

MAGNETOM Flash

SCMR Edition 2022

[siemens-healthineers.com/magnetom-world](https://www.siemens-healthineers.com/magnetom-world)

Page 4

Editorial Comment

From Alpha to Omega: The Breadth in Cardiovascular Magnetic Resonance

Bernd J. Wintersperger

Page 8

Safety, Feasibility, and Clinical Value of Stress Perfusion Vasodilator CMR in Patients with a Pacemaker

Théo Pezel, Jérôme Garot

Page 22

Complete Free-breathing, High-resolution Cardiac MR Studies and their Clinical Impact in Non-ischemic Cardiomyopathies

Guillem Pons-Lladó

Page 28

CMR T2-Mapping Increase as Imaging Biomarker of Myocardial Involvement in Active COVID-19

Marco Francone, et al.

Page 37

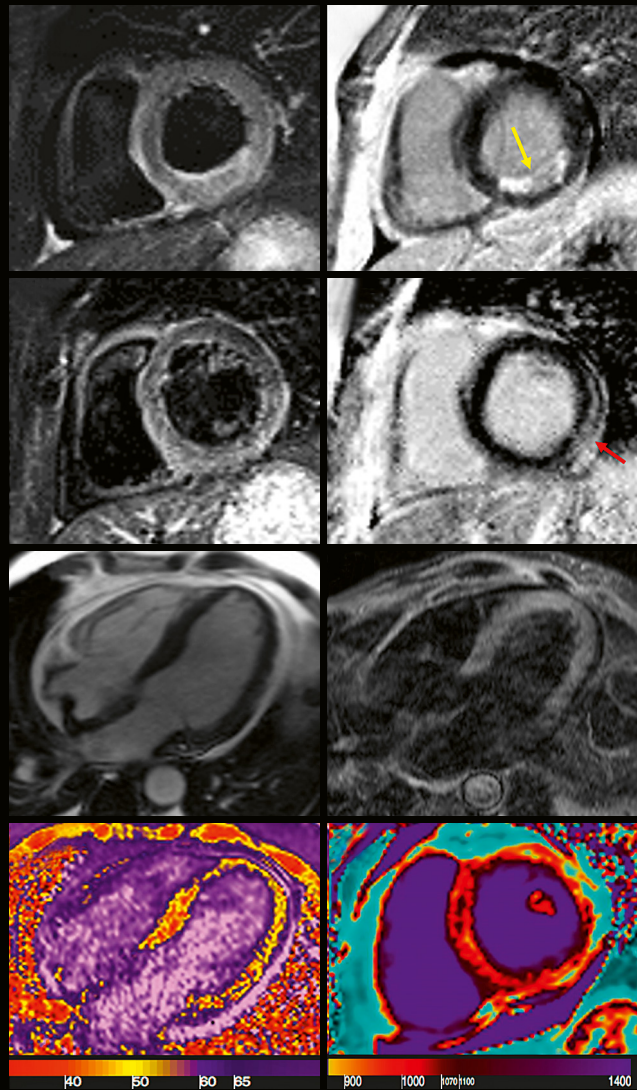
The Added Value of CMRI in the Prevention of Sudden Cardiac Death in Athletes

Hajnalka Vágó

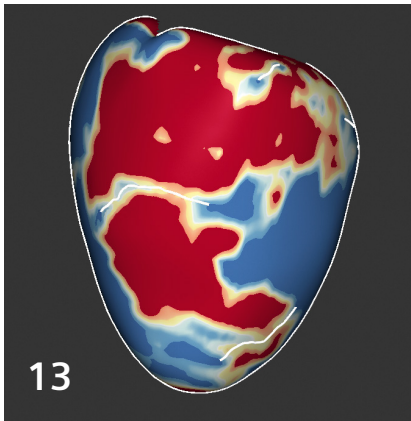
Page 64

Infrared Thermally Enhanced 3D TOF MOTSA MR Angiography for Visualizing the Arteries of the Face

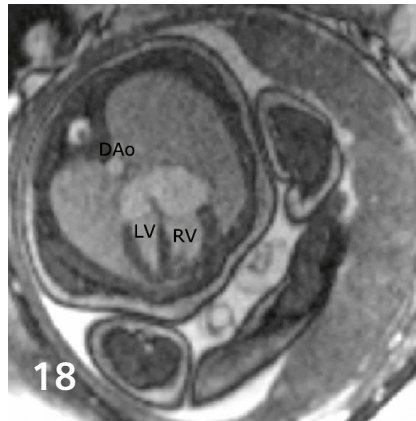
Marc Mespreuve, et al.



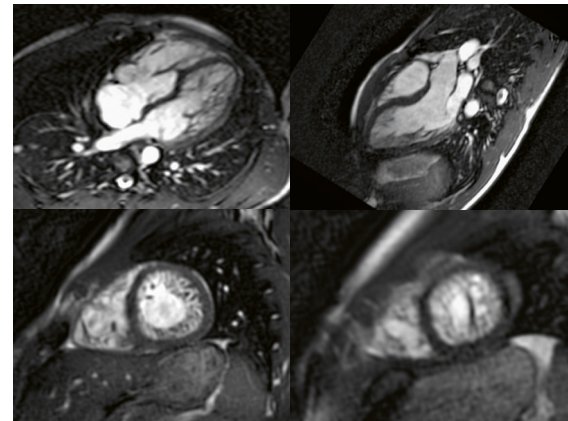
The spectrum of cardiac involvement in COVID-19 patients



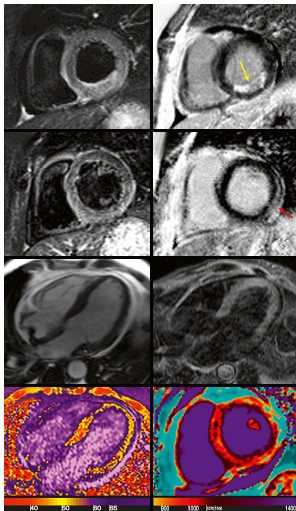
High-bandwidth IR sequences in patients with implants³



Fetal CRM¹ today and in the future



Left ventricular non-compaction: implications for athletes



Cover image: Marco Francone, et al. ("Sapienza" University of Rome, and Humanitas University, Milan, Italy) CMR T2-Mapping Increase as Imaging Biomarker of Myocardial Involvement in Active COVID-19

¹Siemens Healthineers Disclaimer: MR scanning has not been established as safe for imaging fetuses and infants less than two years of age. The responsible physician must evaluate the benefits of the MR examination compared to those of other imaging procedures. Note: This disclaimer does not represent the opinion of the authors.

²Work in progress. The application is currently under development and is not for sale in the U.S. and in other countries. Its future availability cannot be ensured.

³The MRI restrictions (if any) of the metal implant must be considered prior to patient undergoing MRI exam. MR imaging of patients with metallic implants brings specific risks. However, certain implants are approved by the governing regulatory bodies to be MR conditionally safe. For such implants, the previously mentioned warning may not be applicable. Please contact the implant manufacturer for the specific conditional information. The conditions for MR safety are the responsibility of the implant manufacturer, not of Siemens Healthineers.

Editorial Comment

4 From Alpha to Omega: The Breadth in Cardiovascular Magnetic Resonance

Bernd J. Wintersperger
Department of Medical Imaging, University of Toronto / Toronto General Hospital, Toronto, Canada

CMR in Challenging Patient Populations

8 Safety, Feasibility, and Clinical Value of Stress Perfusion Vasodilator CMR in Patients with a Pacemaker³

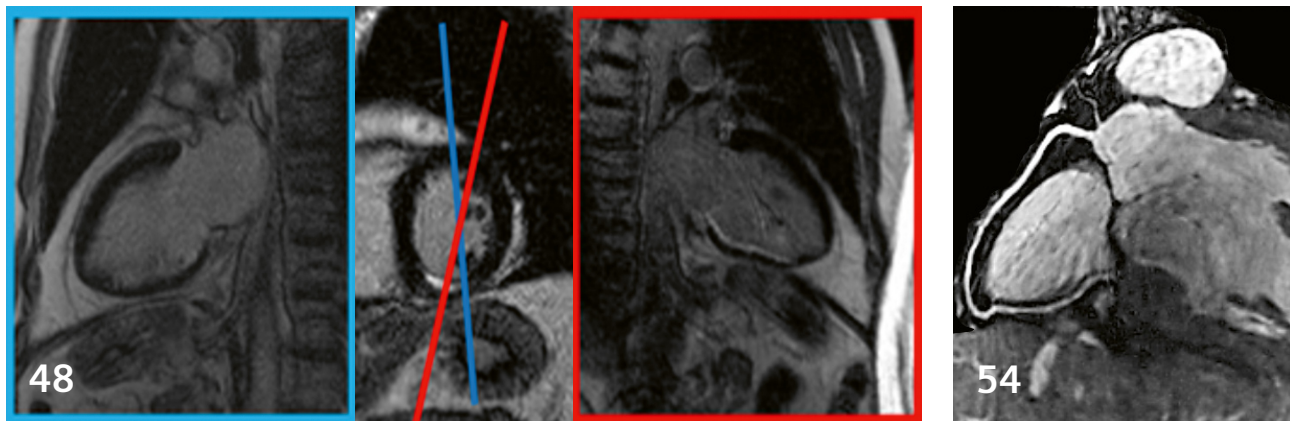
Jérôme Garot, Théo Pezel
Institut Cardiovasculaire Paris Sud—CMR Department
Hôpital Privé Jacques Cartier, Massy, France

13 Clinical Utility of High-Bandwidth Inversion Recovery Sequences in Patients with Cardiac Implanted Electronic Devices³

Hajnalka Vágó, et al.
Semmelweis University, Heart and Vascular Center,
Budapest, Hungary

18 Fetal CMR¹ Today and in the Future

Erik Hedström, Anthony H. Aletras
Lund Cardiac MR Group, Lund University and Skåne
University Hospital, Lund, Sweden



LGE imaging: a technologist's guide

High-resolution motion-corrected 3D CMRA²

CMR in Non-Ischemic Heart Disease

22 Complete Free-breathing, High-resolution Cardiac MR Studies and their Clinical Impact in Non-ischemic Cardiomyopathies

Guillem Pons-Lladó

Cardiac Imaging Unit, Department of Diagnostic Imaging, Clínica Corachán, Barcelona, Spain

28 CMR T2-mapping Increase as Imaging Biomarker of Myocardial Involvement in Active COVID-19

Marco Francone, et al.

Humanitas University, Pieve Emanuele, Milan, Italy

CMR in Athletes

37 The Added Value of CMRI in the Prevention of Sudden Cardiac Death in Athletes

Hajnalka Vágó, et al.

Semmelweis University, Heart and Vascular Center, Budapest, Hungary

43 Left Ventricular Non-Compaction: Implications for Athletes

Giuseppe Femia, Rajesh Puranik

The University of Sydney, Camperdown, NSW, Australia

How I do it

48 Late Gadolinium Enhancement Imaging: A Technologist's Guide

Benny Lawton

St Joseph's Hospital, Malpas, Newport, Wales, UK

MR Angiography

54 High Spatial Resolution Coronary Magnetic Resonance Angiography²: A Single Center Experience

Reza Hajhosseiny, René M. Botnar

King's College London, UK

64 Infrared Thermally Enhanced 3D TOF MOTSA MR Angiography for Visualizing the Arteries of the Face

Marc Mespreuve, et al.

University Hospital Ghent, Belgium

Meet Siemens Healthineers

69 Introducing Solenn Toupin

MR Collaborations

Bordeaux, France



Bernd J. Wintersperger, MD EBCR FAHA, is Director of Magnetic Resonance Imaging and Director of Cardiac Imaging Operations of the Toronto Joint Department of Medical Imaging (JDMI). He is Professor of Radiology at the Department of Medical Imaging at the University of Toronto, and also appointed as Professor of Radiology and Senior Consultant at the Department of Radiology at the University of Munich (LMU), Germany.

Dr. Wintersperger's research interests mainly focus on non-invasive cardiovascular imaging with special emphasis on quantitative methods, quantitative tissue characterization, and innovative accelerated imaging methods. He has over 180 publications listed on PubMed.

Furthermore, he is an active member of various societies (e.g., ISMRM, RNSA, SCMR) and holds various administrative positions in a number of them.

From Alpha to Omega: The Breadth in Cardiovascular Magnetic Resonance

Introduction

Does anyone else have a strong sense of déjà vu? Unfortunately, we will once again be unable to gather in person for the SCMR 2022 scientific sessions. However, we will gather virtually in the spirit of cardiovascular magnetic resonance (CMR) and listen to all the great minds in the fields of CMR (list is purely alphabetical) development, education, engineering, operation, research, and teaching. Ultimately, these magnetic forces will bond all of us for the benefit of our patients.

"Alpha to omega" plots a line from the first to the last letter of the Greek alphabet, and often symbolizes moving from the beginning to the end, or the comprehensiveness of something.

Efforts to image the cardiac affection and myocardial damage related to SARS-CoV-2 infection and the possible effects of vaccinations have been a focus of CMR research throughout the almost two years of the pandemic that has changed today's society in so many ways. However, the entire field of CMR and its broad applications have continued to grow and gain further attention in clinical use and guideline recommendations.

This issue of MAGNETOM Flash highlights some of the many nuances in CMR today, ranging from imaging strategies and technical tips & tricks, to the diagnostic and prognostic use of CMR in various diseases. It highlights the

importance of a team approach and each other's understanding of planning, acquisition, and interpretation. Many people contribute to a successful CMR program, and recognition of everyone's expertise remains a highly important predictor of success. This is in no way different to applications of MR imaging in other parts of the body. Technologists' skills in scanning patients and acquiring data will undoubtedly help the diagnostic assessment by experts interpreting the available data and ultimately support clinical patient management and therapy decisions.

While the following might look like an arbitrary approach, it is meant to capture the bigger picture in CMR – from acquisition to diagnosis viewed from a clinical diagnostic perspective.

The never-ending story

The acquisition of image data undoubtedly represents the beginning (the alpha) of every patient's journey in CMR. Furthermore, the successful sampling of high-quality image data remains key for the diagnostic interpretation and ultimately impacts patient handling, final diagnosis, and therapeutic management.

Simplification of data acquisition and changes in CMR imaging strategies is not a story of the past, but rather one

It highlights the importance of a team approach and each other's understanding of planning, acquisition, and interpretation. Many people contribute to a successful CMR program, and recognition of everyone's expertise remains a highly important predictor of success.

that continues to this day. Besides optimizing image quality and workflows, improving patient comfort and boosting overall efficiency in a busy healthcare environment also remain key for the continued success of CMR in the era of multi-modality approaches to disease assessment. This not only applies to the cardiac component of CMR, but also to the vast field of vascular imaging across the body.

Day optimizing throughput (Dot) engines have been supporting improved and more consistent slice planning as well as patient-adapted workflow strategies for many years. Without doubt, this has improved test-retest comparability in patients with serial CMR exams. Further improvement and integration of AI-based approaches will further reduce the complexity of CMR and increase efficiency. "Lean" imaging with reduced localization aspects compared to diagnostic acquisitions has become a main interest in CMR.

While this may work for most patients, challenges remain in a few, yet important situations. Not only do external factors such as implanted devices pose challenges, but size also matters in terms of whether one is imaging adult coronary arteries or performing CMR in the unborn¹.

For any MR imaging with implants, it is crucial to consider guidelines and recommendations with respect to MR safety, as well as applicable laws and device or MR imager labels. In any case, imaging in the proximity of metal structures remains challenging and while devices may be labeled as MR-conditional, image quality could still become non-diagnostic. In CMR, this specifically poses challenges for late gadolinium enhancement (LGE) imaging and depends on the type of cardiac implantable electronic device (CIED) and specifically also the location of the device generator. Vágó et al. nicely highlight the use of wideband (WB) LGE imaging alternatives in CIED patients where clinical CMR is thought to impact patient management (page 13). While standard LGE strategies specifically fail in the proximity of automated implantable cardioverter

defibrillators (AICD) and cardiac resynchronization therapy (CRT) devices, the application of WB LGE provides scope for diagnostic LGE data sets if clinically appropriate. As such, not only patients with possible need of ablations may benefit but also patients who have received a CIED for various reasons and independent cardiac abnormalities may arise.

Speaking of abnormalities, ischemic heart disease requires not only LGE assessment but also the assessment of hemodynamic relevance of coronary artery stenosis. With the new AHA/ACC/ASE/CHEST/SAEM/SCCT/SCMR guidelines for the evaluation and diagnosis of chest pain, stress perfusion CMR is beginning to take center stage in such scenarios. Garot et al. expand the use of stress perfusion CMR to patients with CIED, on top of LGE scar imaging (page 8). This further supports the continuous improvement of CMR techniques by expanding into challenging territories.

Optimizing LGE imaging in non-CIED patients, and you think you know it all? In over 25 years of CMR experience, I have learned to appreciate every single hint and trick that might help improve overall image quality, speed up acquisition, reduce the need for gadolinium-based contrast agent (GBCA), or tease out subtle differential diagnoses. The ultimate source of many such tricks is still to be found in technologists/radiographers employing their tools regularly. This issue contains a "how-to" overview for implementing the LGE techniques that are currently available on the various platforms from Siemens Healthineers (page 48). Also don't miss the lively discussion of black/gray blood LGE techniques, an approach that specifically aims to improve delineation of subtle LGE in proximity of blood pool (e.g., in subendocardial areas). Such subtle LGE changes can often be the only sign of certain pathologies.

Imaging tiny structures or small patients¹ involves many challenges. Coronary MR angiography is a prime example, specifically given the prevalence of coronary artery disease (CAD) and its impact on healthcare systems

¹Siemens Healthineers Disclaimer: MR scanning has not been established as safe for imaging fetuses and infants less than two years of age. The responsible physician must evaluate the benefits of the MR examination compared to those of other imaging procedures. Note: This disclaimer does not represent the opinion of the authors.

and society. While CMR is undoubtedly the modality of choice for identifying myocardial viability and plays an ever-more important role in the functional testing of potentially hemodynamically relevant stenosis, the holy grail of CAD imaging remains anatomic imaging of the coronary arteries. This is where any potential therapeutic intervention will take place. The hunt for non-invasive coronary imaging began more than two decades ago with the advent of multi-detector row computed tomography (MDCT). In the best interests of our patients and healthcare systems, it remains crucial to consider the benefits and potential limitations of both modalities. Nevertheless, the continuous work by Hajhosseiny et al. (page 54) highlighted in this issue is impressive for its generally high image quality and good to very good diagnostic performance when compared to coronary CT angiography at a 50% stenosis cut-off level. Such work continues to provide confidence that coronary MR angiography² is a technique of the future rather than the past.

Similarly, imaging of the unborn heart presents challenges in the area of spatial and temporal resolution, among others. While fetal MR¹ has been performed for decades, CMR of the fetus, predominately for assessing congenital heart disease (CHD), has only recently attracted more attention – thanks to novel developments and technical improvements. In combination with fetal echocardiography, this aims to further improve pre-natal CHD diagnosis for therapy road-mapping. Hedström et al. (page 18) highlight developments in the field that led to today's advanced approaches. Furthermore, they expand on even more sophisticated non-invasive approaches for assessing physiological parameters such as blood flow and blood oxygenation.

Well, there is no way around this: Given the sheer number of patients in this pandemic and the rapidly growing evidence of myocardium affection by SARS-CoV-2, CMR absolutely had to be investigated in such settings. While the incidence of myocardial inflammation in COVID-19 patients has sparked endless discussions in the community, inoculation with mRNA vaccines and potential adverse cardiac events have also been a focus of debate among CMR professionals. In this issue, Francone's group highlights how quantitative mapping techniques can identify inflammatory changes related to COVID-19 myopericarditis (page 28). Undoubtedly, this confirms the contribution of mapping techniques to the diagnosis of myocarditis and myopericarditis using the modified Lake Louise Criteria.

With cardiomyopathies and their differentiation becoming an important task for CMR, easing and standardizing imaging protocols becomes a highly organizational aspect. One relevant issue is the need for repeated breath-

holds during CMR, a task that can be so complex and demanding for the patient that image quality might substantially degrade. So why breath-holds? Pons-Lladó nicely demonstrates CMR imaging in cardiomyopathy with a free-breathing approach. It has taken a while, but CMR techniques seem to be finally there. With no need for patient recovery periods, such a strategy could cut standard cardiomyopathy CMR protocols to less than 30 minutes' scan time. This would dramatically improve patient comfort, operational workflow, and therefore scanner availability (page 22). Given potential paradigm challenges when applying free-breathing approaches to the employed mapping techniques, the accuracy and precision of quantitative results nevertheless may require further validation.

Athletes aiming to go faster, higher, stronger – in the manner of the Olympic motto *Citius, Altius, Fortius* – frequently need risk assessments or clearance before they can compete. Common protocols in professional and college-level sports have specifically been implemented to clear athletes after COVID-19 infection and thereby minimize risk. However, even without a threat as specific as COVID-19, athletes' hearts may pose challenges in light of their common adaptation to endurance and strength exposure. What many know simply as athlete's heart may show features that are also commonly seen in various cardiomyopathies. If such changes have been identified, CMR plays an increasingly important role in excluding or confirming potentially overlapping cardiomyopathies that could put athletes at risk when exercising. Especially among young athletes, sudden cardiac death (SCD) is of concern and has a number of possible underlying causes. Two articles in this issue cover this important topic and highlight various causes of SCD. They also elaborate on CMR approaches to identify risks and differentiate or confirm potential underlying cardiomyopathies (page 37, 43).

Clearly, after the broad coverage of cardiac topics above, there is an obligation to also highlight vascular imaging innovations. After all, CMR includes vascular imaging as well, doesn't it? To be fair, we may not all be too familiar with the small branches of the facial vasculature. If you want to get more insight into a smart non-contrast MR angiography technique to visualize facial arteries, look no further than this issue. The benefit of compressed sensing in acceleration of time-of-flight (TOF) MR angiography is known, as is the fact that elevated temperature typically results in vascular dilatation and flow increase. Combine the two and you end up with a technique called thermally enhanced 3D TOF MR angiography – with the increased blood flow achieved through heating (with infrared light). This substantially improves TOF MR angiography results,

²Work in progress. The application is currently under development and is not for sale in the U.S. and in other countries. Its future availability cannot be ensured.

as demonstrated by Mespreuve et al. (page 64). Could this potentially be used elsewhere? Watch out for future research endeavors.

Conclusion

We started at alpha, but is there an end for CMR, an omega? Well, that depends on everyone's personal definition. Over recent decades, MR techniques including CMR have hit bumps, but never walls. Technical developments, often based on fancy initial ideas, usually get rolling again and a new era in MR may dawn. Despite this continuous thriving, specifically in technical developments, we should not forget the highly important aspects that are required for the clinical translation of new and innovative CMR techniques. While many new techniques show promise in cohort studies and in predicting future outcomes, the daily diagnostic approach with a single patient being your cohort ($n = 1$) comes with additional needs and requires an especially high discriminatory power of CMR applica-

tions. Our patients are keen to know what their diagnosis is and are not necessarily interested in hearing about the likelihood of a disease and their statistical fate. Back to all the genius minds in CMR: I am more than certain that the translational "dilemma" of some applications will be solved for the benefit of our patients and the healthcare systems.

Bernd J. Wintersperger

Contact

Dr. Bernd J. Wintersperger, MD EBCR FAHA
 Professor of Radiology
 Department of Medical Imaging, University of Toronto, Canada
 Phone: +1 416-340-4800 ex. 8593
 Bernd.Wintersperger@uhn.ca

We appreciate your comments.

Please contact us at magnetomworld.team@siemens-healthineers.com

Editorial Board



Antje Hellwich
Editor-in-chief



Rebecca Ramb, Ph.D.
*Vice President of MR
 Research & Clinical Translation*



Nadine Leclair, M.D.
MR Medical Officer



Wellesley Were
*MR Business Development
 Manager Australia and
 New Zealand*



Jane Kilkenny
*Vice President of MR
 Malvern, PA, USA*



Christian Geppert, Ph.D.
*Head of Cardiovascular
 Applications*

Review Board

Gaia Banks, Ph.D.
*Global Segement Manager
 Cardiovascular MRI*

Daniel Fischer
*Head of Clinical and
 Scientific Marketing*

Daniel Giese, Ph.D.
*Cardiovascular Application
 Development*

Carmel Hayes, Ph.D.
*Cardiovascular Application
 Development*

Michaela Schmidt
*Cardiovascular Application
 Development*

Safety, Feasibility, and Clinical Value of Stress Perfusion Vasodilator Cardiovascular Magnetic Resonance in Patients with a Pacemaker

Théo Pezel, M.D.¹; Solenn Toupin, Ph.D.²; Jérôme Garot, M.D., Ph.D.¹

¹Institut Cardiovasculaire Paris Sud, Cardiovascular Magnetic Resonance Laboratory, Hôpital Privé Jacques Cartier, Massy, France

²Siemens Healthineers, Saint-Denis, France

Introduction

Stress cardiovascular magnetic resonance (CMR) is currently one of the gold standards for the diagnosis of coronary artery disease (CAD) in clinical routine. Indeed, stress CMR imaging is an accurate technique for assessing ventricular function, the presence and extent of inducible ischemia, and the extent of myocardial scar and viability without ionizing radiation. In the MR-INFORM study, an initial stress CMR-based diagnostic strategy was shown to produce outcomes that were noninferior to those of invasive fractional flow reserve in patients with suspected CAD [1]. Therefore, current European and U.S. guidelines recommend stress CMR imaging in symptomatic patients with known or suspected CAD with intermediate risk (class I) [2, 3].

Recent studies have shown that the prevalence of CAD in patients with atrioventricular block or sinus node dysfunction is high, with almost 30% having obstructive CAD [4, 5]. Interestingly, these two conduction disorders are the most frequent conditions for pacemaker (PM) implantation [6]. Moreover, the number of patients treated with a permanently implanted PM has dramatically increased over the last decade [7].

Detecting inducible ischemia by stress CMR plays a crucial role in terms of patient decision-making. Indeed, the patient will be referred to invasive coronary angiography to evaluate the interest of a coronary revascularization by coronary stent or coronary artery bypass graft. In addition, it is recommended to intensify the management of traditional cardiovascular risk factors in these high-risk patients with inducible ischemia.

Although performing CMR exams on patients with a PM¹ in clinical routine often raises practical questions of feasibility, the issue of performing stress CMR on PM patients has become crucial. Indeed, given the high incidence of clinical indications for CMR in these patients,

the technical development of MR-conditional PMs has allowed safe access to this type of exam [8, 9]. Although a PM has long been considered a contraindication for MR scanning [10], several studies have recently demonstrated safety [11, 12] and diagnostic image quality in the vast majority of cases [13–15]. Because PM patients have often been excluded from large-scale CMR outcome studies, very little data assessing the prognostic value of stress CMR in this population exists [16, 17].

The aim of this article is to review our experience with stress CMR in patients with a PM in terms of feasibility and safety, and to discuss the clinical value of performing this type of examination in PM patients.

How to manage pacemaker programming?

In line with AHA guidelines [18], PM programming at our center is performed using a predefined protocol. Immediately before CMR, a full set of device parameters are thoroughly evaluated by a senior electrophysiologist. The evaluation includes lead sensing, lead impedance, battery voltage, state, and capture threshold. Devices are set to MR-safe mode according to the manufacturer's instructions immediately before the CMR exam, and reprogrammed immediately after. The device is programmed to the manufacturer's MR-conditional mode with an appropriate pacing mode: DOO/VOO for PM-dependent patients (defined by a heart rate < 30/min) and VVI/DDI for non-PM-dependent patients [18].

¹The MRI restrictions (if any) of the metal implant must be considered prior to patient undergoing MRI exam. MR imaging of patients with metallic implants brings specific risks. However, certain implants are approved by the governing regulatory bodies to be MR conditionally safe. For such implants, the previously mentioned warning may not be applicable. Please contact the implant manufacturer for the specific conditional information. The conditions for MR safety are the responsibility of the implant manufacturer, not of Siemens Healthineers.

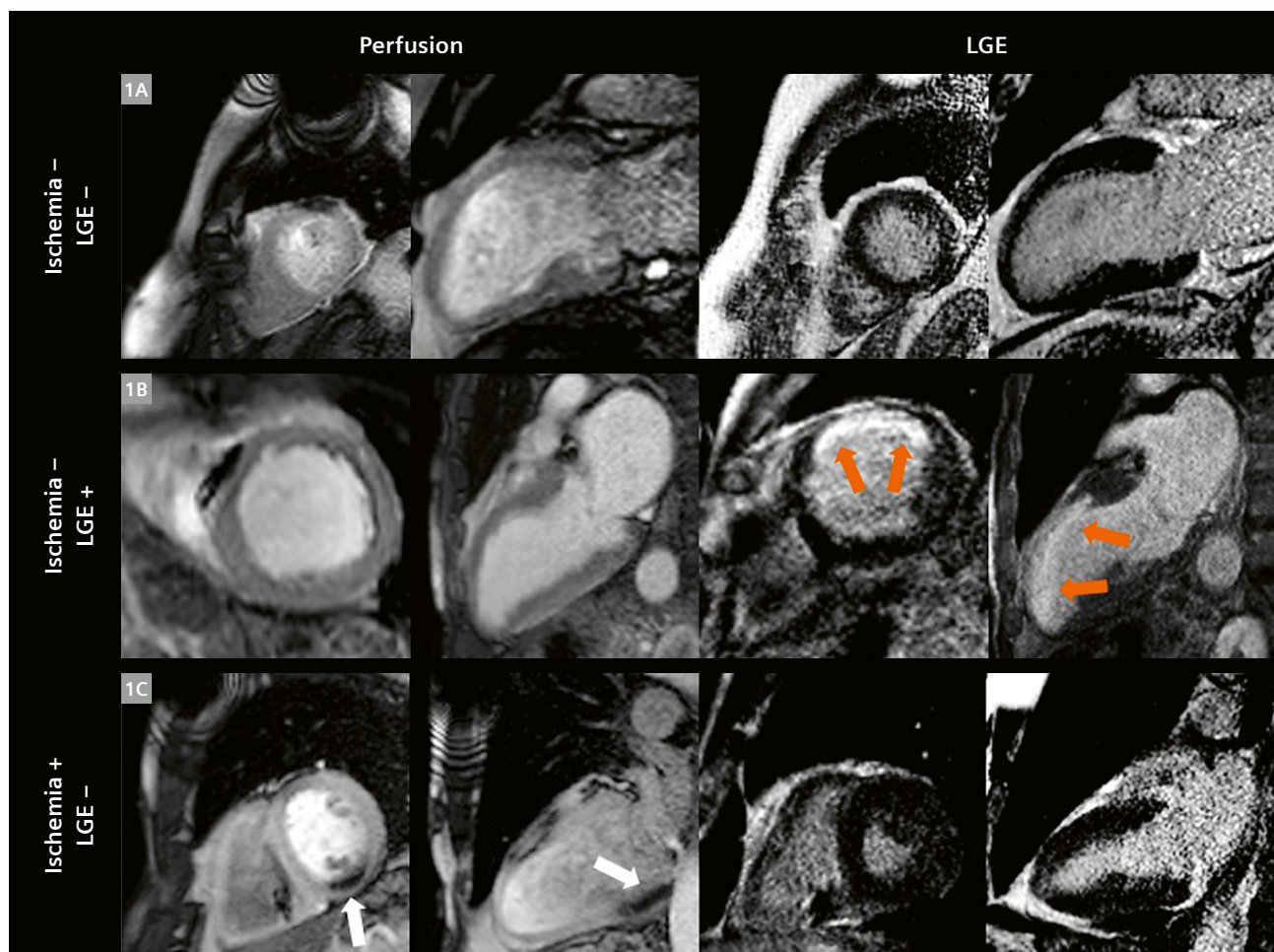
Which safety protocol for a stress CMR?

In our stress CMR protocol, patients are monitored during the scan with continuous electrocardiography, pulse monitoring, oxygen saturation, and visual supervision by a cardiologist present in the control room, with resuscitation equipment and an advanced cardiac life support protocol in the MR environment. Visual and voice contact with the patient is maintained throughout the entire examination. In the scanner, the patient is placed on a carry cart, and staff members are trained to rapidly remove the patient from the scanner room in the event of a cardiovascular emergency. Thus, immediate treatment of severe arrhythmia and reactivation of PM stimulation are

guaranteed within seconds in non-paced patients. Atropine, adrenaline, and theophylline injections are readily available for use in case of bradycardia.

How to check the device integrity?

For device integrity, variations of more than 50% for capture thresholds, 40% for P/R wave-sensing amplitudes, and 30% for impedances are considered to represent significant changes in device performance [19]. Moreover, increases of less than 1.0 V in atrial or ventricular capture thresholds at a pulse duration of 0.4 ms could be considered insignificant [20].



1 Examples of inducible ischemia on stress CMR in patients with a pacemaker

(1A, normal) A 68-year-old male with a pacemaker, presenting with atypical angina. Stress CMR revealed no perfusion defect and no LGE, ruling out a diagnosis of myocardial ischemia.

(1B, myocardial scar without ischemia) A 71-year-old female with a pacemaker and a history of anterior STEMI treated by PCI of the LAD four years ago, presenting with dyspnea on exertion. Stress CMR showed a subendocardial anterior scar on LGE (orange arrow) without any perfusion defect and therefore no inducible ischemia. Coronary angiography confirmed the absence of significant stenosis.

(1C, inducible ischemia) An 82-year-old male with a pacemaker, presenting with atypical angina. First-pass myocardial stress perfusion images revealed a reversible perfusion defect of the inferior wall (white arrows) without LGE, indicating myocardial inducible ischemia suggestive of significant RCA stenosis and confirmed by coronary angiography. In all cases, there were only minor or moderate artifacts from the PM box or leads, and these did not impact diagnostic accuracy (grade 3–4).

Here is the list of parameters often noted by the electrophysiologist to check device integrity before and after the CMR exam:

- P-wave amplitude, mV
- R-wave amplitude, mV
- Atrial lead impedance, ohm
- Ventricular lead impedance, ohm
- Atrial pacing capture threshold, V at a pulse width of 0.4 ms
- Ventricular pacing capture threshold, V at a pulse width of 0.4 ms
- Battery voltage, V

Special features of the stress CMR protocol in patients with a PM

In our center, stress CMR is performed in a dedicated cardiovascular MR laboratory on 1.5T scanners (MAGNETOM Aera, Siemens Healthcare, Erlangen, Germany). According to current guidelines, whole-body specific absorption rate is restricted to 2.0 W/kg bodyweight for all imaging sequences. Moreover, patient-specific energy dose (SED, a measure of the total radiofrequency energy delivered) is ≤ 0.2 kJ/kg for all patients. Cine imaging is initially performed using a retrospectively gated balanced steady-state free-precession (b-SSFP) sequence. If the pacemaker produces significant artifacts that could hamper image analysis, a gradient echo sequence (FGRE) can be used. Vasodilation is induced with dipyridamole, adenosine, or regadenoson. After a bolus of 0.1 mmol/kg of gadolinium-based contrast agent, stress perfusion imaging is performed using a b-SSFP sequence, or a GRE sequence in the case of significant artifacts. A series of six slices (four short-axis views, a 2-chamber view and a 4-chamber view) are acquired. Ten minutes after the contrast injection, late gadolinium enhancement (LGE) images are acquired

using a breath-hold 3D T1-weighted inversion-recovery gradient-echo sequence. Patients are asked to refrain from caffeine for at least 12 hours before CMR. A 12-lead ECG is performed both before and after the CMR examination.

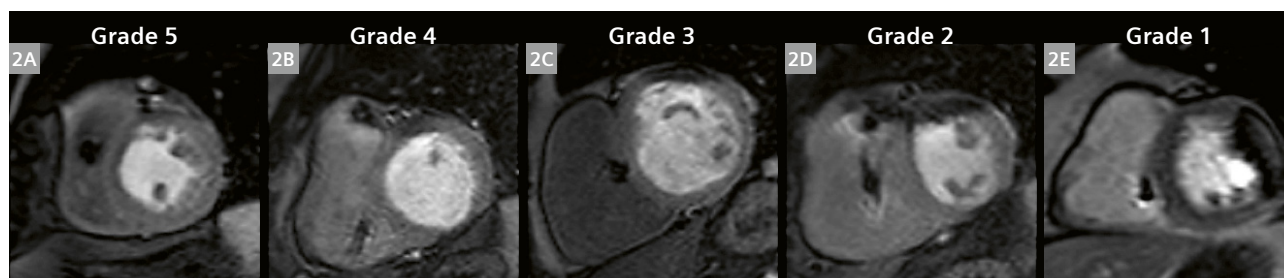
Stress CMR analysis to identify inducible ischemia

The current SCMR guidelines define inducible ischemia as a subendocardial or transmural perfusion defect that

- 1) occurred in at least one myocardial segment;
- 2) persisted for at least three phases beyond peak contrast enhancement;
- 3) followed a coronary distribution;
- 4) occurred in the absence of co-location with LGE (Fig. 1) [21].

Image quality of stress CMR in patients with a PM

In a recent study, our working group showed that stress CMR is feasible and safe in patients with an MR-conditional PM with good or excellent image quality (a score of 4 or 5) in 84% of segments using a validated classification of the level of artifacts (Fig. 2). In the overall population of 203 patients with an MR-conditional PM, 49% had cine and perfusion imaging of diagnostic quality with b-SSFP sequences alone, and 51% required GRE imaging due to the presence of artifacts on the b-SSFP images. The GRE sequences provided better image quality than the b-SSFP sequences (mean score 4.4 vs 3.9; $p < 0.001$). Right-side pectoral devices were associated with significantly better image quality than left-side devices (mean score 4.6 vs 4.1; $p < 0.001$).



2 Classification of the level of artifacts produced by the leads or the pacemaker pacing box [21, 25]

Each myocardial segment is graded using a scale from 5 (excellent image quality) to 1 (non-diagnostic).

Grade 5: very good image quality with no artifacts affecting cardiac anatomy (2A);

Grade 4: good image quality with minor artifacts affecting cardiac anatomy but no impact on diagnostic quality (2B);

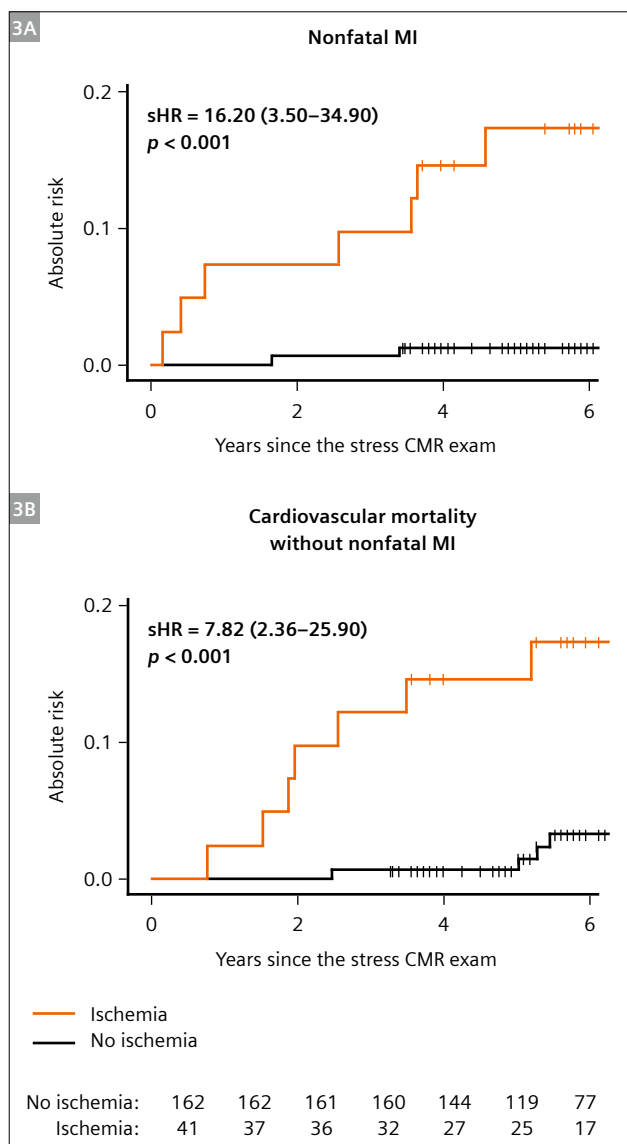
Grade 3: artifacts moderately affect cardiac anatomy but do not impact diagnostic quality (2C);

Grade 2: artifacts moderately affect cardiac anatomy, causing some impact on diagnostic quality (2D);

Grade 1: poor image quality with significant impact of artifacts on cardiac anatomy, resulting in non-diagnostic images (2E).

Safety

Several studies demonstrate the absence of severe CMR-related complications in PM patients with suspected CAD [11, 14, 21]. In our cohort of 203 patients with a PM, no clinical symptoms induced by PM dysfunction were observed and no complications or arrhythmia were induced by the vasodilator agent [21]. Also, device integrity is preserved without significant alterations of lead impedance, pacing capture threshold, and sensing amplitude [11, 14, 21].



3 Prognostic value of inducible ischemia identified by stress CMR to predict nonfatal myocardial infarction (MI) and cardiovascular mortality in patients with a PM [21]

Competitive risk analysis with cumulative incidence uses the subdistribution hazard ratio (sHR) of nonfatal MI (3A) or cardiovascular mortality without nonfatal MI (3B). A test comparing the groups was based on the Fine and Gray's test for trend.

Prognostic value of stress CMR in patients with a PM

Our working group recently described an excellent prognostic value of stress CMR to predict cardiovascular events in consecutive patients with an MR-conditional PM [21]. The presence of inducible ischemia and LGE were independent long-term predictors of cardiovascular events at 7-year median follow-up. Indeed, the presence of inducible ischemia was independently associated with a more than 16-fold increase in the rate of nonfatal myocardial infarction, and with a more than 7-fold increase in the rate of cardiovascular mortality after adjustment for traditional risk factors. The good prognostic value of stress perfusion CMR in PM patients may be explained by the fact that detecting ischemia using a vasodilator does not rely on heart rate response, because relative ischemia is induced by distal vasodilatation and hyperemic response via cardiac A1 receptors and not by positive chronotropy. Although an increased heart rate as a marker of vasodilator response is not valid in PM patients, the good prognostic value of inducible ischemia supports the clinical relevance of stress CMR in this population.

What is the role of stress CMR compared to other non-invasive stress tests?

Functional non-invasive imaging to detect CAD is frequently challenging in patients with PM. Stress echocardiography is often limited by submaximal exercise or by the alternative need for pacing with poor tolerance and segmental wall motion abnormalities caused by focal stimulation [22]. SPECT nuclear perfusion imaging may be hampered by submaximal exercise and artifacts associated with left bundle branch block (LBBB) induced by electrical stimulation and radiation [23]. Coronary computed tomography angiography (CCTA) has some limitations in PM patients as a result of artifacts induced by ventricular leads [24].

Risk stratification of PM patients with suspected or known CAD is not formally specified in the current guidelines [2].

Conclusion

Several studies have shown that stress vasodilator CMR is safe and feasible, providing good or excellent image quality in the vast majority of cases. Some recent studies have described a strong and independent prognostic value of the presence of inducible ischemia detected on stress CMR in patients with an MR-conditional PM. This strategy requires strict compliance with recommended protocols that involve the risk/benefit ratio of undergoing stress CMR and the pre- and post-CMR tuning of the device by an electrophysiologist. In this setting, we can extend the benefits of CMR to patients with an MR-conditional PM.

References

- 1 Nagel E, Greenwood JP, McCann GP, Bettencourt N, Shah AM, Hussain ST, et al. Magnetic Resonance Perfusion or Fractional Flow Reserve in Coronary Disease. *N Engl J Med.* 2019;380(25):2418–2428.
- 2 Knuuti J, Wijns W, Saraste A, Capodanno D, Barbato E, Funck-Brentano C, et al. 2019 ESC Guidelines for the diagnosis and management of chronic coronary syndromes. *Eur Heart J.* 2020;41(3):407–477.
- 3 Writing Committee Members; Gulati M, Levy PD, Mukherjee D, Amsterdam E, Bhatt DL, et al. 2021 AHA/ACC/ASE/CHEST/SAEM/SCCT/SCMR Guideline for the Evaluation and Diagnosis of Chest Pain: A Report of the American College of Cardiology/American Heart Association Joint Committee on Clinical Practice Guidelines. *J Am Coll Cardiol.* 2021;78(22):e187–285.
- 4 Alai MS, Beig JR, Kumar S, Yaqoob I, Hafeez I, Lone AA, et al. Prevalence and characterization of coronary artery disease in patients with symptomatic bradyarrhythmias requiring pacemaker implantation. *Indian Heart J.* 2016;68 Suppl 3:S21–S25.
- 5 Alonso A, Jensen PN, Lopez FL, Chen LY, Psaty BM, Folsom AR, et al. Association of sick sinus syndrome with incident cardiovascular disease and mortality: the Atherosclerosis Risk in Communities study and Cardiovascular Health Study. *PLoS One.* 2014;9(10):e109662.
- 6 Mond HG, Proclemer A. The 11th world survey of cardiac pacing and implantable cardioverter-defibrillators: calendar year 2009--a World Society of Arrhythmia's project. *Pacing Clin Electrophysiol.* 2011;34(8):1013–27.
- 7 Benjamin EJ, Muntner P, Alonso A, Bittencourt MS, Callaway CW, Carson AP, et al. Heart Disease and Stroke Statistics-2019 Update: A Report From the American Heart Association. *Circulation.* 2019;139(10):e56–e528.
- 8 Symons R, Zimmerman SL, Bluemke DA. CMR and CT of the Patient With Cardiac Devices: Safety, Efficacy, and Optimization Strategies. *JACC Cardiovasc Imaging.* 2019;12(5):890–903.
- 9 Shinbane JS, Colletti PM, Shellock FG. MR imaging in patients with pacemakers and other devices: engineering the future. *JACC Cardiovasc Imaging.* 2012;5(3):332–3.
- 10 Brignole M, Auricchio A, Baron-Esquivias G, Bordachar P, Boriani G, Breithardt O-A, et al. 2013 ESC Guidelines on cardiac pacing and cardiac resynchronization therapy: the Task Force on cardiac pacing and resynchronization therapy of the European Society of Cardiology (ESC). Developed in collaboration with the European Heart Rhythm Association (EHRA). *Eur Heart J.* 2013;34(29):2281–329.
- 11 Nazarian S, Hansford R, Rahsepar AA, Weltin V, McVeigh D, Gucuk Ipek E, et al. Safety of Magnetic Resonance Imaging in Patients with Cardiac Devices. *N Engl J Med.* 2017;377(26):2555–2564.
- 12 Schaller RD, Brunker T, Riley MP, Marchlinski FE, Nazarian S, Litt H. Magnetic Resonance Imaging in Patients With Cardiac Implantable Electronic Devices With Abandoned Leads. *JAMA Cardiol.* 2021;6(5):549–556.
- 13 Schwitter J, Kanal E, Schmitt M, Anselme F, Albert T, Hayes DL, et al. Impact of the Advisa MRI pacing system on the diagnostic quality of cardiac MR images and contraction patterns of cardiac muscle during scans: Advisa MRI randomized clinical multicenter study results. *Heart Rhythm.* 2013;10(6):864–72.
- 14 Padmanabhan D, Kella D, Isath A, Tandon N, Mulpuru S, Deshmukh A, et al. Prospective evaluation of the utility of magnetic resonance imaging in patients with non-MRI-conditional pacemakers and defibrillators. *J Cardiovasc Electrophysiol.* 2020;31(11):2931–2939.
- 15 Ning X, Li X, Fan X, Chen K, Hua W, Liu Z, et al. 3.0 T magnetic resonance imaging scanning on different body regions in patients with pacemakers. *J Interv Card Electrophysiol.* 2021;61(3):545–550.
- 16 Kwong RY, Ge Y, Steel K, Bingham S, Abdullah S, Fujikura K, et al. Cardiac Magnetic Resonance Stress Perfusion Imaging for Evaluation of Patients With Chest Pain. *J Am Coll Cardiol.* 2019;74(14):1741–1755.
- 17 Heitner JF, Kim RJ, Kim HW, Klem I, Shah DJ, Debs D, et al. Prognostic Value of Vasodilator Stress Cardiac Magnetic Resonance Imaging: A Multicenter Study With 48 000 Patient-Years of Follow-up. *JAMA Cardiol.* 2019;4(3):256–264.
- 18 Levine GN, Gomes AS, Arai AE, Bluemke DA, Flamm SD, Kanal E, et al. Safety of magnetic resonance imaging in patients with cardiovascular devices: an American Heart Association scientific statement from the Committee on Diagnostic and Interventional Cardiac Catheterization, Council on Clinical Cardiology, and the Council on Cardiovascular Radiology and Intervention: endorsed by the American College of Cardiology Foundation, the North American Society for Cardiac Imaging, and the Society for Cardiovascular Magnetic Resonance. *Circulation.* 2007;116(24):2878–91.
- 19 Nazarian S, Hansford R, Roguin A, Goldsher D, Zviman MM, Lardo AC, et al. A prospective evaluation of a protocol for magnetic resonance imaging of patients with implanted cardiac devices. *Ann Intern Med.* 2011;155(7):415–24.
- 20 Preston TA, Fletcher RD, Lucchesi BR, Judge RD. Changes in myocardial threshold. Physiologic and pharmacologic factors in patients with implanted pacemakers. *Am Heart J.* 1967;74(2):235–42.
- 21 Pezel T, Lacotte J, Toupin S, Salerno F, Said MA, Manenti V, et al. Diagnostic Accuracy of Stress Perfusion CMR for Risk Stratification in Patients With MR-Conditional Pacemakers. *JACC Cardiovasc Imaging.* 2021;14(10):2053–2054.
- 22 Picano E, Alaimo A, Chubuchny V, Plonska E, Baldo V, Baldini U, et al. Noninvasive pacemaker stress echocardiography for diagnosis of coronary artery disease: a multicenter study. *J Am Coll Cardiol.* 2002;40(7):1305–10.
- 23 Einstein AJ, Weiner SD, Bernheim A, Kulon M, Bokhari S, Johnson LL, et al. Multiple testing, cumulative radiation dose, and clinical indications in patients undergoing myocardial perfusion imaging. *JAMA.* 2010;304(19):2137–44.
- 24 Menke J, Kowalski J. Diagnostic accuracy and utility of coronary CT angiography with consideration of unevaluable results: A systematic review and multivariate Bayesian random-effects meta-analysis with intention to diagnose. *Eur Radiol.* 2016;26(2):451–8.
- 25 Raphael CE, Vassiliou V, Alpendurada F, Prasad SK, Pennell DJ, Mohiaddin RH. Clinical value of cardiovascular magnetic resonance in patients with MR-conditional pacemakers. *Eur Heart J Cardiovasc Imaging.* 2016;17(10):1178–85.

Contact

Professor Jérôme Garot, M.D., Ph.D.
IRM cardiovasculaire – ICPS
Hôpital Privé Jacques Cartier
Ramsay Générale de santé
6 Av du Noyer Lambert
91300, Massy
France
jgarot@angio-icps.com



Théo Pezel, M.D.
IRM cardiovasculaire – ICPS
Hôpital Privé Jacques Cartier
Ramsay Générale de santé
6 Av du Noyer Lambert
91300, Massy
France
tpezel@angio-icps.com



Clinical Utility of High-Bandwidth Inversion Recovery Sequences in Patients with Cardiac Implanted Electronic Devices

Zsófia Dohy¹; Liliána Szabó¹; Máté Kiss²; Xiaoming Bi³; Csilla Czibalmos¹; Ferenc Imre Suhai¹; Attila Tóth¹; Vencel Juhász¹; Roland Papp¹; László Gellér¹; Béla Merkely¹; Hajnalka Vágó¹

¹Semmelweis University, Heart and Vascular Center, Budapest, Hungary

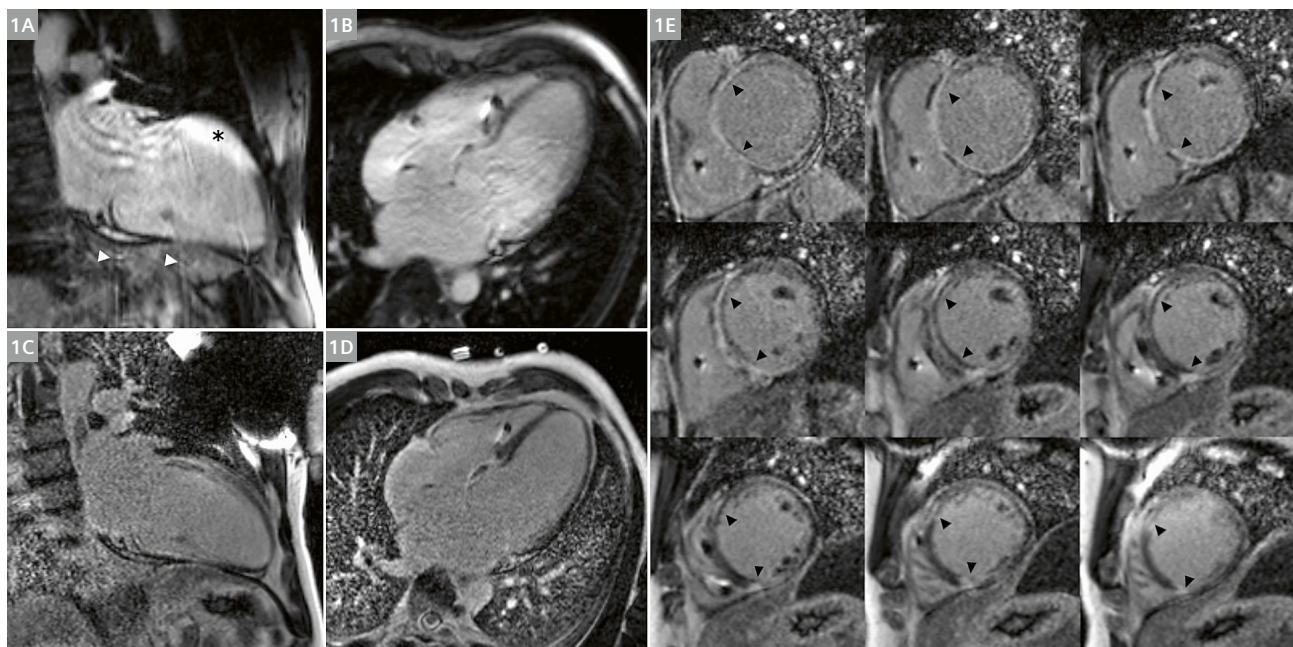
²Siemens Healthineers, Budapest, Hungary

³Siemens Medical Solutions, Los Angeles, USA

Introduction

Myocardial scar detection using cardiac magnetic resonance (CMR) imaging with late gadolinium enhancement (LGE) facilitates diagnosis and clinical management in various cardiac conditions. For instance, it can help determine the etiology of heart failure and arrhythmias, assess myocardial viability, differentiate among cardiomyopathies, and guide electrophysiological interventions

[1–4]. In patients with scar-related ventricular tachycardia (VT), performing CMR imaging before radiofrequency catheter ablation can help pre-procedural planning and scar mapping [5]. However, many patients with an indication for VT ablation already have an implantable cardioverter defibrillator (ICD)¹, and this may be a contraindication to a CMR examination. The population of patients



1 (1A, B) Standard LGE images in 2-chamber (1A) and 4-chamber (1B) views with hyperintensity (black asterisk) and breathing (white arrowheads) artifacts. (1C–E) Wideband LGE images in 2-chamber (1C), 4-chamber (1D), and short axis (1E) views with mid-myocardial contrast enhancement in the basal and midventricular anterior, septal, and inferior segments (black arrowheads).

¹The MRI restrictions (if any) of the metal implant must be considered prior to patient undergoing MRI exam. MR imaging of patients with metallic implants brings specific risks. However, certain implants are approved by the governing regulatory bodies to be MR conditionally safe. For such implants, the previously mentioned warning may not be applicable. Please contact the implant manufacturer for the specific conditional information. The conditions for MR safety are the responsibility of the implant manufacturer, not of Siemens Healthineers.

with different cardiac implanted electronic devices (CIEDs)¹ is growing. Because CIED patients with electrical abnormalities often have underlying structural heart disease, the indications for CMR examinations are expanding in this patient population.

In the past, CMR was contraindicated in patients with CIEDs due to safety concerns. With the advent of MR-conditional CIEDs and the establishment of appropriate and strict safety protocols which allow CMR imaging in patients with CIEDs [6, 7], the number of these examinations is growing. However, device- and lead-related artifacts can limit image interpretability and the clinical applicability of CMR in CIED patients, especially in the case of ICDs and cardiac resynchronization therapy pacemakers (CRT-Ps) or defibrillators (CRT-Ds) [8, 9]. There are two basic device artifacts in late gadolinium enhancement (LGE) imaging:

- 1) Hyperintense regions which were not inverted due to the limited inversion bandwidth
- 2) Signal voids due to dephasing, caused by gradient generally along the widest voxel dimension [10].

A high-bandwidth inversion recovery sequence uses wideband (WB) techniques to reduce susceptibility artifacts². This extends the benefit of tissue characterization to device patients, enabling them to receive diagnostically robust imaging that visualizes myocardial injury. Wideband LGE CMR techniques have been developed to attenuate these image artifacts and enhance the diagnostic value of CMR in CIED patients [10, 11].

At our institution we are using a 1.5T MR scanner (MAGNETOM Aera, Siemens Healthcare, Erlangen, Germany) and two types of WB protocols to reduce susceptibility and off-resonance artifacts in examinations with CIEDs. The spatial resolution is the same for both protocols: 1.4 x 1.4 x 8.0 mm³. The first protocol is a shorter single-shot breath-controlled sequence. The second uses a single-shot data acquisition method in combination with phase-sensitive inversion recovery (PSIR) and motion correction (MoCo) for reconstruction, which allows measurements to be taken under free-breathing conditions [12]. Signal-to-noise ratio (SNR) loss from the accelerated single-shot acquisition is offset by increasing the number of averages. For ICD imaging with more severe artifacts, we suggest at least 24 averages (with thinner slices – e.g., 4 mm). For pacemakers – where the artifacts are less intense – we can reduce the number of averages to 16. Free-breathing measurements take slightly longer, but they provide more stable image quality without SNR loss or device-related image artifacts.

The following two clinical cases demonstrate the clinical impact of the high-bandwidth inversion recovery sequence in everyday routine.

Case 1

A 45-year-old male patient with a CRT-D was referred for CMR imaging before VT ablation for scar mapping.

Patient history: In 2015, the patient had syncope. An electrocardiogram (ECG) showed wide QRS and first-degree AV block, and 24-hour Holter monitoring detected polymorphic ventricular premature beats. The CMR examination in 2015 showed dilated cardiomyopathy with extended LGE with a non-ischemic pattern. During the electrophysiological examination, sustained VT could be induced. After radiofrequency catheter ablation, the VT persisted with altered morphology, which indicated ICD implantation. Over the years, appropriate ICD shocks were detected on several occasions. Because of the progression of heart failure, VT ablation was repeated in 2020 and the ICD was upgraded to a CRT-D (St. Jude Quadra Assura 3371-40C).

The patient has since had repeated VTs, which necessitated another VT ablation and a CMR examination for scar mapping. Before CMR scanning, the patient – who has a non-conditional CIED – underwent device interrogation. As the patient was pacemaker-dependent, the pacing mode was programmed to DOO-RV-only asynchronous bipolar pacing with high pacing energy (5.0 V/1.0 msec). All tachyarrhythmia detection and therapies were switched off. Protocols developed for safely performing CMR imaging in patients with CIEDs were followed [13, 14]. Intra-procedural monitoring was performed with a continuous electrocardiogram, pulse oximetry, and non-invasive blood pressure measurements. The specific absorption rate was limited to 2.0 W/kg. No adverse events occurred. Following completion of the CMR scan, the original device settings were reinstated.

The CMR examination was performed in a 1.5T scanner (MAGNETOM Aera, Siemens Healthcare, Erlangen, Germany). After standard scout slices, spoiled gradient echo imaging was performed to assess cardiac volumes and function. An intravenous bolus of gadobutrol (0.15 mmol/kg) was injected. Ten minutes after the injection, standard LGE and free-breathing WB LGE images were acquired in 2-, 3-, and 4-chamber views. WB LGE images were acquired, as well as short-axis images with full coverage of the left ventricle with free breathing and the MoCo algorithm.

Hyperintensity artifacts in the anterior segments, as well as breathing artifacts, limited the interpretability of standard LGE images (Figs. 1A, B). No artifacts affected the left ventricular segments on the WB LGE images, and midmyocardial contrast enhancement was present in the basal and midventricular anterior, septal, and inferior segments (Figs. 1C–E). The WB LGE images were processed with ADAS-3D software (Galgo Medical SL, Barcelona,

²High-bandwidth Inversion Recovery is a product with software version syngo MR XA 30/31. The sequence used in the article was a prototype.

Spain) for channel detection. Following semiautomatic endo- and epicardial contour detection, ten concentric surface layers were created automatically from endocardium to epicardium. A 3D shell was created for each layer. Based on signal intensities, scar core, border zone, and healthy myocardium were identified. A conducting channel was defined as a corridor in the border zone between two scar-core areas [5].

After invasive electroanatomic mapping (EAM) – supported by the CMR images – VT ablation was repeated in the septal region. During a four-month clinical follow-up, no ventricular arrhythmias were detected.

Case 2

A 64-year-old male patient with prior myocardial infarction and ICD (Biotronic Itevia 5 VR-T DX) implantation was referred for CMR imaging. The patient had an ST-elevated myocardial infarction in 2016, and a percutaneous coronary intervention with stent implantation in the right coronary artery was performed. Six months later, monomorphic VT occurred. Coronary angiography showed in-stent restenosis, which required reintervention with stent implantation. As the VT recurred, VT ablation and ICD implantation were performed in 2016. In 2020 and 2021, appropriate ICD therapies occurred several times, which indicated a repeated VT ablation.

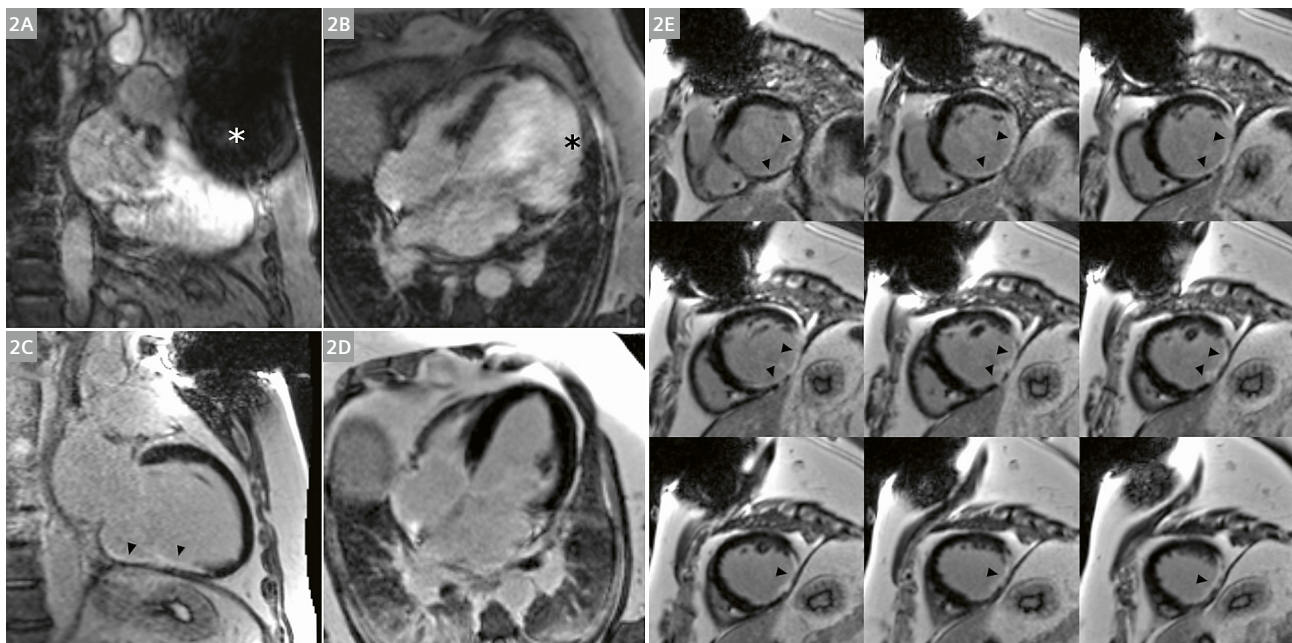
Prior to the VT ablation, CMR for scar mapping was performed with the same protocol described in our first case report. As the patient was not pacemaker-dependent, the MR-conditional ICD was turned off during the CMR examination.

Taking into account the proximity of the ICD, we detected large susceptibility and off-resonance artifacts at the left ventricular anterior and anterolateral segments on the standard LGE images (Figs. 2A, B). Such artifacts would make the correct diagnosis impossible. However, the high-bandwidth inversion recovery sequence allowed us to completely diminish both the off-resonance and susceptibility artifacts, and to detect transmural contrast enhancement in the inferior and inferolateral segments corresponding to the previous myocardial infarction (Figs. 2C–E). Potentially arrhythmogenic conducting channels were identified using the ADAS 3D software (Fig. 3).

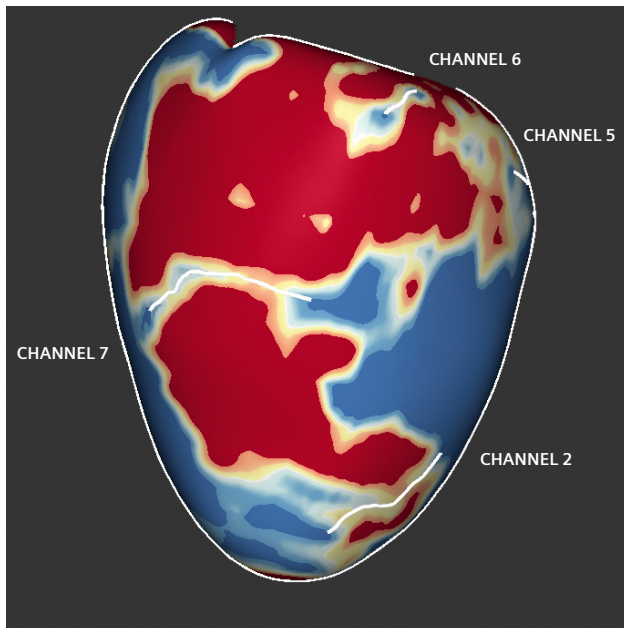
Using the EAM and CMR images, extended epi- and endocardial ablation was performed in the inferior region. During a five-month clinical follow-up, no VT was detected by the ICD.

Discussion

LGE-CMR can accurately identify fibrotic myocardium and the potential arrhythmogenic substrate. It is therefore a



2 (2A, B) Standard LGE images in 2-chamber (2A) and 4-chamber (2B) views with hyperintensity off-resonance artifacts (black asterisk) in the anterior and anterolateral segments, and susceptibility artifacts (white asterisk) in the anterior segments. (2C–E) Wideband LGE images in 2-chamber (2C), 4-chamber (2D), and short axis (2E) views with transmural contrast enhancement in the inferior and inferolateral segments (black arrowheads).



3 Detection of scar in red, border zones in yellow, and normal tissue in blue using ADAS 3D software. Conducting channels were identified as a corridor in the border zone between two core areas.

widely used technique for planning ablation procedures [15, 16]. Previous data demonstrated that CMR-aided VT ablation was associated with a lower need for radio-frequency delivery, lower VT inducibility after substrate ablation, and lower VT recurrence rate [5]. Nevertheless, most patients referred to VT ablation already have a CIED. With conventional CMR, the quality of LGE images is usually poor due to metal-induced artifacts, especially in the left ventricular anterior segments [9]. The device generator causes off-resonance hyperintensity artifacts within the myocardium. These artifacts appear similar to the LGE of scar tissue, which can lead to false diagnoses.

In this report, we presented two patient cases: one with a non-MR-conditional CRT-D, and one with an MR-conditional ICD. The safety protocols were followed and no adverse events occurred. We found that using WB LGE increased the image quality independently of the type of device. Do et al. investigated the safety of CMR and the interpretability of images using WB LGE in 111 patients with a non-MR-conditional CIED, using a self-developed wideband pulse sequence. In 87% of the study population, the WB technique yielded artifact-free images; just 3% of cases had significant artifacts that limited or undermined interpretation of the study [17].

In the CMR studies presented here, free-breathing WB LGE was performed. Previous data suggest that free-breathing WB single-shot LGE and WB-segmented LGE produce similarly improved image quality compared to standard LGE. Schwartz et al. found that the percentage

of diagnostically interpretable myocardial segments was 72% for standard LGE, 89% for WB-segmented LGE, and 94% for free-breathing WB single-shot LGE [18]. According to our experiences, CIED patients may have difficulties with breath-holds because of underlying heart disease. The high-bandwidth inversion recovery application can diminish both the device-related artifacts and the breathing artifacts. However, acquisition times are longer in the free-breathing WB sequence than in a single-shot breath-controlled sequence.

Several studies have demonstrated the clinical benefit of using WB LGE in CIED patients. Bhuva et al. found that WB LGE resulted in changed clinical management in 75% of ICD patients and 19% of pacemaker patients when compared to imaging with standard LGE sequences, based on 136 CMR studies [10]. Singh et al. investigated the agreement between LGE images (standard and WB) and invasive EAM in 27 patients with ICD who underwent VT ablation. With standard LGE, the presence and location of LGE agreed with at least one focus of scar on EAM in 10 out of the 27 cases. In contrast, agreement with EAM was noted in 21 of the 27 cases when WB LGE was used [19]. In another study, conducting channels were identified using ADAS 3D software before VT ablation, based on WB LGE images in 13 ICD patients and on standard LGE images in 26 patients without CIED. The two groups were matched according to the type of cardiomyopathy, scar location, and age. The agreement between CMR and EAM was 85.1% and 92.2% in the WB group and the standard LGE group, respectively. The researchers found no differences in false-positive rates or false-negative rates between the two groups [20].

Conclusion

In this report, we presented our experience with the new high-bandwidth inversion recovery sequence in CIED patients. By reporting on the cases of two patients – one with non-ischemic and one with ischemic cardiac disease – we demonstrated that WB LGE sequences have a substantial impact on diagnosis and treatment in CIED patients.

Funding

Project no. NVKP_16-1–2016-0017 ('National Heart Program') has been implemented with the support provided from the National Research, Development and Innovation Fund of Hungary, financed under the NVKP_16 funding scheme. The research was financed by the Thematic Excellence Programme (2020-4.1.1.-TKP2020) of the Ministry for Innovation and Technology in Hungary, within the framework of the Therapeutic Development and Bioimaging thematic programmes of the Semmelweis University. LS was supported by the ÚNKP-20-3-II-SE-61 New National Excellence Program of the Ministry for Innovation and Technology from the source of the National Research, Development and Innovation Fund. ZD and LS were supported by the "Development of scientific workshops of medical, health sciences and pharmaceutical educations" project. Project identification number: EFOP-3.6.3-VEKOP-16-2017-00009.

References

- 1 Hundley WG, Bluemke DA, Finn JP, Flamm SD, Fogel MA, Friedrich MG, et al. ACCF/ACR/AHA/NASCI/SCMR 2010 expert consensus document on cardiovascular magnetic resonance: a report of the American College of Cardiology Foundation Task Force on Expert Consensus Documents. *J Am Coll Cardiol*. 2010;55(23):2614–62.
- 2 Bello D, Shah DJ, Farah GM, Di Luzio S, Parker M, Johnson MR, et al. Gadolinium cardiovascular magnetic resonance predicts reversible myocardial dysfunction and remodeling in patients with heart failure undergoing beta-blocker therapy. *Circulation*. 2003;108(16):1945–53.
- 3 Kim RJ, Wu E, Rafael A, Chen EL, Parker MA, Simonetti O, et al. The use of contrast-enhanced magnetic resonance imaging to identify reversible myocardial dysfunction. *N Engl J Med*. 2000 Nov;343(20):1445–53.
- 4 Klem I, Weinsaft JW, Bahnson TD, Hegland D, Kim HW, Hayes B, et al. Assessment of myocardial scarring improves risk stratification in patients evaluated for cardiac defibrillator implantation. *J Am Coll Cardiol*. 2012;60(5):408–20.
- 5 Andreu D, Penela D, Acosta J, Fernández-Armenta J, Perea RJ, Soto-Iglesias D, et al. Cardiac magnetic resonance-aided scar dechanneling: Influence on acute and long-term outcomes. *Heart Rhythm*. 2017;14(8):1121–1128.
- 6 Russo RJ, Costa HS, Silva PD, Anderson JL, Arshad A, Biederman RWW, et al. Assessing the Risks Associated with MRI in Patients with a Pacemaker or Defibrillator. *N Engl J Med*. 2017;376(8):755–764.
- 7 Nazarian S, Hansford R, Rahsepar AA, Welton V, McVeigh D, Gucuk Ipek E, et al. Safety of Magnetic Resonance Imaging in Patients with Cardiac Devices. *N Engl J Med*. 2017;377(26):2555–2564.
- 8 Sasaki T, Hansford R, Zviman MM, Kollandavelu A, Bluemke DA, Berger RD, et al. Quantitative assessment of artifacts on cardiac magnetic resonance imaging of patients with pacemakers and implantable cardioverter-defibrillators. *Circ Cardiovasc Imaging*. 2011;4(6):662–70.
- 9 Mesubi O, Ahmad G, Jeudy J, Jimenez A, Kuk R, Saliaris A, et al. Impact of ICD artifact burden on late gadolinium enhancement cardiac MR imaging in patients undergoing ventricular tachycardia ablation. *Pacing Clin Electrophysiol*. 2014;37(10):1274–83.
- 10 Bhava AN, Kellman P, Graham A, Ramlall M, Boubertakh R, Feuchter P, et al. Clinical impact of cardiovascular magnetic resonance with optimized myocardial scar detection in patients with cardiac implantable devices. *Int J Cardiol*. 2019;279:72–8.
- 11 Rashid S, Rapacchi S, Vaseghi M, Tung R, Shivkumar K, Finn JP, et al. Improved late gadolinium enhancement MR imaging for patients with implanted cardiac devices. *Radiology*. 2014;270(1):269–74.
- 12 Kellman P, Xue H, Hansen MS. Free-breathing Late Enhancement Imaging: Phase Sensitive Inversion Recovery (PSIR) with Respiratory Motion Corrected (MOCO) Averaging. *MAGNETOM Flash*. 2016;66(3):65–73.
- 13 Nazarian S, Roguin A, Zviman MM, Lardo AC, Dickfeld TL, Calkins H, et al. Clinical utility and safety of a protocol for noncardiac and cardiac magnetic resonance imaging of patients with permanent pacemakers and implantable-cardioverter defibrillators at 1.5 tesla. *Circulation*. 2006;114(12):1277–84.
- 14 Gupta SK, Ya'qoub L, Wimmer AP, Fisher S, Saeed IM. Safety and Clinical Impact of MRI in Patients with Non-MRI-conditional Cardiac Devices. *Radiol Cardiothorac Imaging*. 2020;2(5):e200086.
- 15 Acosta J, Fernández-Armenta J, Penela D, Andreu D, Borrás R, Vassanelli F, et al. Infarct transmural as a criterion for first-line endo-epicardial substrate-guided ventricular tachycardia ablation in ischemic cardiomyopathy. *Heart Rhythm*. 2016;13(1):85–95.
- 16 Andreu D, Ortiz-Pérez JT, Boussy T, Fernández-Armenta J, De Caralt TM, Perea RJ, et al. Usefulness of contrast-enhanced cardiac magnetic resonance in identifying the ventricular arrhythmia substrate and the approach needed for ablation. *Eur Heart J*. 2014;35(20):1316–26.
- 17 Do DH, Eyvazian V, Bayoneta AJ, Hu P, Finn JP, Bradfield JS, et al. Cardiac magnetic resonance imaging using wideband sequences in patients with nonconditional cardiac implanted electronic devices. *Heart Rhythm*. 2018;15(2):218–25.
- 18 Schwartz SM, Pathrose A, Serhal AM, Ragin AB, Charron J, Knight BP, et al. Evaluation of image quality of wideband single-shot late gadolinium-enhancement MRI in patients with a cardiac implantable electronic device. *J Cardiovasc Electrophysiol*. 2021;32(1):138–47.
- 19 Singh A, Kawaji K, Goyal N, Nazir NT, Beaser A, O'Keefe-Baker V, et al. Feasibility of Cardiac Magnetic Resonance Wideband Protocol in Patients With Implantable Cardioverter Defibrillators and Its Utility for Defining Scar. *Am J Cardiol*. 2019;123(8):1329–35.
- 20 Roca-Luque I, Van Breukelen A, Alarcon F, Garre P, Tolosana JM, Borrás R, et al. Ventricular scar channel entrances identified by new wideband cardiac magnetic resonance sequence to guide ventricular tachycardia ablation in patients with cardiac defibrillators. *Europace*. 2020;22(4):598–606.



Contact

Hajnalka Vágó, M.D.
 Semmelweis University
 Heart and Vascular Center
 Gaál József út 9
 Budapest 1122
 Hungary
 Phone: +36-20-825-8058
 vago.hajnalka@med.semmelweis-univ.hu

Fetal CMR Today and in the Future

Erik Hedström, M.D., Ph.D.; Anthony H. Aletras, Ph.D.

Lund Cardiac MR Group, Lund University and Skåne University Hospital, Lund, Sweden

Benefits of fetal CMR¹ today

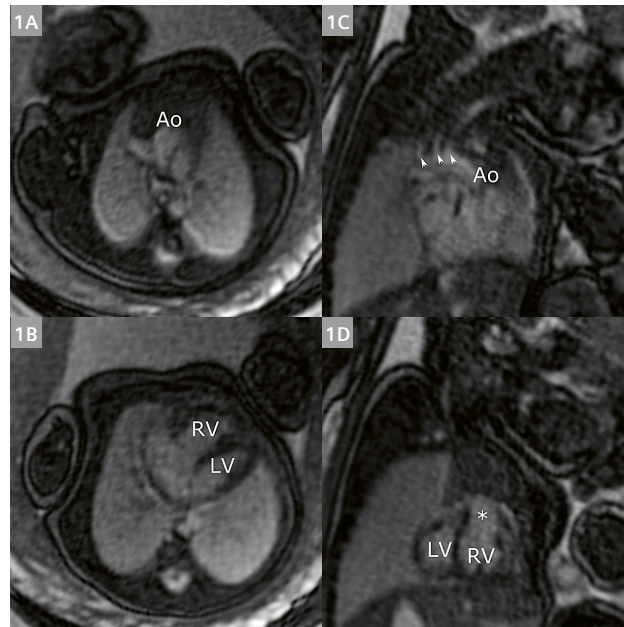
Approximately 1% of neonates are affected by congenital heart defects [1]. Even though prenatal diagnosis has improved, it needs to be further perfected in order to reduce morbidity and mortality [2]. Fetal echocardiography is widely available and plays the main role in enhanced prenatal diagnosis. Ultrasound image quality nowadays is exceptional compared to a decade ago. However, diagnosis based on ultrasound is still limited as it is highly operator-dependent and may be particularly challenging in late pregnancy or in maternal obesity [3, 4].

Fetal magnetic resonance imaging has been used for almost 40 years, mainly for diagnosing fetal thoracic, abdominal, and brain malformations. This is mostly achieved using static anatomical images. Dedicated fetal cardiovascular magnetic resonance (CMR) was performed at only a few centers worldwide 5–10 years ago. Nowadays, approximately 30 centers are running or setting up fetal CMR as part of their clinical service and research. Static balanced steady-state free precession (bSSFP) images (Fig. 1) are more than sufficient to depict anatomy. Early real-time acquisitions depicted fetal cardiac systolic function, but the spatial resolution was too low to clearly portray detailed fetal cardiac anatomy or regional function (Fig. 2A).

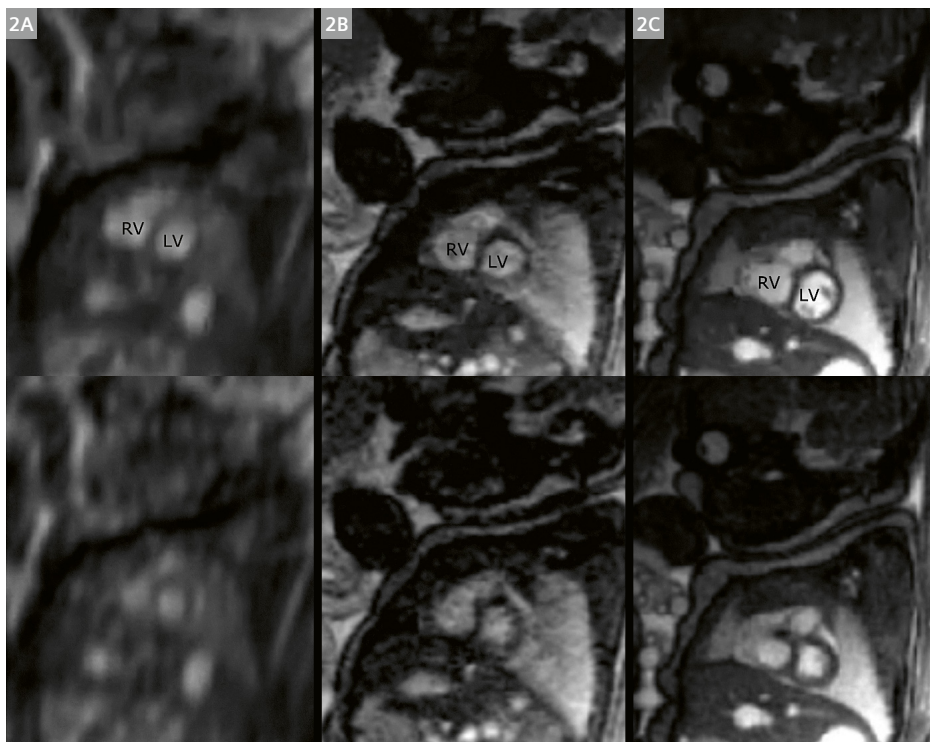
Dynamic fetal CMR took off with the introduction of the metric optimized gating (MOG) postprocessing method for phase-contrast CMR flow measurements [5], which was also applied for fetal cardiac cine imaging (Fig. 2B) [6]. This method introduced sufficient temporal and spatial resolution to study the fetal heart in detail using CMR, and overcame the lack of fetal cardiac gating.

Self-gated postprocessing methods, such as 2D iGRASP (Fig. 2C) [7–9], have since been introduced and used to assess fetal cardiac malformations, along with methods with shorter acquisition times and greater tolerance to fetal motion [10–12]. These methods rely on computationally demanding postprocessing, and currently images are not immediately visualized on the scanner, which

limits the information available directly after the fetal CMR examination. Image reconstruction time depends on local setup and engineering expertise. It is therefore crucial to have local pipelines or faster postprocessing methods in place so that images can be reconstructed soon after data acquisition is complete. On a positive note, imaging sequences and postprocessing methods are quite openly shared and there is a growing community that supports making fetal CMR available for routine patient scans.



1 Static balanced steady-state free precession images of a fetal heart at gestational week 33 with transposition of the great arteries (TGA). Transversal images (1A, B) show the left (LV) and right ventricles (RV) with the aorta (Ao) coming from the right ventricle. Sagittal images (1C, D) correspondingly show the left and right ventricles with the aortic outflow tract (*) from the right ventricle, aortic arch, and normal aortic arch vessels (white arrowheads).



2 A short-axis basal slice in diastole (**top row**) and systole (**bottom row**) showing images acquired using a real-time sequence (**2A**), metric optimized gating (MOG, **2B**) [6], and original 2D iGRASP (**2C**) [7]. Note the higher spatial resolution with MOG and iGRASP compared to the real-time images. A movie showing the three methods side-by-side was published as supplemental material to Haris et al. [7].

The next leap in improving dedicated fetal CMR was the introduction of an MR-compatible cardiac gating device that uses Doppler ultrasound for gating the MR data acquisition to the fetal heartbeat (smart-sync, northh medical GmbH, Hamburg, Germany) [13, 14]. This made it possible to use standard bSSFP cine sequences for fetal CMR. Standard sequence parameters need to be adjusted to the high fetal heart rate of approximately 140 bpm, for the small structures with a total heart diameter of approximately 4 cm (toward term) with myocardium just a few millimeters thick, for vessel diameters of approximately 5–10 mm, and for taking into account SAR and noise levels (Figs. 3, 4).

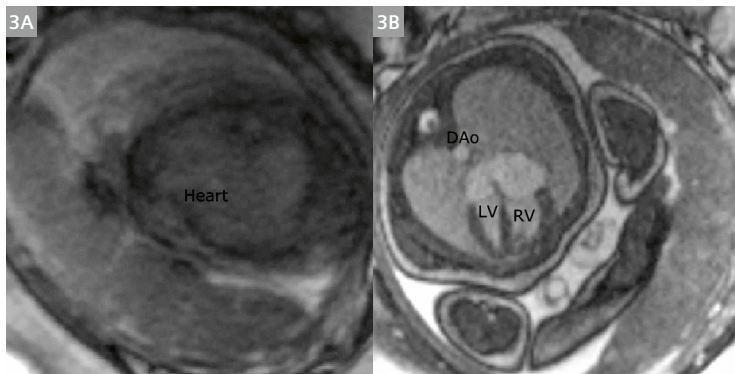
For assessing vascular anatomy, the aforementioned methods also work for producing static and cine white-blood images. An alternative is to use a 2D oversampling method for creating a 3D volume using black-blood images [15]. This is an image-based approach and could be implemented on various MR systems.

Beyond anatomy and cardiac function: Physiology by blood flow and oxygenation

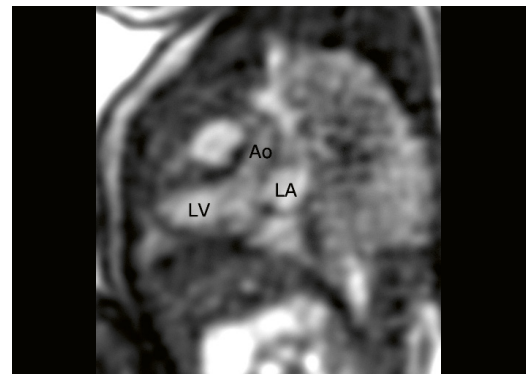
Although anatomy and cardiac function by fetal CMR improve diagnosis and impact clinical decision-making [16], fetal cardiovascular physiology can be assessed more extensively in the same session. This includes blood flow

and oxygenation measurements as well as 3D imaging for fetal weight for normalizing blood flow volumes and for calculating oxygen delivery and consumption [17, 18]. Whereas blood flow is central in pediatric and adult CMR, a clear clinical purpose for blood flow quantification in the individual fetus remains to be seen. However, several studies indicate potential uses, ranging from analysis of blood streaming in cardiac malformations to changes during maternal hyperoxygenation. More recent studies on fetal blood flow show higher accuracy and less variability than in the original studies [19, 20]. Standardization is needed for a wider clinical application, particularly with respect to phase-contrast background phase correction in the moving fetus.

Whereas non-invasive quantification of fetal blood oxygenation has been validated both in vitro [21] and in vivo [22], the concept is still challenging because results are dependent on the specific pulse sequence, and other centers have proposed methods that yield saturation measurements outside the fetal physiological range. One such implementation is available via a C2P exchange from The Hospital for Sick Children (SickKids), Toronto, Canada, and its availability may move the field forward toward standardization. However, in vivo validation is still needed in a multicenter setting and to show that data are of low variability and comparable between centers. Known errors between centers are related to using different T2 fitting



3 An example of a fetal CMR cine image corrupted by fetal motion and lack of gating (3A). No cardiac structures can be clearly seen. Corresponding image (3B) acquired using Doppler-ultrasound gated cine bSSFP optimized for fetal heart size and heart rate. Left (LV) and right (RV) ventricles, atria, mitral and tricuspid valves, and descending aorta (DAo) are clearly depicted. Cf. **Online Movie 1** available at <https://www.magnetomworld.siemens-healthineers.com/clinical-corner/case-studies/fetal-cmr-today-and-in-the-future>



4 An example in which ultrasound was challenging: no fully diagnostic images, but suspicion of ventricular asymmetry with narrow aorta. Fetal CMR in gestational week 35 shows normal systolic function, and in the 3-chamber view a normal-sized aortic annulus and ascending aorta (Ao). LV = left ventricle. LA = left atrium. Cf. **Online Movie 2** available at <https://www.magnetomworld.siemens-healthineers.com/clinical-corner/case-studies/fetal-cmr-today-and-in-the-future>

algorithms and different shimming methods. One also needs to consider that data are sensitive to blood flow, with fetal data commonly acquired over both systole and diastole [23, 24]. Acquisition of oxygenation data using the aforementioned MR-compatible ultrasound device for gating is not yet possible because the acquisition is too long for the short fetal RR interval. Sequence development is needed before taking this approach, which would otherwise be interesting for decreasing the impact of different flow profiles.

Conclusion

Fetal CMR is increasingly used and offers benefits for patients and clinical decision-makers. Although echocardiography is and should remain the first-line examination and screening tool, fetal CMR will likely strengthen its position as an important tool for further improving the prenatal diagnosis of cardiovascular malformations and reducing morbidity and mortality. For this to happen, standardization of both pulse sequences and analysis methods is crucial, in conjunction with simpler methods for acquisition, motion correction, and online image reconstruction.

¹Siemens Healthineers Disclaimer:

MR scanning has not been established as safe for imaging fetuses and infants less than two years of age. The responsible physician must evaluate the benefits of the MR examination compared to those of other imaging procedures. Note: This disclaimer does not represent the opinion of the authors.

References

- van der Linde D, Konings EEM, Slager MA, Witsenburg M, Helbing WA, Takkenberg JJM, et al. Birth prevalence of congenital heart disease worldwide: a systematic review and meta-analysis. *J Am Coll Cardiol*. 2011;58(21):2241–7.
- Bensemlali M, Stirnemann J, Le Bidois J, Lévy M, Raimondi F, Hery E, et al. Discordances Between Pre-Natal and Post-Natal Diagnoses of Congenital Heart Diseases and Impact on Care Strategies. *J Am Coll Cardiol*. 2016;68(9):921–30.
- Tegnander E, Eik-Nes SH. The examiner's ultrasound experience has a significant impact on the detection rate of congenital heart defects at the second-trimester fetal examination. *Ultrasound Obstet Gynecol*. 2006;28(1):8–14.
- Thornburg LL, Miles K, Ho M, Pressman EK. Fetal anatomic evaluation in the overweight and obese gravida. *Ultrasound Obstet Gynecol*. 2009;33(6):670–5.
- Jansz MS, Seed M, van Amerom JFP, Wong D, Grosse-Wortmann L, Yoo S-J, et al. Metric optimized gating for fetal cardiac MRI. *Magn Reson Med*. 2010;64(5):1304–14.
- Roy CW, Seed M, van Amerom JFP, Nafisi AI B, Grosse-Wortmann L, Yoo S-J, et al. Dynamic imaging of the fetal heart using metric optimized gating. *Magn Reson Med*. 2013;70(6):1598–607.
- Haris K, Hedström E, Bidhult S, Testud F, Maglaveras N, Heiberg E, et al. Self-gated fetal cardiac MRI with tiny golden angle iGRASP: A feasibility study. *J Magn Reson Imaging*. 2017;46(1):207–217.
- Bhat M, Haris K, Bidhult S, Liuba P, Aletras AH, Hedström E. Fetal iGRASP cine CMR assisting in prenatal diagnosis of complicated cardiac malformation with impact on delivery planning. *Clin Physiol Funct Imaging*. 2019;39(4):231–235.
- Haris K, Hedström E, Kording F, Bidhult S, Steding-Ehrenborg K, Ruprecht C, et al. Free-breathing fetal cardiac MRI with doppler ultrasound gating, compressed sensing, and motion compensation. *J Magn Reson Imaging*. 2020;51(1):260–272.
- Roy CW, Seed M, Macgowan CK. Accelerated MRI of the fetal heart using compressed sensing and metric optimized gating. *Magn Reson Med*. 2017;77(6):2125–2135.

11 van Amerom JFP, Lloyd DFA, Price AN, Kuklisova Murgasova M, Aljabar P, Malik SJ, et al. Fetal cardiac cine imaging using highly accelerated dynamic MRI with retrospective motion correction and outlier rejection. *Magn Reson Med*. 2018;79(1):327–338.

12 Berggren K, Ryd D, Heiberg E, Aletras AH, Hedström E. Super-Resolution Cine Image Enhancement for Fetal Cardiac Magnetic Resonance Imaging. *J Magn Reson Imaging*. 2021 Oct 15. Online ahead of print.

13 Kording F, Yamamura J, Much C, Adam G, Schoennagel B, Wedegärtner U, et al. Evaluation of an Mr Compatible Doppler-Ultrasound Device as a New Trigger Method in Cardiac MRI: A Quantitative Comparison to ECG. *Biomed Tech (Berl)*. Epub 2013 Sep 7.

14 Kording F, Yamamura J, de Sousa MT, Ruprecht C, Hedström E, Aletras AH, et al. Dynamic fetal cardiovascular magnetic resonance imaging using Doppler ultrasound gating. *J Cardiovasc Magn Reson*. 2018;20(1):17.

15 Lloyd DFA, Pushparajah K, Simpson JM, van Amerom JFP, van Poppel MPM, Schulz A, et al. Three-dimensional visualisation of the fetal heart using prenatal MRI with motion-corrected slice-volume registration: a prospective, single-centre cohort study. *Lancet*. 2019;393(10181):1619–1627.

16 Salehi D, Fricke K, Bhat M, Arheden H, Liuba P, Hedström E. Utility of Fetal Cardiovascular Magnetic Resonance for Prenatal Diagnosis of Complex Congenital Heart Defects. *JAMA Netw Open*. 2021;4(3):e213538.

17 Seed M, van Amerom JFP, Yoo S-J, Nafisi Al B, Grosse-Wortmann L, Jaeggi E, et al. Feasibility of quantification of the distribution of blood flow in the normal human fetal circulation using CMR: a cross-sectional study. *J Cardiovasc Magn Reson*. 2012;14(1):79.

18 Sun L, Macgowan CK, Sled JG, Yoo S-J, Manlhiot C, Porayette P, et al. Reduced fetal cerebral oxygen consumption is associated with smaller brain size in fetuses with congenital heart disease. *Circulation*. 2015;131(15):1313–23.

19 Salehi D, Sun L, Steding-Ehrenborg K, Bidhult S, Kording F, Ruprecht C, et al. Quantification of blood flow in the fetus with cardiovascular magnetic resonance imaging using Doppler ultrasound gating: validation against metric optimized gating. *J Cardiovasc Magn Reson*. 2019;21(1):74.

20 Goolaub DS, Xu J, Schrauben E, Sun L, Roy CW, Marini D, et al. Fetal Flow Quantification in Great Vessels Using Motion-Corrected Radial Phase Contrast MRI: Comparison With Cartesian. *J Magn Reson Imaging*. 2021;53(2):540–551.

21 Portnoy S, Seed M, Sled JG, Macgowan CK. Non-invasive evaluation of blood oxygen saturation and hematocrit from T1 and T2 relaxation times: In-vitro validation in fetal blood. *Magn Reson Med*. 2017;78(6):2352–2359.

22 Saini BS, Darby JRT, Portnoy S, Sun L, Amerom J, Lock MC, et al. Normal human and sheep fetal vessel oxygen saturations by T2 magnetic resonance imaging. *J Physiol*. 2020;598(15):3259–3281.

23 Johansson SL, Testud F, Hedström E, Aletras AH. T2 measurements in blood with T2-prepared SSFP: Effects of shimming and trigger delay at high flow velocity. *SCMR* 2021.

24 Johansson SL, Testud F, Hedström E, Aletras AH. T2 measurements in blood with T2-prepared SSFP: Effects of varying imaging parameters and flow. *SCMR* 2021.



Contact

Associate Professor Erik Hedström, M.D., Ph.D.
Lund Cardiac MR Group, Lund University
Centre for Medical Imaging and Physiology
Skåne University Hospital
Entrégatan 7
222 42 Lund
Sweden
Phone: +46 46 17 30 79
erik.hedstrom@med.lu.se

Further Reading

Small Structures Big Challenges: Fetal Cardiac Magnetic Resonance Imaging

Veronica Bianchi¹; Jérôme Yerly^{1,2}; Jerome Chaptinel¹; Yvan Mivelaz³; Milan Prsa³; Leonor Alamo¹; Chantal Rohner¹; Jean-Baptiste Ledoux^{1,2}; Davide Piccini^{1,5}; Chris Roy¹; Matthias Stuber^{1,2}

¹Department of Radiology, University Hospital (CHUV) and University of Lausanne (UNIL), Lausanne, Switzerland
²Center for Biomedical Imaging (CIBM), Lausanne, Switzerland
³Department of Pediatrics, University Hospital (CHUV) and University of Lausanne (UNIL), Lausanne, Switzerland
⁴Department of Gynecology-Obstetrics, University Hospital (CHUV) and University of Lausanne (UNIL), Lausanne, Switzerland
⁵Advanced Clinical Imaging Technology, Siemens Healthineers, Lausanne, Switzerland

Read the article at <https://www.magnetomworld.siemens-healthineers.com/clinical-corner/case-studies/fetal-cardiac-mri.html>

Advertisement

Small Structures Big Challenges: Fetal Cardiac Magnetic Resonance Imaging

Veronica Bianchi¹, Jérôme Yerly^{1,2}, Jerome Chaptinel¹, Yvan Mivelaz³, Milan Prsa³, Leonor Alamo¹, Chantal Rohner¹, Jean-Baptiste Ledoux^{1,2}, Davide Piccini^{1,5}, Chris Roy¹, Matthias Stuber^{1,2}

Introduction

Cardiac cine MRI (CMR) is the gold standard for fetal cardiac imaging. However, it is limited by low temporal resolution and motion artifacts. This study aims to evaluate a new MRI sequence for fetal cardiac imaging, which is more robust to motion and provides higher temporal resolution. The new sequence is based on a combination of a high-resolution cine MRI sequence and a motion correction algorithm. The results show that the new sequence provides better image quality and is more robust to motion compared to the standard cine MRI sequence.

Image acquisition and analysis

The new MRI sequence was evaluated in a cohort of 10 fetuses. The results show that the new sequence provides better image quality and is more robust to motion compared to the standard cine MRI sequence. The new sequence also provides higher temporal resolution, which is important for the detection of small structures.

Image reconstruction framework

The reconstruction framework for the new MRI sequence is based on a combination of a high-resolution cine MRI sequence and a motion correction algorithm. The results show that the new sequence provides better image quality and is more robust to motion compared to the standard cine MRI sequence.

Results and discussion

The new MRI sequence provides better image quality and is more robust to motion compared to the standard cine MRI sequence. The new sequence also provides higher temporal resolution, which is important for the detection of small structures. The results show that the new sequence is a promising alternative to the standard cine MRI sequence for fetal cardiac imaging.

Conclusion

The new MRI sequence provides better image quality and is more robust to motion compared to the standard cine MRI sequence. The new sequence also provides higher temporal resolution, which is important for the detection of small structures. The results show that the new sequence is a promising alternative to the standard cine MRI sequence for fetal cardiac imaging.

Complete Free-breathing, High-resolution Cardiac MR Studies and their Clinical Impact in Non-ischemic Cardiomyopathies

Guillem Pons-Lladó, M.D., Ph.D.

Cardiac Imaging Unit, Department of Diagnostic Imaging, Clínica Corachán, Barcelona, Spain

Abstract

Cardiovascular magnetic resonance imaging (CMR) has become an irreplaceable tool since it was introduced in clinical practice in the 1990s. Useful in every aspect of cardiac diseases, its role is particularly valuable in the study of non-ischemic cardiomyopathies (NICMs), due to the unique body of information it provides on these diseases. Referential data on morphology and function of the ventricles and, notably, on myocardial tissue characterization mean that the technique is now ordered in every patient with NICM.

The performance of studies, however, has traditionally required a large number of breath-hold maneuvers from the patient. These, combined with an uncomfortable position in the magnet, have resulted in the test being perceived as rather unpleasant, particularly among cardiac patients.

Recent advances in the field of sequence acceleration and the development of motion-correction algorithms, however, have turned into reality the option of a whole cardiac exam without the need for patients to hold their breath during acquisitions.

As illustrated in the present article, a complete study of patients with NICM can be performed during free

breathing, including cine sequences accelerated with Compressed Sensing reconstruction and adaptive triggering, and tissue characterization studies using late gadolinium enhancement and T1/T2 mapping sequences with motion correction. When available in an MR system, in this case a 3T MAGNETOM Vida scanner, this exam can be done within 30 minutes, and may provide the same valuable information as that obtained with conventionally equipped systems.

Introduction

Since the integration of cardiovascular magnetic resonance imaging (CMR) into the field of diagnostic imaging in the late 1990s [1], the technique has become a true subspecialty in itself [2]. Continuous technical developments have widened its scope and have led to its present consideration as a first-line diagnostic tool.

Some inconvenient aspects of the acquisition of exams, however, have been recognized: isolation of the patient within the magnet in an uncomfortable position, need for repeated breath-holding, and a relatively long



1 Window of the physiology signal during the planning of a study with short-axis cine images and a free-breathing RT sequence. For a mean heart rate of 69 bpm in this case, slab of 10 prospectively gated, contiguous slices will be executed in 18 seconds. As 25 phases of the heart cycle are extracted by INTP, the resulting temporal resolution is 35 seconds.

exam duration. Considering the relevant information provided by the technique, these drawbacks are considered a tolerable burden by operating personnel and well-informed patients alike. Despite this, when patients are asked about their acceptance of the examination, some say they would prefer to undergo a different kind of non-invasive diagnostic imaging exam. Moreover, in the case of patients with cardiac conditions, maintaining the supine position and holding their breath repeatedly can be particularly strenuous.

Manufacturers and investigators have therefore both made efforts to counteract these inconveniences by devising strategies for acquiring and processing sequences aimed at shortening the exam time and minimizing the number and duration of breath-hold periods required. As a general rule, however, speeding up the acquisition results in ill-defined images [3]. Therefore, advances in faster acquisition schemes can only be realized if the resolution of the reconstructed images is preserved [4].

The present state of the art in CMR has notably achieved this goal, and the purpose of this brief article is to illustrate how these improvements have been integrated into clinical routine for the benefit of patients undergoing CMR, in this case on a 3T MAGNETOM Vida system. We have chosen to focus on the diagnostic workup of patients with suspected non-ischemic cardiomyopathy (NICM), as they represent a subset of patients for whom a CMR study is most frequently prescribed.

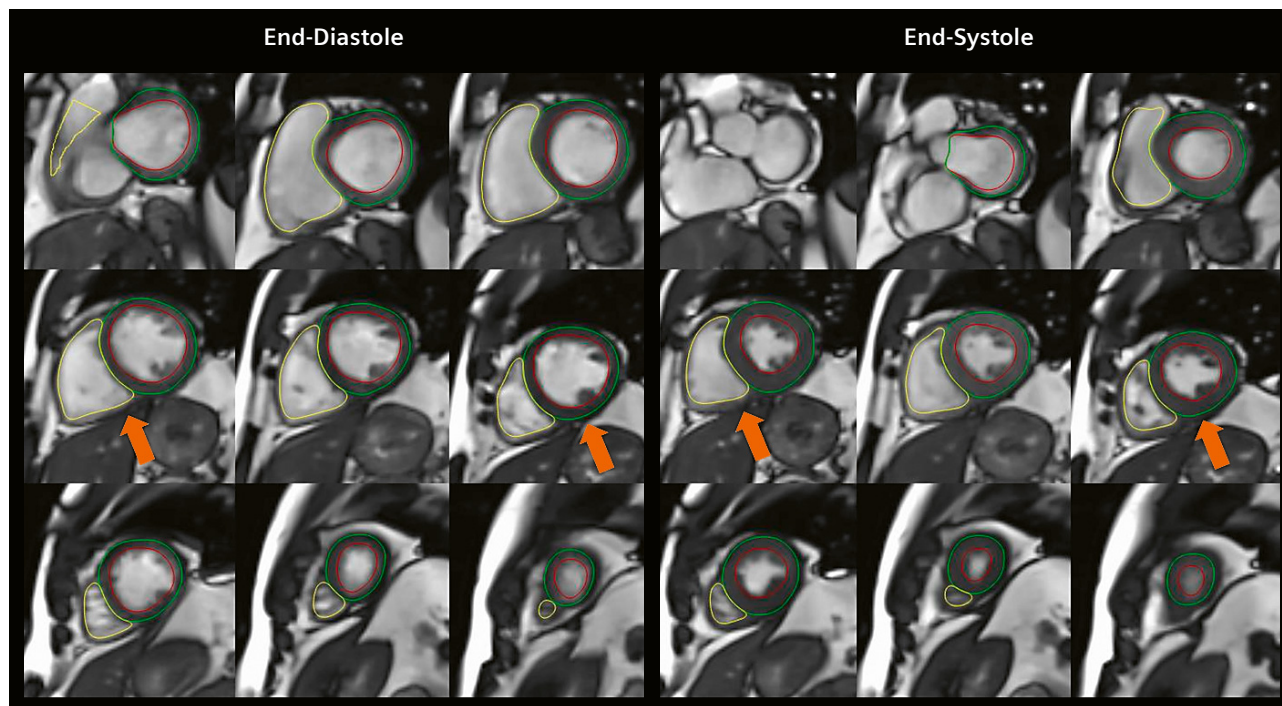
Planning of a conventional CMR study in patients with known or suspected NICM

CMR is considered as a Class I indication in patients who present with signs, symptoms, and/or findings from other diagnostic techniques consistent with NICM [5]. This is because CMR may provide, in every case, a body of information potentially useful for diagnosis, prognosis, and therapeutic decisions.

NICMs are a group of fairly distinct diseases that include hypertrophic, dilated, and restrictive cardiomyopathies – either primary or secondary. The CMR study protocols to be applied in each of these cases are detailed in official guidelines [6] and essentially aim to cover two aspects: data on the structure and function of the heart chambers and, importantly, information on myocardial tissue characteristics.

Most conventional MR systems equipped for cardiovascular applications are able to perform these studies nowadays. In addition to the pilot scans, the required sequences are as follows:

1. A complete series of cine sequences in both long and short axis views, usually obtained by a segmented, retrospectively ECG-gated, balanced steady-state free precession (bSSFP) technique.
2. Late gadolinium enhancement (LGE) sequences in the same orientations as those of the cine slices, obtained 10 minutes after the injection of a gadolinium-based contrast agent.



2 Free-breathing Compressed Sensing Cardiac Cine RT sequence obtained with adaptive ECG triggering and interpolative reconstruction to 25 phases of the cardiac cycle. Note the variable position of the diaphragm in the different slices (arrows) due to spontaneous breathing, and how the efficient tracking of the acquisition enables reliable border detection.

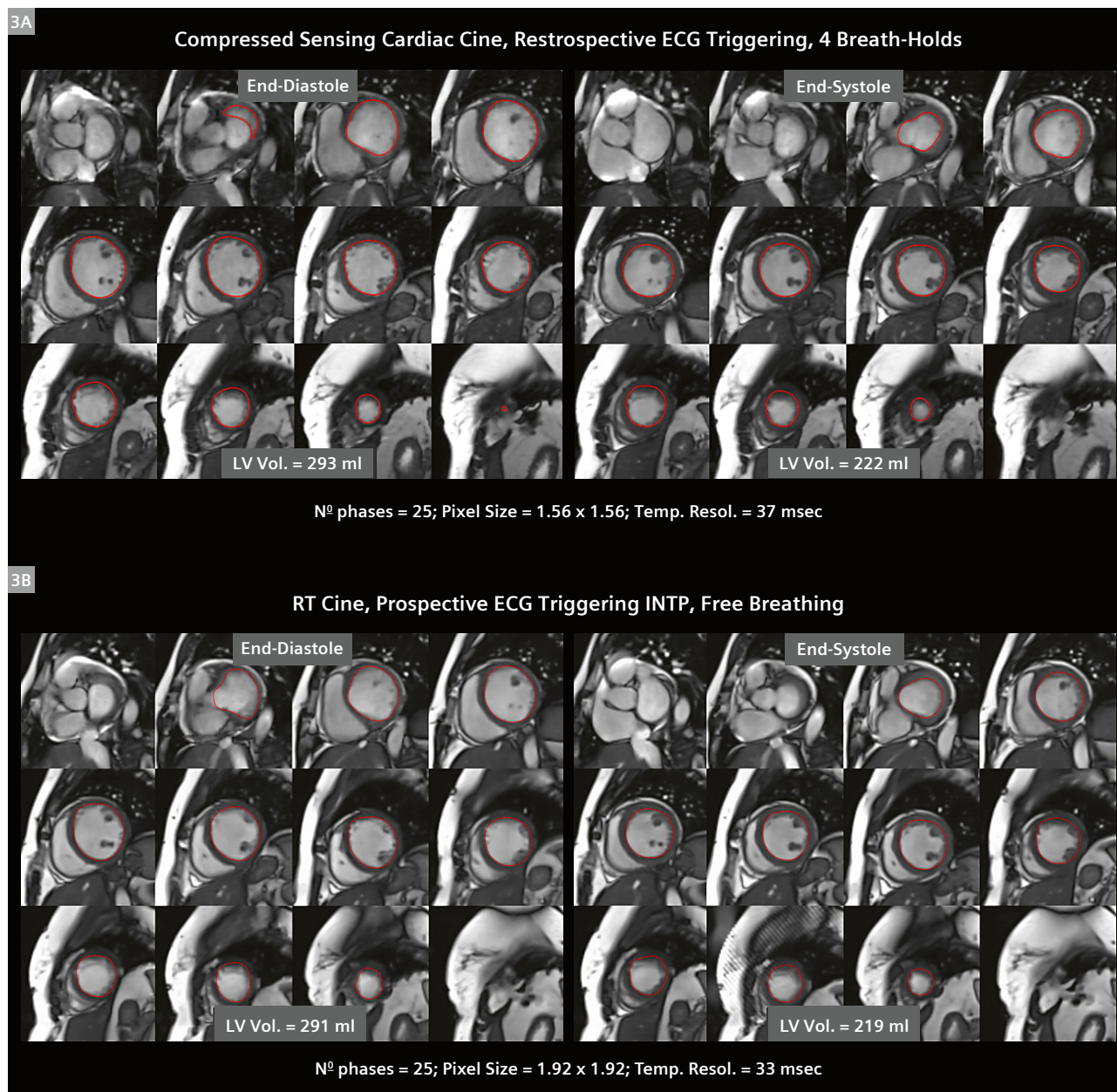
3. T1 and T2 mapping sequences. Each slice from these sequences must be acquired during breath-hold to achieve appropriate image quality, free of movement interference.

A standard study comprising all these sequences might require the performance of at least 30 breath-hold maneuvers, with a total exam time of nearly 45 minutes.

Advantages of a CMR exam performed with advanced technology to study NICM

The study of morphology and function

The acceleration of bSSFP cine sequences using parallel imaging techniques that allow for simultaneous (rather than sequential) gathering of data has contributed to a significant improvement in the acquisition of functional studies



3 (3A) End-diastolic and end-systolic frames, and calculated LV volumes using a Compressed Sensing Cardiac Cine sequence obtained with four breath-hold periods in a patient with dilated NICM. (3B) The corresponding study with a free-breathing RT INTP cine sequence. Both sequences render a cardiac cycle with 25 phases with a temporal resolution of 35 ms, the spatial resolution being slightly higher in the case of the CS sequence. Pixel sizes are 1.56 vs 1.92 mm² for the RT sequence. Note the excellent agreement between volume calculations and, therefore, between values of ejection fraction: 24.2 and 24.7%, respectively.

of the heart [7]. Really fast and efficient cine sequences, however, have become an option in CMR with the implementation of acceleration schemes based on Compressed Sensing (CS), which reconstructs good-quality sparse images from highly undersampled k -space data [8]. By applying CS, the slab of short-axis cine images with complete ventricular coverage can be obtained with 1–2 breath-holds [9], instead of the 10–12 required by conventional techniques.

Real-time (RT) free-breathing cine sequences using CS on our 3T MAGNETOM Vida system are prospectively gated and render 15–20 phases per slice (depending on the heart rate), with an in-plane pixel size of around 1.5 mm² and a temporal resolution between phases of nearly 60 milliseconds. In addition, the option of adaptive triggering (AT) enables real-time adaptation of the acquisition to changes in heart rate. This strategy detects and reacts to changes in the cardiac cycle, effectively acquiring data between triggers. Combined with retrospective temporal interpolation (INTP) during postprocessing [10], it enables calculation of a predefined number of cardiac phases in cine acquisitions (usually 25), which further increases temporal resolution to nearly 30 milliseconds. The acquisition of every slice takes just 1–2 seconds, meaning that the total scan of the short-axis slab (10–12 slices) requires only 20–25 continuous heart beats during free breathing (Figs. 1, 2).

Comparisons of free-breathing RT sequences with conventional breath-hold cine studies have shown adequate agreement regarding volume calculations and ejection fraction values [10, 11], which validates the technique as a true alternative in practice (Fig. 3).

Although useful as a routine in most patients with NICM, the RT cine sequences still have some inherent limitations. As a prospective acquisition, there can still be slight differences in the number of reconstructed phases per slice and, particularly, in the time points of end-diastolic and end-systolic frames [11]. AT and INTP techniques are efficient for reconstructing robust, homogeneous sets of cine slices, but may also lead to some spatial blurring of images [10], which can be prominent in the case of the right ventricle [12] due to its complex anatomy. Finally, the presence of arrhythmias – particularly atrial fibrillation, which is frequent in NICM patients – poses a further challenge to RT cine imaging. While prospective acquisition has advantages in this case, highly increased heart rates drastically reduce the number of reconstructed cardiac phases and, therefore, the reliability of volume calculations at end-diastole and end-systole.

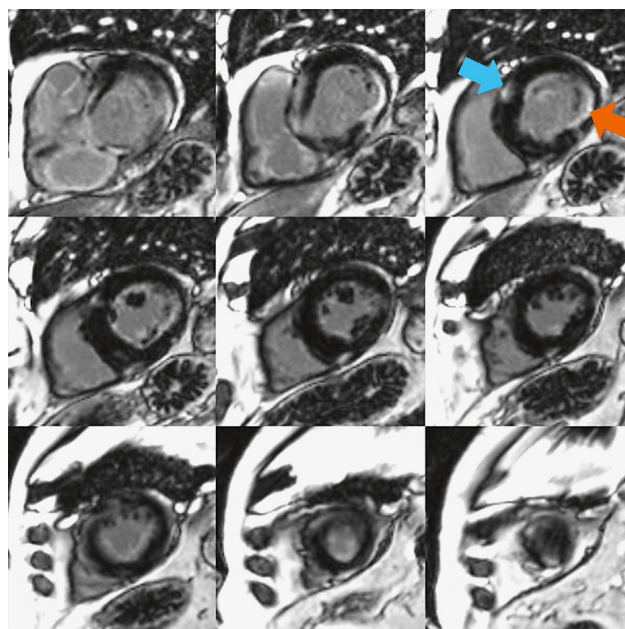
These drawbacks account for the need to have operator supervision for every study in order to guarantee the acquisition of adequately reconstructed images. In particular cases, this may lead to a move to breath-hold and/or

retrospective types of acquisition, either with CS or RT cine sequences [13].

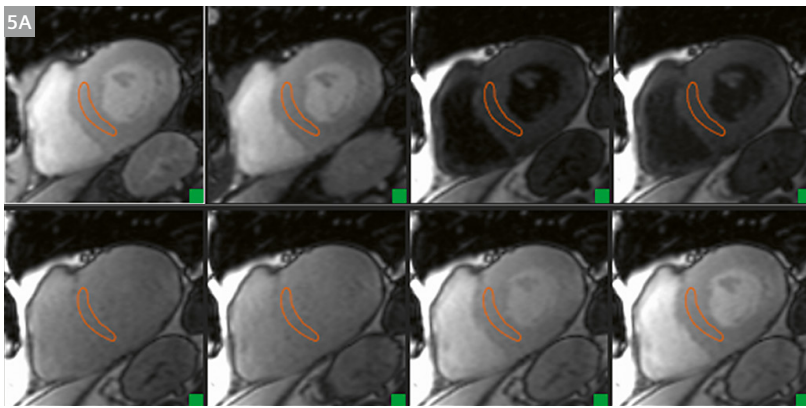
The study of tissue characterization

This part of the exam for patients with NICM is essential, as it provides information with proven prognostic value [14, 15]. Fortunately, it poses fewer challenges than cine studies for a free-breathing acquisition. LGE imaging, the cornerstone of myocardial tissue characterization, can be easily performed by sequences that retrospectively combine and average images at different respiratory phases using motion correction (MOCO) algorithms [16] (Fig. 4). A complete free-breathing LGE study on the short axis may be taken in 2–3 minutes, depending on the heart rate.

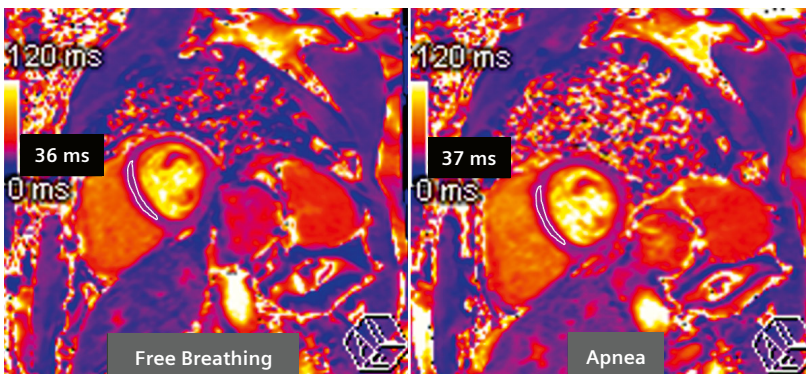
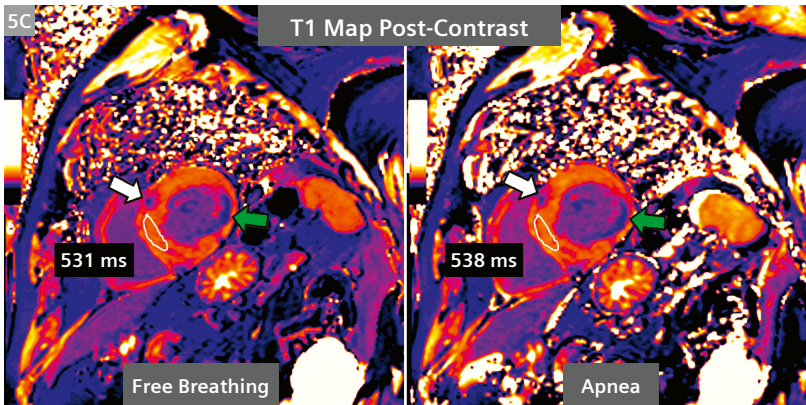
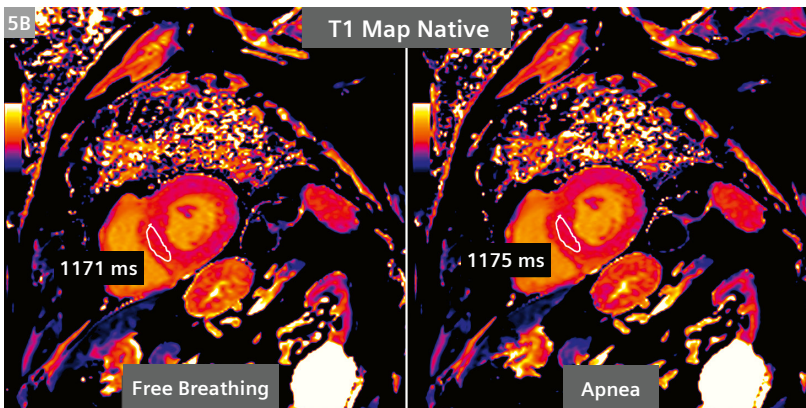
Myocardial T1 and T2 maps constitute an essential part of the study of tissue composition nowadays. These sequences are easy to perform as they require a single acquisition, which is recommended to be obtained during breath-hold, as MOCO algorithms in this case are less efficient at correcting through-plane motion [17]. In patients with difficult apnea maintenance, however, these sequences may be obtained in free breathing, asking the patient to keep a regular, calm respiratory pattern (Figs. 5, 6). Inspection of the resulting set of source images, however, is recommended in order to detect potential co-registration failure.



4 Single shot PSIR-SSFP free-breathing MOCO LGE in short-axis orientation in a patient with hypertrophic cardiomyopathy. Note the presence of focal, intramyocardial fibrosis (blue arrow) and, also, of subendocardial enhancement (orange arrow) indicating the coexistence of ischemic necrosis.



5 (5A) Set of raw source images from a T1 mapping sequence obtained during free breathing in the same patient as in Figure 4. Note the adequate co-registration of images. (5B) Resulting parametric image compared with a repeat measurement using breath-hold. Note the close agreement of native T1 values. (5C) The same studies after contrast: observe also the comparable resolution in the detection of areas of striking T1 reduction due to myocardial fibrosis (white arrow) and ischemic necrosis (green arrow).



6 Parametric images of T2 mapping sequences obtained during free-breathing and with breath-holding on the same patient showing comparable results.

Final comments

A complete CMR study of patients with NICM can currently be performed with sequences obtained during free breathing when using the most updated technology – in this case, a 3T MAGNETOM Vida system, as illustrated here. This makes the examination particularly comfortable for the patient and reduces the total exam time to 30 minutes (including the time lapse of waiting for the LGE study), which should impact positively on overloaded workflows. It is worth noting that the set of sequences discussed here, although robust, are more sensitive than conventional breath-hold sequences to interference caused by either an irregular pattern of respiration or arrhythmias, which might lead to suboptimal image reconstruction. This underlines the role of the operator, who should supervise the output of images after each acquisition to check for proper quality.

Acknowledgements

The author wishes to recognize the kind assistance provided by Marta Vidorreta, MR Clinical Scientist at Siemens Healthineers Spain, on technical aspects of the article.

References

- Budinger TF, Berson A, McVeigh ER, Pettigrew RI, Pohost GM, Watson JT, Wickline SA. Cardiac MR imaging: report of a working group sponsored by the National Heart, Lung, and Blood Institute. *Radiology*. 1998;208(3):573–6.
- Pohost GM. Certification of competence in cardiovascular magnetic resonance. *J Cardiovasc Magn Reson*. 1999;1(2):ix–x.
- Xu J, Kim D, Otazo R, Srichai MB, Lim RP, Axel L, Mccorty KA, Niendorf T, Sodickson DK. Towards a five-minute comprehensive cardiac MR examination using highly accelerated parallel imaging with a 32-element coil array: feasibility and initial comparative evaluation. *J Magn Reson Imaging*. 2013;38(1):180–8.
- Hansen MS, Kellman P. Image reconstruction: an overview for clinicians. *J Magn Reson Imaging*. 2015;41(3):573–85.
- Leiner T, Bogaert J, Friedrich MG, Mohiaddin R, Muthurangu V, Myerson S, Powell AJ, Raman SV, Pennell DJ. SCMR Position Paper (2020) on clinical indications for cardiovascular magnetic resonance. *J Cardiovasc Magn Reson*. 2020;22(1):76.
- Kramer CM, Barkhausen J, Bucciarelli-Ducci C, Flamm SD, Kim RJ, Nagel E. Standardized cardiovascular magnetic resonance imaging (CMR) protocols: 2020 update. *J Cardiovasc Magn Reson*. 2020;22(1):17.
- Mascarenhas NB, Muthupillai R, Cheong B, Pereyra M, Flamm SD. Fast 3D cine steady-state free precession imaging with sensitivity encoding for assessment of left ventricular function in a single breath-hold. *AJR Am J Roentgenol*. 2006;187(5):1235–9.
- Lustig M, Donoho D, Pauly JM. Sparse MRI: The application of compressed sensing for rapid MR imaging. *Magn Reson Med*. 2007 Dec;58(6):1182–95.
- Vincenti G, Monney P, Chaptinel J, Rutz T, Coppo S, Zenge MO, Schmidt M, Nadar MS, Piccini D, Chèvre P, Stuber M, Schwitler J. Compressed sensing single-breath-hold CMR for fast quantification of LV function, volumes, and mass. *JACC Cardiovasc Imaging*. 2014;7(9):882–92.
- Saybasili H, McNeal GR, Zuehlsdorff S, Schmidt M, Kellman P, Zenge MO. Temporal interpolation of real-time cine images for ventricular function assessment. *J Cardiovasc Magn Reson*. 2014;16(Suppl 1):O42.
- Haji-Valizadeh H, Rahsepar AA, Collins JD, Bassett E, Isakova T, Block T, Adluru G, DiBella EVR, Lee DC, Carr JC, Kim D; CKD Optimal Management with Binders and Nicotinamide (COMBINE) Study Group. Validation of highly accelerated real-time cardiac cine MRI with radial *k*-space sampling and compressed sensing in patients at 1.5T and 3T. *Magn Reson Med*. 2018;79(5):2745–2751.
- Rahsepar AA, Saybasili H, Ghasemiesfe A, Dolan RS, Shehata ML, Botelho MP, Markl M, Spottiswoode B, Collins JD, Carr JC. Motion-Corrected Real-Time Cine Magnetic Resonance Imaging of the Heart: Initial Clinical Experience. *Invest Radiol*. 2018;53(1):35–44.
- Xue H, Kellman P, Larocca G, Arai AE, Hansen MS. High spatial and temporal resolution retrospective cine cardiovascular magnetic resonance from shortened free breathing real-time acquisitions. *J Cardiovasc Magn Reson*. 2013;15(1):102.
- Halliday BP, Baksi AJ, Gulati A, Ali A, Newsome S, Izgi C, Arzanauskaite M, Lota A, Tayal U, Vassiliou VS, Gregson J, Alpendurada F, Frenneaux MP, Cook SA, Cleland JGF, Pennell DJ, Prasad SK. Outcome in Dilated Cardiomyopathy Related to the Extent, Location, and Pattern of Late Gadolinium Enhancement. *JACC Cardiovasc Imaging*. 2019;12(8 Pt 2):1645–1655.
- Puntmann VO, Carr-White G, Jabbour A, Yu CY, Gebker R, Kelle S, Hinojar R, Doltra A, Varma N, Child N, Rogers T, Suna G, Arroyo Ucar E, Goodman B, Khan S, Dabir D, Herrmann E, Zeiher AM, Nagel E; International T1 Multicentre CMR Outcome Study. T1-Mapping and Outcome in Nonischemic Cardiomyopathy: All-Cause Mortality and Heart Failure. *JACC Cardiovasc Imaging*. 2016;9(1):40–50.
- Kellman P, Arai AE. Cardiac imaging techniques for physicians: late enhancement. *J Magn Reson Imaging*. 2012;36(3):529–42.
- Messroghli DR, Moon JC, Ferreira VM, Grosse-Wortmann L, He T, Kellman P, Mascherbauer J, Nezafat R, Salerno M, Schelbert EB, Taylor AJ, Thompson R, Ugander M, van Heeswijk RB, Friedrich MG. Clinical recommendations for cardiovascular magnetic resonance mapping of T1, T2, T2* and extracellular volume: A consensus statement by the Society for Cardiovascular Magnetic Resonance (SCMR) endorsed by the European Association for Cardiovascular Imaging (EACVI). *J Cardiovasc Magn Reson*. 2017;19(1):75.



Contact

Guillem Pons-Lladó, MD, PhD
Cardiac Imaging Unit
Department of Diagnostic Imaging
Clínica Corachán
Buigas 19
08017 Barcelona
Spain
Phone: +34 607 26 38 48
gponsllado@gmail.com

CMR T2-Mapping Increase as Imaging Biomarker of Myocardial Involvement in Active COVID-19

Nicola Galea, M.D., Ph.D.^{1,2}; Livia Marchitelli, M.D.²; Giacomo Pambianchi, M.D.²; Federica Catapano, M.D.²; Giulia Cundari, M.D.²; Lucia Ilaria Birtolo, M.D.³; Viviana Maestrini, M.D., Ph.D.³; Massimo Mancone, M.D.³; Francesco Fedele, M.D.³; Carlo Catalano, M.D.²; Marco Francone, M.D., Ph.D.^{4,5}

¹Department of Experimental Medicine, "Sapienza" University of Rome, Italy

²Department of Radiological, Oncological, and Pathological Sciences, "Sapienza" University of Rome, Italy

³Department of Cardiovascular and Respiratory Diseases, "Sapienza" University of Rome, Italy

⁴Department of Biomedical Sciences, Humanitas University, Pieve Emanuele, Milan, Italy

⁵IRCCS Humanitas Research Hospital, Rozzano, Milan, Italy

Abstract

Background

Early detection of myocardial involvement in COVID-19 patients can be relevant for targeting symptomatic treatment in a timely manner and decreasing the occurrence of the cardiac sequelae of the infection.

The aim of the present study was to assess the clinical value of Cardiovascular Magnetic Resonance (CMR) in characterizing myocardial damage in active COVID-19 patients, using the correlation of qualitative and quantitative imaging biomarkers with clinical and laboratory evidence of myocardial injury.

Methods

In this retrospective observational cohort study, we enrolled 22 patients who had been diagnosed with active COVID-19 and suspected cardiac involvement, and referred to our institution for CMR between March and October 2020.

Clinical and laboratory characteristics, including high-sensitivity troponin T (hs-cT), and CMR imaging data were obtained. Relationships between CMR parameters and clinical and laboratory findings were explored.

Results

The median (IQR) time interval between COVID-19 diagnosis and CMR examination was 20.5 (11–52) days. Hs-cT values were collected within 24 hours prior to CMR and were abnormally increased in 14 patients (64%). A total of 16 cases (73%) presented tissue signal abnormalities, including increased myocardial native T1 (n = 9), myocardial T2 (n = 11), ECV (n = 8), LGE (n = 10), and pericardial enhancement (n = 2). A CMR diagnosis of myocarditis was established in 7 (31.81%), pericarditis in 2 (9%) and myocardial infarction with non-obstructive coronary arteries in 2 (9%) patients. T2 mapping values showed a moderate positive linear correlation with high-sensitivity troponin T ($r = 0.6$; $p = 0.03$). A highly positive linear correlation between ECV and high-sensitivity troponin T was also found ($r = 0.879$; $p = 0.0001$).

Conclusions

CMR allowed in vivo recognition and characterization of myocardial damage in a cohort of selected individuals with COVID-19 using a multiparametric scanning protocol including conventional imaging and T1–T2 mapping sequences. Abnormal T2 mapping was the most common abnormality observed in our cohort and it correlated positively with hs-cT values, reflecting the predominant edematous changes characterizing the active phase of the disease.

Introduction

Myocardial injury is not uncommon in coronavirus disease (COVID-19) and has a complex multifactorial pathogenesis, including direct viral toxicity, uncontrolled immune activation (known as the “cytokine storm”), stress cardiomyopathy, mismatch ischemia, and prothrombotic activation with plaque formation and microvascular disease [1]. By definition, the term refers to any patient presenting with at least one cardiac troponin (cT) concentration above the 99th percentile upper reference limit [2]. Reported rates of increased cT levels range from 7% to 36% of COVID-19 inpatients and are associated with a higher prevalence of cardiovascular (CV) diseases [1, 3, 4].

This heterogeneity is probably due to the different thresholds applied in cT assays, and to the clinical severity of the cases included, which has proven to be significantly related to the extent of myocardial damage. A recent meta-analysis summarized that the acute myocardial injury rate was 13-fold higher in intensive care unit (ICU) patients than in those with mild forms of infection [5]. Nevertheless, limited evidence exists on the assessment of myocardial damage in patients with mild disease.

Although it remains debated whether cT elevation necessarily reflects direct cardiac infection, there is a clear independent association between myocardial injury and mortality rate. Fatal outcomes were reported in 37.5% of patients with elevated levels of cT, and they increased to 69.4% in the presence of pre-existing cardiovascular comorbidities [6]. This data was confirmed by two independent studies reporting sudden cardiac arrest as a fatal outcome in both in-hospital [7] and out-of-hospital [8] settings/frameworks.

Despite the evidence, the American College of Cardiology does not recommend routinely testing cT levels in COVID-19 patients unless the diagnosis of acute myocardial infarction (MI) is suspected on clinical grounds [9].

This potentially excludes from screening most paucisymptomatic or asymptomatic patients in whom myocardial injury has prognostic significance. In this scenario, early detection of myocardial involvement can be relevant for targeting symptomatic treatment in a timely manner and decreasing the occurrence of the devastating cardiac sequelae of the infection.

Our endpoint is to assess the clinical value of a non-invasive and highly sensitive tool – cardiovascular magnetic resonance (CMR) – in characterizing myocardial damage in COVID-19 patients, using the correlation of qualitative and quantitative CMR features with clinical and laboratory evidence of myocardial injury. Our quantitative analysis relies on parametric mapping, which is an innovative and reproducible method of providing unique quantitative data about changes in T1 and T2 relaxation times in the myocardium.

As a further advantage, CMR can be integrated into comprehensive assessments of the heart, pulmonary vessels, and lung parenchyma as part of a one-stop-shop approach. This makes CMR potentially suitable for ruling out thromboembolic complications and following up on pulmonary disease progression in COVID-19 patients using a radiation-free imaging procedure [10].

Methods

Study population

This was a single-center observational retrospective study of a cohort of 22 patients with a confirmed diagnosis of active COVID-19 by reverse transcription-polymerase chain reaction (RT-PCR) on nasopharyngeal swabs.

Patients were considered eligible for CMR if they fulfilled at least one of the following inclusion criteria:

- At least one high-sensitivity troponin T (hs-cT) measurement above the 99th percentile (> 0.014 ng/mL) in the absence of ST elevation or other signs of myocardial infarction
- Newly observed reduced ($< 50\%$) left ventricle (LV) ejection fraction (EF) detected by rapid bedside echocardiography
- No obstructive coronary artery disease (CAD) on coronary angiography, despite infarct-like clinical presentation

Exclusion criteria were general contraindications to magnetic resonance imaging (MRI), unstable clinical conditions, or inability to perform repeated breath-holds.

In all patients, the following routine blood tests and arterial blood gas tests were collected in the 48 hours before the CMR examination: C-reactive protein (CRP), D-dimer, white blood cell (WBC) count, lymphocyte count, and arterial oxygen partial pressure/fraction of inspired oxygen ($\text{PaO}_2/\text{FiO}_2$) ratio.

In addition, all patient blood samples collected 24 hours prior to CMR were processed using standardized, commercially available test kits for analysis of hs-cT, and values above the 99th percentile (0.014 ng/mL) were considered abnormal. Data on respiratory rate and O_2 saturation were also reported.

Disease severity score was evaluated for all individuals using the Chinese Center for Disease Control and Prevention (China CDC) criteria [11]. Mild, severe, and critical categories were assigned accordingly. Depending on the time of symptom onset, patients were also classified as having early-stage (0–7 days) or late-stage (> 7 days) disease [12]. Furthermore, the time interval between diagnosis with severe acute respiratory syndrome coronavirus 2 (SARS-CoV-2) infection and the CMR exam date was calculated.

Based on computed tomography (CT) scoring by Pan et al. [13], a semi-quantitative evaluation of pulmonary involvement was performed and a global CT score (0–25) was obtained by adding a single score (0–5) for each pulmonary lobe [14].

Access to MRI scanner and sanitization procedures

All CMR examinations were performed between March and October 2020 on a fully dedicated COVID-19 1.5T scanner (MAGNETOM Avanto, Siemens Healthcare, Erlangen, Germany) equipped with SQ-engine gradients (amplitude: 45 mT/m; slew rate: 200 mT/m/ms) and a 16-channel phased-array cardiac coil. According to international recommendations [15], staffing was strictly limited to three individuals: one technologist and one radiologist in the control room, and one nurse in the scanning room.

A full set of personal protective equipment (PPE), including FFP2 mask, gloves, gown, goggles, and/or face shield was provided to all exposed healthcare professionals, who were trained on the correct use of PPE. Sanitization of the MRI facility was performed at the end of the dedicated CMR session. In cases of known or suspected bacterial superinfection, the facility was cleaned in between scanning two patients with SARS-CoV-2.

CMR scanning protocol

All patients enrolled gave written informed consent to participate in the study.

A dose of 0.25 mmol/kg of contrast media (CM) (gadoteric acid, Claricyclic, GE Healthcare, USA) was injected intravenously at a flow rate of 2.5 mL/sec.

The CMR protocol included the following:

- Black blood T2-weighted short tau inversion recovery (STIR) images acquired on multiple cardiac axes, including a stack of short-axis views covering the entire left ventricle
- Modified Look-Locker inversion recovery (MOLLI) images acquired before and 15 minutes after CM injection on three matched short-axis slices at basal, mid, and apical views, and one four-chamber view
- T2-prepared TrueFISP (T2 map) images acquired on three matched short-axis slices at basal, mid, and apical planes, and one four-chamber view
- Balanced steady state free precession cine MRI (SSFP cine MRI) images acquired in short-axis (a stack of contiguous planes from the base to the apex), 2-chamber, 4-chamber and 3-chamber planes
- Contrast-enhanced inversion recovery T1-weighted (IR-CE T1w) images acquired on a stack of short-axis views covering the entire left ventricle, long-axis and four-chamber views, between 15 and 20 minutes after CM injection, during breath-hold at end-diastole

In selected patients, when clinically indicated, we embedded chest sequences in the CMR protocol in order to perform a comprehensive cardiothoracic MRI evaluation, as described elsewhere [10].

Image analysis

CMR images were analyzed in consensus by two experienced cardiovascular radiologists with three and ten years of experience respectively, using a commercially available post-processing workstation (cmr42© v.5.3.0, Circle Cardiovascular Imaging Inc., Calgary, Canada). LV volumes and mass were calculated from the short-axis SSFP cines.

Extracellular volume fraction (ECV) maps were generated by combining MOLLI images acquired before and 15 minutes after CM administration as demonstrated elsewhere [16].

Myocardial native T1 (nT1), T2, and ECV values were assessed by manually tracing subepicardial and subendocardial contours carefully (excluding the epicardial fat and ventricular cavity) on respective maps for each slice. The highest nT1, T2, and ECV values among all slices were considered for each patient.

Late gadolinium enhancement (LGE) was identified with a signal intensity (SI) > 5 standard deviation (SD) compared to the remote myocardium [17]. Depending on the LGE distribution pattern, myocardial fibrosis/necrosis was classified as “ischemic” (subendocardial or transmural extension) or “non-ischemic” (subepicardial or mid-myocardial) [18]. Myocardial edema was identified on STIR images as areas with an SI increase of 2 SD above the remote myocardium, or with a myocardium-to-skeletal muscle T2 ratio ≥ 1.9 [19].

Abnormal native T1, T2, and ECV parameters were defined as having a value beyond a predefined threshold (T1 > 1027 ms, T2 > 49.9 ms, and ECV > 29.5%), which corresponds to the 95th percentile values of a large age- and gender-matched healthy control group that was retrospectively recruited from our database, had already been examined in our center, and had been previously selected to assess the center-specific normal range.

According to new Lake Louise criteria [20], myocarditis diagnosis was established when at least one T2-based and one T1-based-criteria were present.

Statistical analysis

Data are presented as counts and percentages for categorical data, and as means or medians for continuous data. Normal distribution of all variables was tested using the Kolmogorov-Smirnov and the Shapiro-Wilk tests.

The Pearson correlation coefficient was used to analyze the linear correlation between continuous variables. The T-test for independent samples was applied to continuous and categorical variables.

All the quantitative parameters (hs-cT, T1, T2, ECV, etc.) were studied as categorical variables by dichotomizing them into “altered” and “normal” in order to investigate the relationship between abnormal clinical and imaging features.

The chi-squared (χ^2) test was performed to assess the dependency between two categorical variables. To evaluate the correspondence between hs-cT and T2 values, a stepwise linear regression model was carried out. A receiver operator characteristic (ROC) curve was used to determine the diagnostic accuracy of hs-cT in predicting myocardial involvement assessed by T2 mapping. Youden’s test was applied to identify the optimal hs-cT cut-off value. All the tests were 2-tailed, and only p-values < 0.05 were considered statistically significant. Analysis was performed using SPSS software version 26.0 (IBM Corp., Armonk, NY, USA).

Results

Study population

From March to October 2020, a total of 22 patients were included; the most significant clinical and laboratory parameters are displayed in Table 1.

The mean age was 56 ± 12 (range 28–75) years, and 18/22 patients (81.8%) were male. The most common symptoms were fever (20/22; 90.8%), cough (11/22; 50%), and dyspnea (5/22; 22.7%).

Increased hs-cT levels (> 0.014 ng/mL) were reported in 14/22 patients (63.6%) with a median (interquartile range) of 0.027 (0.01–0.09) ng/mL.

Given the time of symptom onset [12], all patients were classified as having late-phase disease (> 7 days); in addition, the median time between diagnosis of SARS-CoV-2 infection and CMR was 20.5 (11–52) days.

Increased D-dimer levels (> 500 ng/mL) were found in 18/22 patients (81.8%) with a median value of 818 (600–1916) ng/mL. Increased CRP levels (> 0.5 mg/dL) were found in 16/22 patients (72.7%) with a median value of 1.3 (0.45–3.89) mg/dL. WBC count was elevated (> $11.3 \times 10^9/L$) in 7/22 patients (31.8%).

Decreased lymphocyte count (< $1 \times 10^9/L$) was observed in 7/22 patients (31.8%), decreased O₂ saturation ($\leq 95\%$) in 5/22 patients (23%), and decreased PaO₂/FiO₂ ratio (< 300) in 3/22 patients (13.6%).

Based on the China CDC clinical scoring for COVID-19 [11], 1/22 patients (4.5%) was classified as having severe disease, and 21/22 patients (95.5%) were classified as having mild disease.

Signs of interstitial pneumonia were detected on chest CT in most patients (20/22; 95.5%), corresponding to a mean global CT score of 8.91 ± 5.03 (range 0–14).

Underlying CV comorbidities were present in 10/22 patients (45.5%), including hypertension (8/22; 36.4%)

and type II diabetes (2/22; 9.1%). No patients had known previous cardiac diseases or history of obstructive CAD.

CMR data

No procedural complications were observed in any of the 22 participants, even though four patients interrupted the exam before post-contrast MOLLI acquisition.

The CMR features are displayed in Table 2. LV dilation (abnormal increase of end-diastolic volume) was found in 5/22 patients (22.7%), while 10/22 patients (45.5%) showed impaired LV systolic function (LV-EF < 50%).

Clinical and laboratory parameters	Values
Age, mean (SD)	56 (12)
Gender male, No. (%)	18 (81.8)
CV comorbidities, No. (%)	
Hypertension	8 (36.4)
CAD	0
Diabetes	2 (9.1)
Smoking	0
Dyslipidemia	0
Laboratory findings, median (IQR)	
hs-cT, ng/mL	0.027 (0.01–0.09)
CRP, mg/dL	1.3 (0.45–3.89)
D-dimer, ng/dL	818 (600–1916)
WBC	5.11 (4.67–6.31)
Lymphocytes $\times 10^9/L$	1.12 (0.94–1.97)
Clinical findings, mean (SD)	
Respiratory rate, breaths/min	19.8 (2.2)
O ₂ sat %	96.8 (1.5)
PaO ₂ /FiO ₂ ratio	377.5 (68)
Chest CT score	8.9 (5)
Time from COVID-19 diagnosis to CMR, median (IQR)	20.5 (11–52)

Table 1: Patient characteristics and laboratory data

Abbreviations: CAD, coronary artery disease; CMR, cardiovascular magnetic resonance; COVID-19, coronavirus disease 2019; CRP, c-reactive protein; CT, computed tomography; CV, cardiovascular; hs-cT, high-sensitivity troponin T; IQR, interquartile range; O₂ sat, oxygen saturation; PaO₂/FiO₂, arterial oxygen partial pressure/fraction of inspired oxygen; SD, standard deviation; WBC, white blood cells

A total of 16/22 patients showed tissue signal abnormalities, including at least one of the following: increased myocardial nT1 (9/22), T2 (11/22) and ECV (8/22), areas of LGE (10/22) or edema on STIR images (7/22), pericardial enhancement (2/22).

Eight patients had a non-ischemic-type pattern of myocardial LGE, while only two showed transmural LGE.

CMR feature	Value
LVEDV/BSA, mean (SD), mL/m ²	72.4 (16.9)
LVESV/BSA, mean (SD), mL/m ²	35.5 (10.7)
LVSV/BSA, mean (SD), mL/m ²	36.1 (7.37)
LVEF, mean (SD), %	51.2 (6)
LVEF < 50%, No. (%)	11 (50)
MASS/BSA, mean (SD), g/m ²	62.8 (11)
RVEDV/BSA, mean (SD), mL/m ²	76.98 (13.4)
RVESV/BSA, mean (SD), mL/m ²	40.62 (11)
RVSV/BSA, mean (SD), mL/m ²	36.36 (7.3)
RVEF, mean (SD), %	48 (7.5)
nT1, mean (SD), ms	1038.3 (57.2)
nT1 > 1027 ms, No. (%)	9 (40.9)
T2, mean (SD), ms	52.5 (4.8)
T2 > 49.9 ms, No. (%)	11 (50)
ECV, mean (SD), %	29.2 (4.9)
ECV > 29.5%, No. (%)	8 (44.4)
Edema on STIR, No. (%)	7 (31.8)
LGE, No. (%)	10 (45.5)
Ischemic pattern, No. (%)	2 (20)
Nonischemic pattern, No. (%)	8 (80)
Pericardial, No. (%)	2 (20)

Table 2: Cardiovascular magnetic resonance (CMR) findings in COVID-19 patients

Abbreviations: BSA, body surface area; ECV, extracellular volume; LGE, late gadolinium enhancement; LV, left ventricle; LVEDV, left ventricular end-diastolic volume; LVEF, left ventricular ejection fraction; LVESV, left ventricular end-systolic volume; LVSV, left ventricular stroke volume; nT1, native T1; RV, right ventricle; RVEDV, right ventricular end-diastolic volume; RVEF, right ventricular ejection fraction; RVESV, right ventricular end-systolic volume; RVSV, right ventricular stroke volume; STIR, short tau inversion recovery; SD, standard deviation

Isolated elevation of one myocardial parametric value was found in 6/22 patients (3/22 with increased nT1 and 3/22 with increased T2 mapping).

Final diagnosis of myocarditis was established in 7/22 patients (31.81%), pericarditis in 2/22 patients (9%), and myocardial infarction with non-obstructive coronary arteries (MINOCA) in 2/22 patients (9%) (Figure 1).

Moreover, impaired biventricular contractile performance without myocardial signal alteration was found in 2/22 patients.

Correlations between clinical and CMR features

A significant dependence between T2 and the hs-cT values was found using the X² test ($p = 0.035$) when these variables were considered as categorical. The correlation analysis using the Pearson correlation index showed a moderate positive linear relationship between the T2 and the hs-cT values ($r = 0.583$; $p = 0.004$).

The linear regression analysis was conducted to examine the relationship between the T2 and hs-cT values. In particular, the best-fitting model was obtained in five steps using hs-cT, WBC count, lymphocyte count, CRP value, with an r^2 of 0.714 and an r of 0.845.

No significant correlation was found between the nT1 and the hs-cT values in our population, either as a categorical or quantitative variable ($p = 0.176$ – 0.104).

We also documented that all the patients with an increased ECV showed altered hs-cT values. Therefore, we demonstrated a significant dependence between the altered ECV and hs-cT values using the X² test ($p = 0.04$) and a highly positive correlation between these two parameters using the Pearson correlation index ($r = 0.803$; $p < 0.001$).

ROC analysis of our data identified a hs-cT value > 0.022 ng/mL as the best cut-off for distinguishing between the healthy controls and patients with myocardial edema (sensitivity: 90.9%; specificity: 81.8%; $p = 0.002$; area under the curve: 0.818). Adapted to all patients, this threshold identified 10 of 11 patients as having myocardial involvement on T2 maps.

Applying the cut-off of 0.022 divided the cohort into 2 groups. Significant differences were found between them in terms of T2 ($p = 0.007$) and ECV ($p = 0.024$) values. No significant differences were found regarding nT1 values ($p = 0.189$).

It should be noted that no differences were found in terms of CT scores between patients with abnormal nT1 ($p = 0.815$), T2 ($p = 0.414$), and ECV ($p = 0.205$) values.

Discussion

To the best of our knowledge, this is the first study using CMR imaging to explore the nature of myocardial damage in a selected cohort of individuals with active COVID-19 disease.

Besides the definition of myocardial injury, corresponding to a rise of cT levels above the 99th percentile upper reference limit [2], our research provides a broader insight into the possible underlying pathological substrates associated with SARS-CoV-2 infection.

The heterogeneity of CMR patterns observed in our population reflects the complexity of disease pathogenesis and offers insight into the main mechanisms involved (e.g., inflammatory, cytokine-mediated, direct cytotoxicity of the virus, intra-coronary thrombosis), with potential implications for patient management and prognosis.

As expected, the most common CMR disease pattern observed in our series (31.8% of patients) was consistent with a diagnosis of clinically suspected acute myocarditis, characterized by the combination of myocardial edema with evidence of non-ischemic myocardial injury, as suggested by the new CMR diagnostic criteria [20].

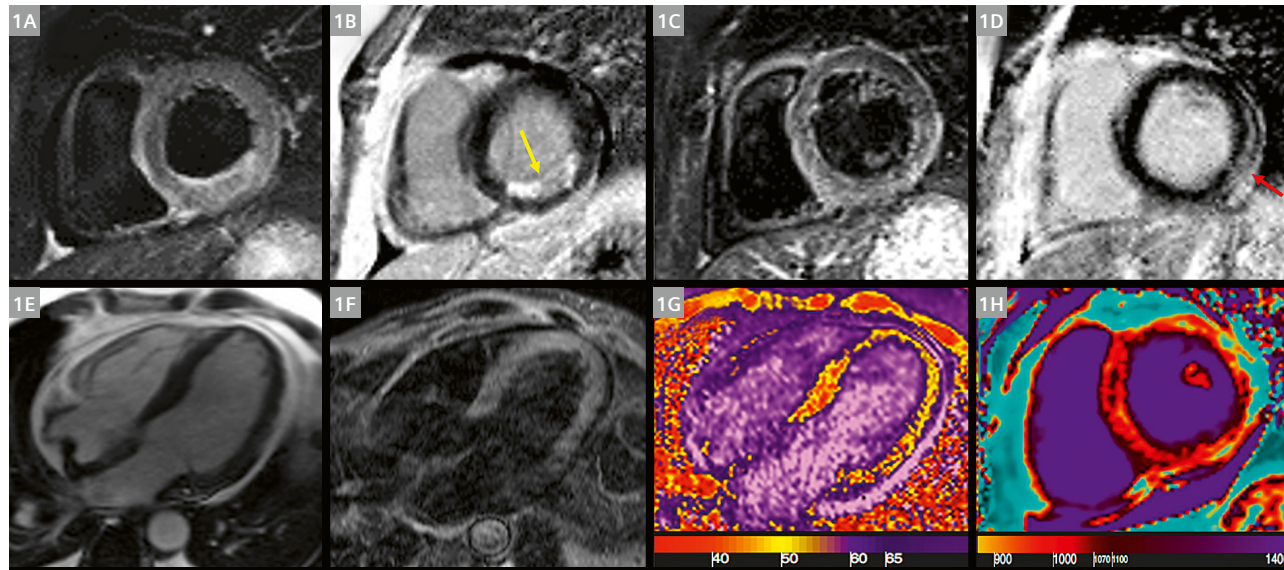
CMR patterns of diffuse inflammation were more commonly detected, probably reflecting the increased

interstitial macrophage recruitment and, in a limited percentage of cases, the multifocal lymphocytic infiltration that has been reported in previous pathological studies [21].

In line with the acute phase of COVID-19-related myocardial involvement that characterized our study population, the most commonly observed CMR feature was the increase of myocardial T2 values (abnormal T2 in 11/22 patients). This mirrors numerous studies published in non-COVID-19 literature and reflects the predominantly edematous expression of the process [22].

Our average T2 values (51 ms) significantly differed from an earlier publication by Esposito et al. [23], which reported remarkably increased levels of T2 values (62 ms, using a reference normal value < 50 ms) in patients consecutively referred for suspected COVID-19 myocarditis. The most likely explanation for this discrepancy is the large heterogeneity of the clinical presentations observed in our cohort, which included subjects without CMR evidence of myocardial injury.

Similar observations were published by Puntmann et al. [24], who found increased T2 mapping values in 60% of 100 patients with convalescent-stage disease (average interval between the last positive PCR and CMR examination was 71 days). Their findings suggest



1 The spectrum of cardiac involvement in coronavirus disease 2019 (COVID-19) patients

Acute myocardial infarction (1A, B) showed by edema (1A) and subendocardial LGE (1B, yellow arrow) at inferior segments on basal planes. Mild pericardial effusion was also present. Acute myocarditis (1C, D). A diffuse myocardial edema at inferior and inferolateral segments on midventricular planes (1A) with a subepicardial stria on the same cardiac segments on LGE images (1D, red arrow) satisfied Lake Louise criteria for CMR diagnosis of myocardial inflammation. Isolated T2 mapping increase (1E–H). The patient had normal ejection fraction on cine images (1E) and showed no edema in STIR T2-weighted images (1F); T2 mapping sequences revealed a diffuse increase in T2 values (1G, mean values: 55–60 ms; normal values: < 50 ms), especially in mid and apical planes. Native T1 mapping values were within the normal range (1H, 950–1030 ms). Patient also showed pericardial and bilateral pleural effusion.

Abbreviations: CMR, cardiac magnetic resonance; LGE, late gadolinium enhancement; STIR, short tau inversion recovery

persistence of the inflammatory cascade beyond the acute phase of the infection, potentially triggered by the activation of an autoimmune process.

In our investigation, the main differential diagnoses of acute myocarditis were pericarditis and MINOCA. Pericardial inflammation in COVID-19 has been described as a purely inflammatory response to the systemic insult rather than a local infectious process [25]. Accordingly, the two cases of acute pericarditis in our population showed typical hallmarks of transudative pericardial effusions with associated edematous thickening of the layers [26]. MINOCA, defined by the presence of ischemic LGE with tissue edema in CMR images and not associated with epicardial coronary obstruction, was observed in two cases.

Possible explanations have focused on the presence of high levels of angiotensin-converting enzyme 2 receptors in pericytes and endothelial cells, which causes severe microvascular dysfunction enhanced by the cytokine storm [27]. A mismatch between oxygen supply and demand was reported to be a second potential mechanism of injury [28].

A further pathological CMR pattern (observed in three patients) showed an isolated increase of T2 values without associated CMR features of myocardial damage on LGE, nT1, and ECV. This CMR phenotype, which does not correspond to a diagnosis of acute myocarditis, likely represents the imaging correlate of the diffuse edematous myocardial involvement induced by the uncontrolled cytokine release that characterizes the late phases of the infection. Presence of myocardial interstitial macrophage infiltration without myocyte injury was reported in 86% of cases from a recent multicenter study that included the autopsies of 21 consecutive COVID-19 patients [21]. The authors' hypothesis was that the characteristics of tissue damage suggest etiologies other than viral myocarditis, more likely depending on a combination of elevated proinflammatory cytokines, hypoxemia, right ventricular overload, and thrombotic complications [21].

Similar findings were published by Xu et al. [29], who reported the presence of few interstitial mononuclear inflammatory infiltrates and no evidence of substantial damage in the heart tissue of a post-mortem biopsy.

Systemic capillary leak syndrome has been proposed as a possible mechanism of pathogenesis in COVID-19 patients [30]. It causes acute loosening of the endothelial junctions, resulting in extravasation and shift of fluids, electrolytes, and proteins toward the extravascular space and leading to myocardial edema [31]. This paroxysmal permeability phenomenon is frequently associated with contractile dysfunction and tends to regress generally without any permanent sequelae. This might explain the increase of ECV fraction values found in our population, which correlated with hs-cT values. Corresponding

CMR follow-up data are missing in the literature and will certainly provide better comprehension of the underlying mechanism of injury and its transient nature with or without permanent tissue abnormalities.

Interestingly, two patients showed a newly diagnosed mild reduction of biventricular function in the absence of myocardial signal alterations both in conventional sequences (T2 STIR and LGE) and in relaxometric imaging. Interpreting these findings remains challenging, as a pre-existing ventricular impairment cannot be excluded and could not be differentiated from a chronic evolution of myocardial damage.

Correlation between CMR parameters and hs-cT values (clinical variables)

As expected, we found a positive linear relationship between the T2 mapping and hs-cT values.

Besides myocardial necrosis, hs-cT assays can be detectable in COVID-19 as the consequence of the transient ischemic or inflammatory conditions associated with the disease, which include respiratory and renal failure, hypoxemia, tachyarrhythmias, and thromboembolic disease [32].

Regardless of the underlying pathogenetic mechanisms, troponin levels have been hypothesized to be the expression of a general hyperinflammatory status [33]. At the level of the heart, this leads to the accumulation of interstitial edema, which proportionally increases T2 relaxation times and explains the observed positive correlation. Accordingly, the significant dependence observed in our cohort between the altered ECV and hs-cT likely depends on the water-dependent expansion of interstitial space.

In addition, the stepwise linear regression analysis showed that the increase in each of the inflammatory biomarker values (WBC, lymphocyte count, and CRP) was associated with higher T2 mapping values. These results confirm that patients with myocardial injury showed a more pronounced inflammatory response with direct impact on T2 measurements.

ROC analysis indicated that a hs-cT value >0.022 ng/mL would be the best cut-off value to differentiate normal versus increased T2 mapping values (sensitivity: 83.3%; specificity: 80%). This threshold identified 11/12 patients as having evidence of myocardial pathological involvement on T2 maps, and may represent a potential cut-off value to direct patients to CMR examination.

A further interesting finding is the lack of correlation between the extent of pulmonary disease and the occurrence of myocardial involvement. This further supports the theory that cardiac involvement is not affected or is a complication of pulmonary pathology, even though they likely share common pathogenic mechanisms.

Study limitations

Our sample size was limited to 22 patients, but nonetheless represents, to date, one of the largest cohorts of individuals who have undergone CMR with active COVID-19.

Due to the complexity of the diagnostic exam, which requires repeated breath-holds and an average scanning time of 50 minutes, we had a selection bias regarding the clinical stage of patients enrolled, with almost all of them presenting with a mild form of disease.

Myocardial injury proportionally correlated with the severity of the clinical manifestations of COVID-19 and potentially identifies patients with worse baseline clinical status. This has an obvious impact on the prevalence and extent of tissue damage observed in our study.

Similarly, no early-stage disease patients (i.e., less than seven days after positive PCR) were included in our cohort. This indirectly confirms that myocardial involvement begins or persists days after disease onset.

Our study did not provide prognostic data, which is likely to further refine the role of CMR imaging in this complex clinical scenario and to better clarify possible inclusion criteria for patient selection.

None of our patients received an endomyocardial biopsy, therefore the diagnosis of myocarditis in our patients could be considered definitively confirmed.

Finally, we did not include asymptomatic individuals, in whom multiparametric imaging data would allow subclinical detection of structural damage with potentially relevant implications for early diagnosis and clinical decision-making.

Conclusions

CMR allowed recognition and characterization of myocardial damage in a cohort of selected COVID-19 patients with active disease. This consisted of heterogeneous patterns of injury ranging from acute myocarditis to MINOCA, pericarditis, and CMR evidence of isolated edematous changes. The prompt recognition of disease patterns is pivotal to drive therapy and patient management. Myocardial T2 appears to be the prevalent imaging biomarker in active COVID-19 patients, and the most closely related to hs-cT values.

Abbreviations

ACS:	Acute coronary syndrome
AHA:	American Heart Association
China CDC:	Chinese Center for Disease Control and Prevention
CM:	Contrast media
CMR:	Cardiovascular magnetic resonance
COVID-19:	Coronavirus disease 2019

CRP:	C-reactive protein
CT:	Computed tomography
cT:	Cardiac troponin
CV:	Cardiovascular
DWI:	Diffusion-weighted imaging
ECV:	Extracellular volume
EDV/BSA:	End-diastolic volume/body surface area
EF:	Ejection fraction
FLASH 3D:	Fast low angle shot 3D
hs-cT:	High-sensitive troponin T
IR-CE T1w:	Contrast-enhanced inversion recovery T1-weighted
LGE:	Late gadolinium enhancement
LV:	Left ventricle
MINOCA:	Myocardial infarction with non-obstructive coronary arteries
MOLLI:	Modified Look-Locker inversion recovery
MR:	Magnetic resonance
PaO ₂ /FiO ₂ :	Arterial oxygen partial pressure/fraction of inspired oxygen
PD-TSE:	Proton-density weighted fat-saturated turbo spin echo
PPE:	Personal protective equipment
ROI:	Region of interest
RT-PCR:	Reverse transcription–polymerase chain reaction
SARS-CoV-2:	Severe acute respiratory syndrome coronavirus 2
SD:	Standard deviation
SGRE:	Spoiled gradient echo
SI:	Signal intensity
SSFP:	Balanced steady state free precession
STIR:	Short tau inversion recovery
WBC:	White blood cells
X ² :	Chi-squared

Declarations

- *Ethics approval and consent to participate:* The ethics approval was waived because of the observational nature of the study. The study was conducted in line with the Declaration of Helsinki and good clinical practice. Informed consent was obtained from all participants.
- *Availability of data and materials:* All data generated or analyzed during this study will be available at the request of the referees and will be included in the published article as supplementary information files, once the manuscript is accepted.
- *Competing interests:* The authors declare that they have no competing interests.
- *Funding:* No specific funds have been employed.

References

- 1 Atri D, Siddiqi HK, Lang J, Nauffal V, Morrow DA, Bohula EA. COVID-19 for the Cardiologist: A Current Review of the Virology, Clinical Epidemiology, Cardiac and Other Clinical Manifestations and Potential Therapeutic Strategies. *JACC Basic Transl Sci.* 2020;5(5):518–536.
- 2 Alpert JS, Antman E, Apple F, Armstrong PW, Bassand JP,

- Bayés de Luna A, et al. Myocardial infarction redefined – a consensus document of the Joint European Society of Cardiology/ American College of Cardiology Committee for the redefinition of myocardial infarction. *Eur Heart J*. 2000;21:1502–1513.
- 3 Lala A, Johnson KW, Januzzi JL, Russak AJ, Paranjpe I, Richter F, et al. Prevalence and Impact of Myocardial Injury in Patients Hospitalized With COVID-19 Infection. *J Am Coll Cardiol*. 2020;76(5):533–546.
 - 4 Wei JF, Huang FY, Xiong TY, Liu Q, Chen H, Wang H, et al. Acute myocardial injury is common in patients with COVID-19 and impairs their prognosis. *Heart* 2020;106(15):1154–1159.
 - 5 Li B, Yang J, Zhao F, Zhi L, Wang X, Liu L, et al. Prevalence and impact of cardiovascular metabolic diseases on COVID-19 in China. *Clin Res Cardiol*. 2020;109(5):531–538.
 - 6 Guo T, Fan Y, Chen M, Wu X, Zhang L, He T, et al. Cardiovascular Implications of Fatal Outcomes of Patients with Coronavirus Disease 2019 (COVID-19). *JAMA Cardiol*. 2020;5(7):811–818.
 - 7 Thapa SB, Kakar TS, Mayer C, Khanal D. Clinical Outcomes of In-Hospital Cardiac Arrest in COVID-19. *JAMA Intern Med*. 2021;181(2):279–281.
 - 8 Baldi E, Sechi GM, Mare C, Canevari F, Brancaglione A, Primi R, et al. Out-of-Hospital Cardiac Arrest during the Covid-19 Outbreak in Italy. *N Engl J Med*. 2020;383(5):496–498.
 - 9 Januzzi Jr JL. Troponin and BNP Use in COVID-19 [Internet]. Washington, DC: American College of Cardiology; March 18, 2020 [cited November 24, 2021]. Available from: <https://www.acc.org/latest-in-cardiology/articles/2020/03/18/15/25/troponin-and-bnp-use-in-covid19>
 - 10 Galea N, Catapano F, Marchitelli L, Cundari G, Maestrini V, Panebianco V, et al. How to perform a cardio-thoracic magnetic resonance imaging in COVID-19: comprehensive assessment of heart, pulmonary arteries, and lung parenchyma. *Eur Hear J Cardiovasc Imaging*. 2021;22(7):728–731.
 - 11 Wu Z, McGoogan JM. Characteristics of and Important Lessons From the Coronavirus Disease 2019 (COVID-19) Outbreak in China: Summary of a Report of 72 314 Cases From the Chinese Center for Disease Control and Prevention. *JAMA*. 2020;323(13):1239–1242.
 - 12 Zhou S, Wang Y, Zhu T, Xia L. CT Features of Coronavirus Disease 2019 (COVID-19) Pneumonia in 62 Patients in Wuhan, China. *AJR Am J Roentgenol*. 2020;214(6):1287–1294.
 - 13 Pan F, Ye T, Sun P, Gui S, Liang B, Li L, et al. Time Course of Lung Changes At Chest CT during Recovery from Coronavirus Disease 2019 (COVID-19). *Radiology*. 2020;295(3):715–721.
 - 14 Francone M, Iafate F, Masci GM, Coco S, Cilia F, Manganaro L, et al. Chest CT score in COVID-019 patients: correlation with disease severity and short-term prognosis. *Eur Radiol* 2020;30(12):6808–6817.
 - 15 Beitzke D, Salgado R, Francone M, Kreitner KF, Natale L, Bremerich J, et al. Cardiac imaging procedures and the COVID-19 pandemic: recommendations of the European Society of Cardiovascular Radiology (ESCR). *Int J Cardiovasc Imaging*. 2020;36(10):1801–1810.
 - 16 Messroghli DR, Moon JC, Ferreira VM, Grosse-Wortmann L, He T, Kellman P, et al. Clinical recommendations for cardiovascular magnetic resonance mapping of T1, T2, T2* and extracellular volume: A consensus statement by the Society for Cardiovascular Magnetic Resonance (SCMR) endorsed by the European Association for Cardiovascular Imaging (EACVI). *J Cardiovasc Magn Reson*. 2017;19(1):75.
 - 17 Bondarenko O, Beek AM, Hofman MBM, Kühl HP, Twisk JWR, Van Dockum WG, et al. Standardizing the definition of hyperenhancement in the quantitative assessment of infarct size and myocardial viability using delayed contrast-enhanced CMR. *J Cardiovasc Magn Reson*. 2005;7(2):481–485.
 - 18 Mahrholdt H, Wagner A, Judd RM, Sechtem U, Kim RJ. Delayed enhancement cardiovascular magnetic resonance assessment of non-ischaemic cardiomyopathies. *Eur Heart J*. 2005;26(15):1461–74.
 - 19 Friedrich MG, Sechtem U, Schulz-Menger J, Holmvang G, Alakija P, Cooper LT, et al. Cardiovascular Magnetic Resonance in Myocarditis: A JACC White Paper. *J Am Coll Cardiol*. 2009;53(17):1475–87.
 - 20 Ferreira VM, Schulz-Menger J, Holmvang G, Kramer CM, Carbone I, Sechtem U, et al. Cardiovascular Magnetic Resonance in Nonischemic Myocardial Inflammation: Expert Recommendations. *J Am Coll Cardiol*. 2018;72(24):3158–3176.
 - 21 Basso C, Leone O, Rizzo S, De Gaspari M, Van Der Wal AC, Aubry MC, et al. Pathological features of COVID-19-associated myocardial injury: A multicentre cardiovascular pathology study. *Eur Heart J*. 2020;41(39):3827–3835.
 - 22 Cundari G, Galea N, De Rubeis G, Frustaci A, Cilia F, Mancuso G, et al. Use of the new Lake Louise Criteria improves CMR detection of atypical forms of acute myocarditis. *Int J Cardiovasc Imaging*. 2021;37(4):1395–1404.
 - 23 Esposito A, Palmisano A, Natale L, Ligabue G, Peretto G, Lovato L, et al. Cardiac Magnetic Resonance Characterization of Myocarditis-Like Acute Cardiac Syndrome in COVID-19. *JACC Cardiovasc Imaging*. 2020;13(11):2462–2465.
 - 24 Puntmann VO, Carerj ML, Wieters I, Fahim M, Arendt C, Hoffmann J, et al. Outcomes of Cardiovascular Magnetic Resonance Imaging in Patients Recently Recovered from Coronavirus Disease 2019 (COVID-19). *JAMA Cardiol*. 2020;5(11):1265–1273.
 - 25 Allam HH, Kinsara AJ, Tuaima T, Alfakh S. Pericardial Fluid in a COVID-19 Patient: Is It Exudate or Transudate? *Eur J Case Rep Intern Med*. 2020;7(6):001703.
 - 26 Bogaert J, Francone M. Pericardial disease: Value of CT and MR imaging. *Radiology*. 2013;267(2):340–56.
 - 27 Guzik TJ, Mohiddin SA, Dimarco A, Patel V, Savvatis K, Marelli-Berg FM, et al. COVID-19 and the cardiovascular system: Implications for risk assessment, diagnosis, and treatment options. *Cardiovasc Res*. 2020;116(10):1666–1687.
 - 28 DeFilippis AP, Nasir K, Blaha MJ. Myocardial Infarction as a Clinical End Point in Research. *Circ Res*. 2019;124(12):1701–1703.
 - 29 Xu Z, Shi L, Wang Y, Zhang J, Huang L, Zhang C, et al. Pathological findings of COVID-19 associated with acute respiratory distress syndrome. *Lancet Respir Med*. 2020;8(4):420–422.
 - 30 Cosyns B, Lochy S, Luchian ML, Gimelli A, Pontone G, Allard SD, et al. The role of cardiovascular imaging for myocardial injury in hospitalized COVID-19 patients. *Eur Heart J Cardiovasc Imaging*. 2020;21(7):709–714.
 - 31 Wu MA, Catena E, Cogliati C, Ottolina D, Castelli A, Rech R, et al. Myocardial edema in paroxysmal permeability disorders: The paradigm of Clarkson's disease. *J Crit Care*. 2020;57:13–18.
 - 32 Giustino G, Croft LB, Stefanini GG, Bragato R, Silbiger JJ, Vicenzi M, et al. Characterization of Myocardial Injury in Patients With COVID-19. *J Am Coll Cardiol*. 2020;76(18):2043–2055.
 - 33 Lombardi CM, Carubelli V, Iorio A, Inciardi RM, Bellasi A, Canale C, et al. Association of Troponin Levels with Mortality in Italian Patients Hospitalized with Coronavirus Disease 2019: Results of a Multicenter Study. *JAMA Cardiol*. 2020;5(11):1274–1280.

Contact

Marco Francone, M.D., Ph.D.
 Radiology Full Professor
 Department of Biomedical Sciences
 Humanitas University
 Via Rita Levi Montalcini 4
 20072 Pieve Emanuele, Milan
 Italy
 Tel.: +39 335 7550688
marco.francone@hunimed.eu



The Added Value of Cardiac Magnetic Resonance Imaging in the Prevention of Sudden Cardiac Death in Athletes

Liliána Szabó¹, Zsófia Dohy¹, Vencel Juhász¹, Máté Kiss², Karl P. Kunze³, Béla Merkely^{*1,4}, Hajnalka Vágó^{*1,4}

¹Semmelweis University, Heart and Vascular Center, Budapest, Hungary

²Siemens Healthineers, Budapest, Hungary

³MR Research Collaborations, Siemens Healthineers, Frimley, UK

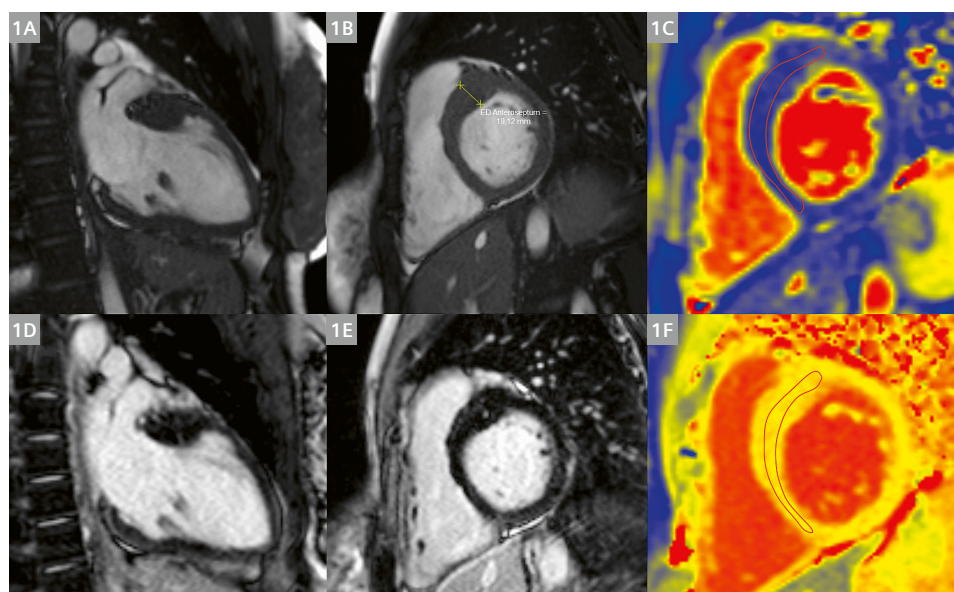
⁴Semmelweis University, Department of Sport Medicine, Budapest, Hungary

*Equal contribution

Introduction

Early differentiation of pathological alterations from physiological cardiac adaptation in highly trained athletes is key to preventing sudden cardiac death (SCD) [1]. Athletes engaging in high training loads develop a complex electrical, volumetric adaptation to sport, known as “the athlete’s heart” [2, 3]. While not all aspects of physiological adaptation are fully understood today, many characteristics are well described. The imaging features of the athlete’s heart include a balanced elevation in left and right cavity sizes, increased myocardial mass and wall thickness, and normal or low normal systolic function at rest compared to sedentary controls [4]. The main factors contributing to the extensiveness of the morphological attributes can be categorized as physiological and pathological. The physiological factors are age, gender, ethnicity, body size, and sports discipline. The pathological factors are illegal perfor-

mance-enhancing drugs and underlying heart disease [3]. Cardiac magnetic resonance (CMR) imaging is increasingly recognized as an essential second-line imaging modality to diagnose, follow-up, and inform risk stratification in several myocardial diseases such as hypertrophic or arrhythmogenic cardiomyopathy, or acute myocarditis. Recent efforts using novel techniques such as strain analysis or mapping enable more sophisticated differentiation, even in so-called “gray-zone” cases [3]. As CMR is becoming more broadly available, some initiatives have used it as a screening method in collegiate athletes after COVID-19 infection [5]. While this might not be suitable in all cases and could even lead to overdiagnosis of several entities [6], the application of CMR is undoubtedly widening. We summarize the primary applications of CMR in the context of highly trained athletes, and illustrate some real-life CMR cases using a MAGNETOM Area 1.5T MRI scanner from Siemens Healthineers.



1 Young female basketball player with mild phenotypic hypertrophic cardiomyopathy. Images 1A and 1B show cine images in 2-chamber (1A) and short-axis (1B) views using the CINE segmented (b-SSFP/TrueFISP) sequences. The maximum end-diastolic wall thickness is 19 mm in the basal anteroseptal segment. The T2 mapping (1C) is normal (47 ms). Images (1D, E) show a very small late gadolinium enhancement in the hypertrophic segment. Image (1F) shows a slightly elevated native T1 mapping value (1012 ms) in the basal septum compared to our in-house normal female athletic values.

Applications of CMR imaging in athletes

Cine sequences are well suited to assessing the athlete's heart in terms of biventricular volumes, function, and myocardial mass. CMR measures these parameters very accurately, showing minimal intra- and interobserver variability [7]. It is also worth mentioning that echocardiography and CMR measurements are not directly comparable. CMR systematically shows larger volumes and smaller wall thickness than echocardiography [8]. Volumetric evaluation of athletes requires athletic controls to prevent false diagnoses and unnecessary restrictions on participating in the competitive sport activity. The cardiac adaptation varies according to gender: Male athletes generally show more pronounced ventricular volumes and myocardial mass than female athletes [9, 10]. Different sports disciplines also lead to slightly altered morphological features: Endurance athletes tend to present with robust cardiac adaptation primarily due to the volume load of the heart, while power athletes such as weightlifters experience states of extreme pressure overload that lead to increased LV wall thickness with virtually unchanged LV volumes [11]. Myocardial deformation imaging has been shown to detect early dysfunction in a number of cardiovascular diseases. Various imaging techniques (e.g., feature tracking, SENC, or DENSE) help to assess myocardial deformation in CMR [12]. Nowadays, thanks to their ease of use, feature-tracking applications using cine images are also gaining popularity in the post-processing analysis of strain imaging. However, there is little data about the typical strain pattern of the athlete's heart.

In addition to precise volumetric measurements and exact morphological evaluation in all myocardial segments, CMR is also capable of non-invasive tissue characterization [7]. Edema is visualized qualitatively with T2-weighted and early gadolinium-enhanced images, and T2 mapping sequences can be used for quantitative assessments. In young athletes, edema-specific sequences are used in acute settings such as acute myocarditis or contusion. Necrosis and fibrosis of the myocardium are visualized on the late gadolinium-enhanced (LGE) images. We acquire LGE images after administering extracellular, gadolinium-based contrast media. At the same time, native T1 mapping and extracellular volume (ECV) provide invaluable information regarding the diffuse extracellular fibrosis or necrosis of the heart. In athletes aged < 35 years, LGE is often caused by myocarditis or different types of cardiomyopathies [3, 7].

It is worth noting that novel evidence also supports the use of normal values for athletic T1 mapping, rather than just site-specific normal values, because native T1 might decrease slightly in cases of physiological hypertrophy [13, 14].

Differential diagnosis and risk stratification in the athlete's heart

Due to the phenotypic overlap between the athlete's heart and early or mild forms of cardiomyopathies, highly trained athletes must be evaluated in cardiovascular centers that deal with a high volume of athletic patients. The use of specific novel CMR techniques is pivotal in some gray-zone cases.

Hypertrophic cardiomyopathy

According to a sizeable forensic registry of competitive athletes in the USA, hypertrophic cardiomyopathy (HCM) is the single most common cause of SCD and it affects male minority athletes even more seriously than other demographic groups [15]. Not surprisingly, diagnosing HCM in highly trained athletes is a considerable challenge, especially in the case of gray-zone left ventricular (LV) hypertrophy with a wall thickness of 13–16 mm [16, 17]. There are, however, some distinctive characteristics that might aid the diagnosis. In a CMR imaging study, the following clues are of importance: focal areas of hypertrophy, where typically asymmetric septal and apical forms are suspicious of pathological alterations, as well as the application of sport indices, showing the ratio between maximum end-diastolic wall width or mass and the end-diastolic volume index for the identification of pathological hypertrophy. Tissue-specific information is invaluable in HCM: LGE shows a midmyocardial pattern in the hypertrophic areas or elevated T1/ECV values, suggesting diffuse fibrosis in the affected segments. In a small set of HCM patients, athletes, and controls, elevated T2 mapping and global longitudinal strain values (absolute value) helped to distinguish HCM from the athlete's heart [18]. In the differential diagnosis of hypertrophy among highly trained athletes, it is also worth mentioning that decreased native T1 values as assessed by T1 mapping help to distinguish Fabry disease, a rare storage disease that causes LV hypertrophy [13]. Finally, it is of the utmost importance that while CMR might provide important clues for the differential diagnosis of HCM, the final decision *must only* be made with the clinicians' assessment of symptoms, family history, and 12-lead ECG [3, 19].

For demonstration purposes, we present the case of a young female elite athlete (Fig. 1). On CMR, asymmetric hypertrophy (19 mm) with slight T1 elevation and a small LGE was present. She was diagnosed with a mild phenotype of HCM. After a comprehensive risk assessment as per the ESC Guideline on sports cardiology and exercise in patients with cardiovascular disease, she was cleared to return to high levels of sporting activity with close supervision [1].

Arrhythmogenic cardiomyopathy

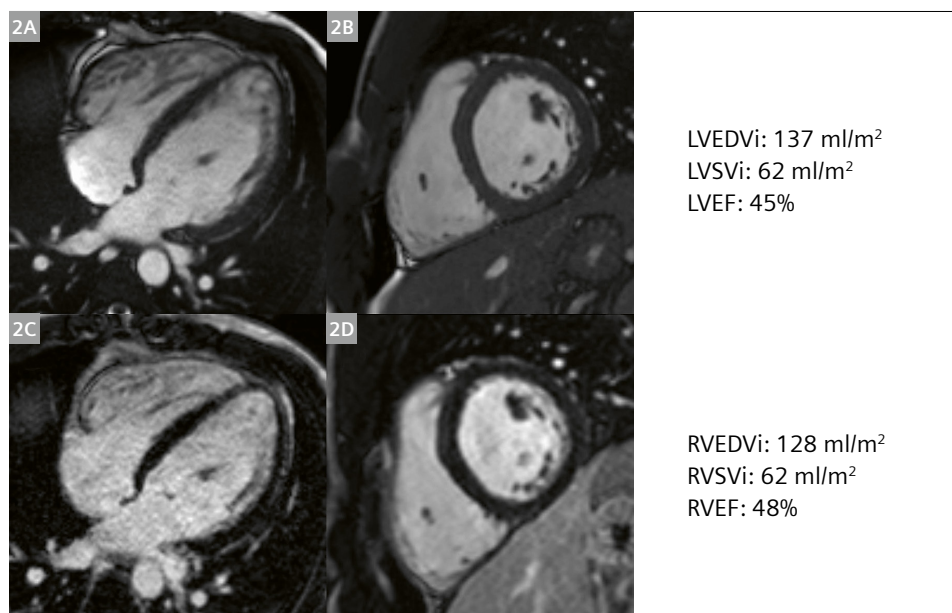
Arrhythmogenic cardiomyopathy (AC) was first described as a fatty-fibrotic replacement predominantly affecting the right ventricle (RV), although LV involvement also occurs [3]. It is often associated with ventricular arrhythmias and SCD – so much so that, according to Italian data, AC accounted for 23% of SCD among young athletes. The diagnosis of AC is quite complex and is currently based on the modified Task Force Criteria that include anamnestic, electrophysiological, and imaging data [20]. Overall, CMR plays a prominent role in the detailed evaluation of RV volumes, function, and regional wall motion abnormalities compared to echocardiography. As the dimensional criteria for AC were described based on the comparison between sedentary controls and AC patients, the European Association of Cardiovascular Imaging (EACVI) suggested applying only “major” volumetric criteria to elite athletes [3]. Nevertheless, elevated volumes (men: RVEDVi > 110 ml/m²; women: > 100 ml/m²) only fulfil AC criteria in combination with decreased systolic function and regional akinesia, dyskinesia, or aneurysmal deformation of the RV. While LGE is not currently part of the Task Force Criteria, it can be present in up to 40% of cases [3, 20]. Regional RV feature-tracking strain may also help identify AC in athletes with preserved RV ejection fraction [21].

Dilated cardiomyopathy

Endurance and mixed sports are often associated with biventricular dilatation at rest. They can sometimes be associated with mildly reduced systolic function, which raises the suspicion of dilated cardiomyopathy (DCM) [3].

This presents an important diagnostic challenge and requires a series of examinations, ideally including CMR. DCM also provides some vital imaging clues that can help with the final decision. In athletic adaptation, biventricular cavity enlargement is usually associated with normal systolic function and increased wall thickness [9]. In mild functional impairment (LVEF approximately 50–45%), it might be beneficial to assess the improvement during exercise. Stress CMR is a valuable tool for detecting reduced cardiac functional reserve and early pathological alterations that are not present at rest. This might be beneficial to recognizing DCM in the early stages of the disease [22]. The presence and pattern of LGE are paramount for the differential diagnosis and risk stratification of DCM, though the absence of LGE does not exclude the disease. Among other forms of LV scar, septal midmyocardial fibrosis was linked to ventricular arrhythmias [3, 23, 24]. While there is currently little data on the subject, T1 mapping could potentially play a role, as the physiological hypertrophy in athletes causes a slight decrease in native T1 values, and diffuse fibrosis that is not visible on LGE images can elevate T1 and ECV values [25].

Figure 2 shows the CMR images of an asymptomatic young male kayaker who was referred for CMR due to elevated volumes on echocardiography. CMR found elevated LV volumes exceeding the 95th percentile of normal athletic values, and an LVEF lower than the normal athletic value with mild LV hypokinesis at rest. We did not find signs of regional or diffuse LV fibrosis. Examinations and risk stratification are currently underway for the athlete. His imaging will include stress CMR using an MR-conditional bicycle to establish his reaction to physiological exercise.



2 Young male kayaker with early signs of dilated cardiomyopathy. Cine images in 4-chamber (**2A**) and short-axis (**2B**) view show dilated left (LV) and right ventricles with slightly elevated LV trabeculation. Images (**2C**, **D**) show no pathological late gadolinium enhancement in the myocardium.

Left ventricular non-compaction

LV non-compaction is characterized by a distinctive double-layer appearance: compact myocardial wall and pronounced myocardial trabeculation with or without deep inter-trabecular recesses. Currently, the most widely used CMR criteria for diagnosis is a non-compacted-to-compacted layer ratio of > 2.3 in diastole [26]. A debate is still ongoing as to whether or not this morphologically and clinically heterogeneous group of individuals should be classified as pathological. High preload conditions such as pregnancy or athletic training are commonly associated with increased LV trabeculation. While LV trabeculation was found in 18–19% of asymptomatic athletic and adolescent populations [27, 28], cardiac pathology should be considered in cases of cardiac symptoms, decreased systolic function, or a family history of heart failure or SCD [1]. Novel proof-of-concept studies show abnormal strain patterns in LV non-compaction [29], and the presence of LGE suggests “cardiomyopathic process”, though the overall prevalence of LGE is currently unclear [3].

Myocarditis

Acute myocarditis causing electrical instability of the heart is also linked to cases of sudden cardiac death in young athletes [3, 30]. A recent history of viral infection and indicative symptoms of chest pain, palpitation, and fever are key factors in the workup of acute myocarditis – though with young athletes, toxins should also be considered and excluded. From an imaging perspective, CMR is very well suited to confirm or exclude the diagnosis of myocarditis [31, 32]. The updated Lake Louise Criteria from 2018 require the following main findings at a

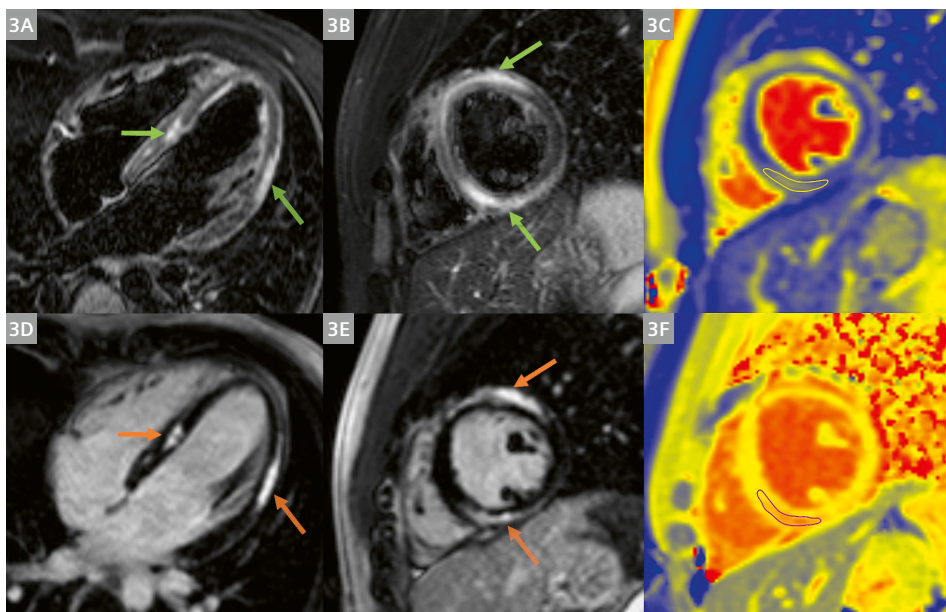
regional or global level: myocardial edema on T2 mapping or T2-weighted images and non-ischemic myocardial injury presenting as an abnormal T1 mapping value, elevation of the extracellular volume, or LGE. The supportive features are as follows: pericarditis presenting as effusion in cine images; abnormal LGE, T2, or T1 mapping; and systolic LV dysfunction presenting with regional or global wall motion abnormality [31].

At the beginning of the COVID-19 pandemic, the first results among athletes suggested that myocarditis occurred at an alarmingly high rate, even without symptoms [33]. However, more than a year into the pandemic, we found that the prevalence of definitive acute myocarditis is as low as 1–2% [34–36].

We present the case of a young male floorball player who presented at the emergency room after a short viral infection with considerable chest pain and ECG alteration. Coronary angiography showed no obstruction in the coronary arteries. Therefore, the patient was referred to CMR with the suspicion of myocarditis. CMR confirmed the diagnosis, showing an extensive non-ischemic pattern of myocardial edema and necrosis in the basal and midventricular septal segments and in the apical lateral segment (Fig. 3). The athlete was prohibited from participating in competitive sport for at least three months. After that, he will return to our clinic for a reevaluation [1].

Congenital coronary artery anomalies

While congenital coronary artery anomalies are rare and only affect approximately 0.4% of the adolescent population [28], they are present in as many as 19% of all cases of SCD in young athletes [11]. Two forms are



3 Young male floorball player presenting with acute myocarditis. Edema images using fat-suppressed T2-weighted TIRM sequences in 4-chamber (**3A**) and short-axis (**3B**) views show elevated signal intensity in midmyo/subepicardial pattern (green arrows). On image (**3C**), T2 mapping values are elevated (56 ms) in the areas showing signal intensity elevation on T2-weighted images compared to our normal values. Late gadolinium enhancement in the same non-ischemic pattern is visible on images (**3D, E**) (orange arrows). Image (**3F**) shows native T1 mapping elevation (1151 ms).



4 Adolescent male basketball player's coronary origin. Images (4A–C) were acquired using a prototype 3D T2-prep non-contrast MR angiography¹ with isotropic spatial resolution [1.2 x 1.2 x 1.2 mm] in free breathing [38]. Image (4A) shows the origin of the right coronary artery from the right sinus, while (4B, C) depict the origin of the left main coronary artery from slightly above the left sinus.

associated with the most pronounced risk of SCD: an anomalous vessel coursing between the aorta and the pulmonary artery, and an anomalous vessel with an interseptal course that requires surgical repair [1]. In patients with suspected congenital coronary artery anomalies, CT or CMR angiography is recommended. CMR angiography is a non-invasive, radiation-free method of visualizing the coronary origins [37, 38].

Figure 4 shows the non-contrast CMR angiography¹ of a young basketball player who experienced fatigue and presented with ECG abnormalities on exertion. The CMR angiography revealed no coronary artery anomaly, but the left main coronary originates slightly higher up than the usual spot in the left coronary sinus.

Conclusions

CMR plays an essential role both in the assessment and risk stratification of cardiovascular diseases in highly trained athletes. The overlapping phenotypic features of the athlete's heart and mild or early characteristics of cardiomyopathies still constitute a considerable challenge, but these difficulties can be overcome by applying novel CMR techniques such as mapping, strain, or stress imaging.

Funding

Project no. NVKP_16-1-2016-0017 (National Heart Program) has been implemented with the support provided from the National Research, Development and Innovation Fund of Hungary, financed under the NVKP_16 funding scheme. The research was financed by the Thematic Excellence Programme (2020-4.1.1.-TKP2020) of the Ministry for Innovation and Technology in Hungary, within the framework of the Therapeutic Development and Bioimaging thematic programmes of the Semmelweis University. LS was supported by the ÚNKP-20-3-II-SE-61 New National Excellence Program of the Ministry for Innovation and Technology from the source of the National Research, Development and Innovation Fund. ZD and LS were supported by the "Development of scientific workshops of medical, health sciences and pharmaceutical educations" project. Project identification number: EFOP-3.6.3-VEKOP-16-2017-00009.

References

- Pelliccia A, Sharma S, Gati S, Bäck M, Börjesson M, Caselli S, et al. 2020 ESC Guidelines on sports cardiology and exercise in patients with cardiovascular disease. *Eur Heart J*. 2021;42(1):17–96.
- Maron BJ, Towbin JA, Thiene G, Antzelevitch C, Corrado D, Arnett D, et al. Contemporary definitions and classification of the cardiomyopathies: An American Heart Association Scientific Statement from the Council on Clinical Cardiology, Heart Failure and Transplantation Committee; Quality of Care and Outcomes Research and Functional Genomics and Translational Biology Interdisciplinary Working Groups; and Council on Epidemiology and Prevention. *Circulation*. 2006;113(14):1807–1816.
- Pelliccia A, Caselli S, Sharma S, Basso C, Bax JJ, Corrado D, et al. European Association of Preventive Cardiology (EAPC) and European Association of Cardiovascular Imaging (EACVI) joint position statement: Recommendations for the indication and interpretation of cardiovascular imaging in the evaluation of the athlete's heart. *Eur Heart J*. 2018;39(21):1949–1969.
- Galderisi M, Cardim N, D'Andrea A, Bruder O, Cosyns B, Davin L, et al. The multi-modality cardiac imaging approach to the Athlete's heart: an expert consensus of the European Association of Cardiovascular Imaging. *Eur Heart J Cardiovasc Imaging*. 2015;16(4):353.
- Daniels CJ, Rajpal S, Greenshields JT, Rosenthal GL, Chung EH, Terrin M, et al. Prevalence of Clinical and Subclinical Myocarditis in Competitive Athletes With Recent SARS-CoV-2 Infection: Results From the Big Ten COVID-19 Cardiac Registry. *JAMA Cardiol*. 2021:e212065.
- Moulson N, Baggish A. Subclinical COVID-19 Cardiac Imaging Findings: Resurgence of the Athletic "Grey-Zone". *JACC Cardiovasc Imaging*. 2021;14(3):556–558.
- Scharhag J, Wu KC, Bohm P, Basso C. Athlete's heart and prevention of sudden cardiac death in athletes. In: Lombardi M, Plein S, Petersen S, Bucciarelli-Ducci C, Buechel EV, Basso C, et al. *The EACVI Textbook of Cardiovascular Magnetic Resonance*. Oxford: Oxford University Press; 2018. p. 387–394.
- Prakken NH, Teske AJ, Cramer MJ, Mosterd A, Bosker AC, Mali WP, et al. Head-to-head comparison between echocardiography and cardiac MRI in the evaluation of the athlete's heart. *Br J Sports Med*. 2012;46(5):348–54. Epub 2011 Jan 29.
- Finocchiaro G, Dhutia H, D'Silva A, Malhotra A, Steriotes A, Millar L, et al. Effect of Sex and Sporting Discipline on LV Adaptation to Exercise. *JACC Cardiovasc Imaging*. 2017;10(9):965–72.
- Csecs I, Czibalmos C, Toth A, Dohy Z, Suhai IF, Szabo L, et al.

¹Work in progress. The application is currently under development and is not for sale in the U.S. and in other countries. Its future availability cannot be ensured.

- The impact of sex, age and training on biventricular cardiac adaptation in healthy adult and adolescent athletes: Cardiac magnetic resonance imaging study. *Eur J Prev Cardiol.* 2020;27(5):540–549.
- 11 Caruso MR, Garg L, Martinez MW. Cardiac Imaging in the Athlete: Shrinking the “Gray Zone”. *Curr Treat Options Cardiovasc Med.* 2020;22(2):5.
 - 12 Amzulescu MS, De Craene M, Langet H, Pasquet A, Vancraeynest D, Pouleur AC, et al. Myocardial strain imaging: review of general principles, validation, and sources of discrepancies. *Eur Heart J Cardiovasc Imaging.* 2019;20(6):605–619.
 - 13 Messroghli DR, Moon JC, Ferreira VM, et al. Clinical recommendations for cardiovascular magnetic resonance mapping of T1, T2, T2* and extracellular volume: A consensus statement by the Society for Cardiovascular Magnetic Resonance (SCMR) endorsed by the European Association for Cardiovascular Imaging (EACVI). *J Cardiovasc Magn Reson.* 2017;19(1):75.
 - 14 McDiarmid AK, Swoboda PP, Erhayiem B, Lancaster RE, Lyall GK, Broadbent DA, et al. Athletic Cardiac Adaptation in Males Is a Consequence of Elevated Myocyte Mass. *Circ Cardiovasc Imaging.* 2016;9(4):e003579.
 - 15 Maron BJ, Haas TS, Ahluwalia A, Murphy CJ, Garberich RF. Demographics and Epidemiology of Sudden Deaths in Young Competitive Athletes: From the United States National Registry. *Am J Med.* 2016;129(11):1170–1177.
 - 16 Pelliccia A, Maron BJ, Spataro A, Proschan MA, Spirito P. The upper limit of physiologic cardiac hypertrophy in highly trained elite athletes. *N Engl J Med.* 1991;324(5):295–301.
 - 17 Sheikh N, Papadakis M, Schnell F, Panoulas V, Malhotra A, Wilson M, et al. Clinical Profile of Athletes with Hypertrophic Cardiomyopathy. *Circ Cardiovasc Imaging.* 2015;8(7):e003454.
 - 18 Gastl M, Lachmann V, Christidi A, Janzarik N, Veulemans V, Haberkorn S, et al. Cardiac magnetic resonance T2 mapping and feature tracking in athlete’s heart and HCM. *Eur Radiol.* 2021;31(5):2768–2777. Epub 2020 Oct 15.
 - 19 Pelliccia A, Sharma S, Gati S, Bäck M, Börjesson M, Caselli S, et al. 2020 ESC Guidelines on sports cardiology and exercise in patients with cardiovascular disease. *Eur Heart J.* 2021;42(1):17–96.
 - 20 Marcus FI, McKenna WJ, Sherrill D, Basso C, Bauce B, Bluemke DA, et al. Diagnosis of arrhythmogenic right ventricular cardiomyopathy/dysplasia: proposed modification of the task force criteria. *Circulation.* 2010;121(13):1533–1541.
 - 21 Czibalmos C, Csecs I, Dohy Z, Toth A, Suhai FI, Müssigbrodt A, et al. Cardiac magnetic resonance based deformation imaging: role of feature tracking in athletes with suspected arrhythmogenic right ventricular cardiomyopathy. *Int J Cardiovasc Imaging.* 2019;35(3):529–538.
 - 22 De Innocentiis C, Ricci F, Khanji MY, Aung N, Tana C, Verrengia E, et al. Athlete’s Heart: Diagnostic Challenges and Future Perspectives. *Sports Med.* 2018;48(11):2463–2477.
 - 23 Zorzi A, Perazzolo Marra M, Rigato I, De Lazzari M, Susana A, Niero A, et al. Nonischemic Left Ventricular Scar as a Substrate of Life-Threatening Ventricular Arrhythmias and Sudden Cardiac Death in Competitive Athletes. *Circ Arrhythm Electrophysiol.* 2016;9(7):e004229.
 - 24 Perazzolo Marra M, De Lazzari M, Zorzi A, Migliore F, Zilio F, Calore C, et al. Impact of the presence and amount of myocardial fibrosis by cardiac magnetic resonance on arrhythmic outcome and sudden cardiac death in nonischemic dilated cardiomyopathy. *Heart Rhythm.* 2014;11(5):856–63.
 - 25 Malek LA, Bucciarelli-Ducci C. Myocardial fibrosis in athletes—Current perspective. *Clin Cardiol.* 2020;43(8):882–888.
 - 26 Petersen SE, Selvanayagam JB, Wiesmann F, Robson MD, Francis JM, Anderson RH, et al. Left ventricular non-compaction: Insights from cardiovascular magnetic resonance imaging. *J Am Coll Cardiol.* 2005;46(1):101–105.
 - 27 Gati S, Chandra N, Bennett RL, Reed M, Kervio G, Panoulas VF, et al. Increased left ventricular trabeculation in highly trained athletes: Do we need more stringent criteria for the diagnosis of left ventricular non-compaction in athletes? *Heart.* 2013;99(6):401–8.
 - 28 Angelini P, Cheong BY, Lenge De Rosen VV, Lopez JA, Uribe C, Masso AH, et al. Magnetic Resonance Imaging–Based Screening Study in a General Population of Adolescents. *J Am Coll Cardiol.* 2018;71(5):579–580.
 - 29 Szűcs A, Kiss AR, Gregor Z, Horváth M, Tóth A, Dohy Z, et al. Changes in strain parameters at different deterioration levels of left ventricular function: A cardiac magnetic resonance feature-tracking study of patients with left ventricular noncompaction. *Int J Cardiol.* 2021;331:124–30.
 - 30 Corrado D, Basso C, Rizzoli G, Schiavon M, Thiene G. Does sports activity enhance the risk of sudden death in adolescents and young adults? *J Am Coll Cardiol.* 2003;42(11):1959–63.
 - 31 Ferreira VM, Schulz-Menger J, Holmvang G, Kramer CM, Carbone I, Sechtem U, et al. Cardiovascular Magnetic Resonance in Nonischemic Myocardial Inflammation: Expert Recommendations. *J Am Coll Cardiol.* 2018;72(24):3158–3176.
 - 32 Friedrich MG, Sechtem U, Schulz-Menger J, Holmvang G, Alakija P, Cooper LT, et al. Cardiovascular magnetic resonance in myocarditis: A JACC White Paper. *J Am Coll Cardiol.* 2009;53(17):1475–87.
 - 33 Rajpal S, Tong MS, Borchers J, Zareba KM, Obarski TP, Simonetti OP, et al. Cardiovascular Magnetic Resonance Findings in Competitive Athletes Recovering from COVID-19 Infection. *JAMA Cardiol.* 2021;6(1):116–118.
 - 34 Starekova J, Bluemke DA, Bradham WS, Eckhardt LL, Grist TM, Kusmirek JE, et al. Evaluation for Myocarditis in Competitive Student Athletes Recovering From Coronavirus Disease 2019 With Cardiac Magnetic Resonance Imaging. *JAMA Cardiol.* 2021;6(8):945–950.
 - 35 Moulson N, Petek BJ, Drezner JA, Harmon KG, Kliethermes SA, Patel MR, et al. SARS-CoV-2 Cardiac Involvement in Young Competitive Athletes. *Circulation.* 2021;144(4):256–266. Epub 2021 Apr 17.
 - 36 Vago H, Szabo L, Dohy Z, et al. Cardiac Magnetic Resonance Findings in Patients Recovered From COVID-19: Initial Experiences in Elite Athletes. *JACC Cardiovasc Imaging.* 2021;14(6):1279–1281. Epub 2021 Dec 16.
 - 37 Bluemke DA, Achenbach S, Budoff M, et al. Noninvasive coronary artery imaging: Magnetic resonance angiography and multidetector computed tomography angiography: A scientific statement from the American Heart Association committee on cardiovascular imaging and intervention of the council on cardiovascular radiology and intervention, and the councils on clinical cardiology and cardiovascular disease in the young. *Circulation.* 2008;118(5):586–606.
 - 38 Hajhosseiny R, Rashid I, Bustin A, Munoz C, Cruz G, Nazir MS, et al. Clinical comparison of sub-mm high-resolution non-contrast coronary CMR angiography against coronary CT angiography in patients with low-intermediate risk of coronary artery disease: a single center trial. *J Cardiovasc Magn Reson.* 2021;23(1):57.

Contact

Hajnalka Vágó, M.D.
 Semmelweis University
 Heart and Vascular Center
 Gaál József út 9
 Budapest 1122
 Hungary
 Phone: +36-20-825-8058
 vago.hajnalka@med.semmelweis-univ.hu



Left Ventricular Non-Compaction: Implications for Athletes

Giuseppe Femia^{1,2}, Rajesh Puranik^{1,2}

¹Sydney Medical School, Faculty of Medicine and Health, The University of Sydney, Camperdown, NSW, Australia

²Department of Cardiology, Royal Prince Alfred Hospital, Camperdown, NSW, Australia

Abstract

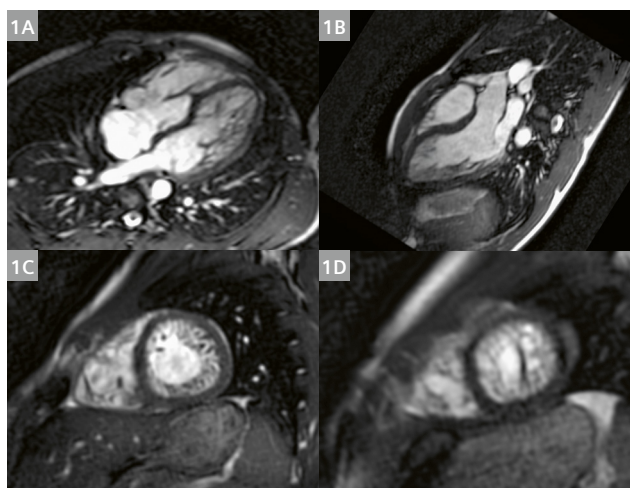
Left ventricular non-compaction (LVNC) is a complex clinical condition with no diagnostic gold standard. At present, there is uncertainty about securing the diagnosis, correlation to clinical outcomes, and long-term medical management. Furthermore, the consequences of LV hypertrabeculation in athletes is even more problematic as this may reflect an adaptive physiologic response. We review the available literature to provide clinical guidance to assist in diagnosis and patient management.

Introduction

Left ventricular non-compaction (LVNC) is an unclassified cardiomyopathy characterized by an abnormally thick trabeculated non-compacted myocardial layer with adjacent deep intra-trabecular recesses and a thin compacted myocardial layer [1]. Although the underlying etiology of LVNC remains uncertain, evidence suggests that the excessive trabeculation may result from a disturbance in the compaction process during early myocardial development [2–4].

Although specific genes have been found to contribute to LVNC, there is pronounced genetic variability and a low diagnostic yield of genetic testing [5, 6]. For some individuals, abnormal trabeculations may develop in conjunction with other cardiovascular or systemic conditions [7, 8]. In some athletes, it remains unclear whether the abnormal myocardial morphology is representative of pathological LVNC or an epiphenomenon of cardiac adaptations from increased loading conditions [9] (Fig. 1). Overall, the clinical manifestations are heterogeneous and include no symptoms, ventricular arrhythmias, left ventricular (LV) dysfunction, stroke, and/or sudden cardiac death [10].

Heightened awareness and improved imaging techniques have led to inaccurate diagnoses, clinical challenges, and unwarranted restriction from competitive sport [11, 12]. Presently, there are several criteria based on 2-dimensional echocardiographic (2D-echo) and cardiac magnetic resonance (CMR) imaging, but no diagnostic gold standard or specific clinical guidelines to help differentiate physiological hypertrabeculation from pathological LVNC [13–20]. Using a novel semi-automated thresholding CMR technique for LVNC evaluation, we have previously demon-



1 Patient with left ventricular non-compaction (LVNC);
(1A) 4-chamber CINE;
(1B) Left ventricular outflow tract (LVOT);
(1C) Short-axis CINE mid ventricular level view;
(1D) Short-axis CINE apical view

	Petersen	Jacquier	Grothoff	Captur
Year	2005	2010	2012	2013
Total patients; patients with LVNC	177; 7	64; 16	57; 12	135; 30
Age range	14 to 25 years	25 to 74 years	11 to 71 years	18 to 85 years
Description of criteria	1. 2-layered myocardium with a compacted epicardial and non-compacted endocardial layer 2. NC/C ratio ≥ 2.3 in any long-axis LV image	1. Total LV trabeculated mass $\geq 20\%$ of the global LV mass	1. Percentage of non-compacted mass $> 25\%$ 2. Total indexed myocardial mass $> 15 \text{ g/m}^2$ 3. A non-compacted to compacted myocardial ratio of $\geq 3:1$ in segments 1–3 or 7–16 excluding the apex 4. A non-compacted to compacted myocardial ratio of $\geq 2:1$ in segments 4–6	1. Fractal analysis with elevated fractal dimension, global LV trabecular complexity as a continuous variable
View	Any long-axis image	Short-axis stack	Short-axis stack	Short-axis stack
Phase	End-diastole	End-diastole	End-diastole	End-diastole
Outcomes	No	No	No	No

Table 1: CMR-based diagnostic criteria for LVNC

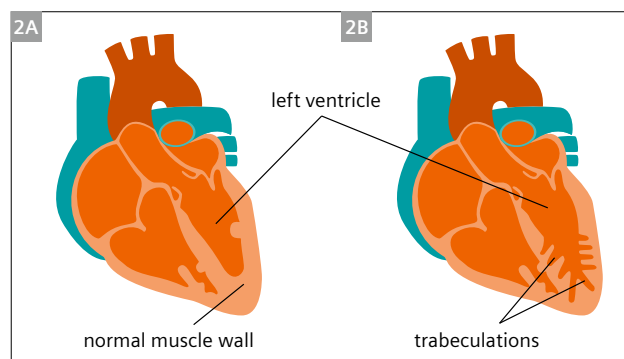
strated that impaired LV function and/or LV late gadolinium enhancement (LGE) is associated with major adverse cardiac and cerebrovascular events (MACCE), rather than non-compacted mass [21]. In this review, we discuss issues relating to CMR diagnosis and evaluation of LV hypertrabeculation, and the implications for athletes [22].

Diagnosis of hyper-trabeculation by CMR

CMR is generally used to supplement and confirm 2D-echo findings by providing better spatial resolution in all LV segments (especially the apex), detailed visualization of cardiac morphology, robust volumetrics, myocardial T1/2 mapping, and the ability to identify fibrosis with LGE. There are currently four validated CMR-based criteria, but again no gold standard has been established (Table 1).

Limitations of CMR imaging

Several concerns have been highlighted about CMR and the current criteria. First, the four criteria are based on small cohorts and the data are not prospectively derived. Even though the criteria have been shown to accurately differentiate LVNC from other cardiomyopathies, none of the criteria have been correlated to clinical outcomes. In fact, only one study showed a strong association between end-systolic measures of LVNC and adverse events such as congestive heart failure [23]. In addition, none of the current CMR-based criteria include other LV parameters



2 (2A) Normal heart. (2B) Heart with left ventricular non-compaction (LVNC) cardiomyopathy.

such as LV ejection fraction or LV scar in the assessment of LVNC, despite recent evidence showing that LV non-compaction alone is not predictive of clinical events. In a study of 113 patients with a diagnosis of LVNC, the degree of LV trabeculation has no prognostic impact over and above LV dilation, LV systolic dysfunction, and the presence of LGE [11]. In another study, the authors evaluated hyper-trabeculation in 162 consecutive patients with dilated cardiomyopathy and found that only LV ejection fraction and scar as determined by LGE were independent predictors of MACE-free survival [24]. Although CMR can more easily differentiate compacted from non-compacted myocardium throughout the entire LV cavity, the rate of diagnosis has been shown to be higher compared to 2D

echo. A recent systematic review of 59 studies reporting LVNC prevalence in adults found a higher prevalence with CMR imaging and criteria [12]. Given the poor correlation to clinical outcomes, there are concerns that not all hyper-trabeculation is pathological.

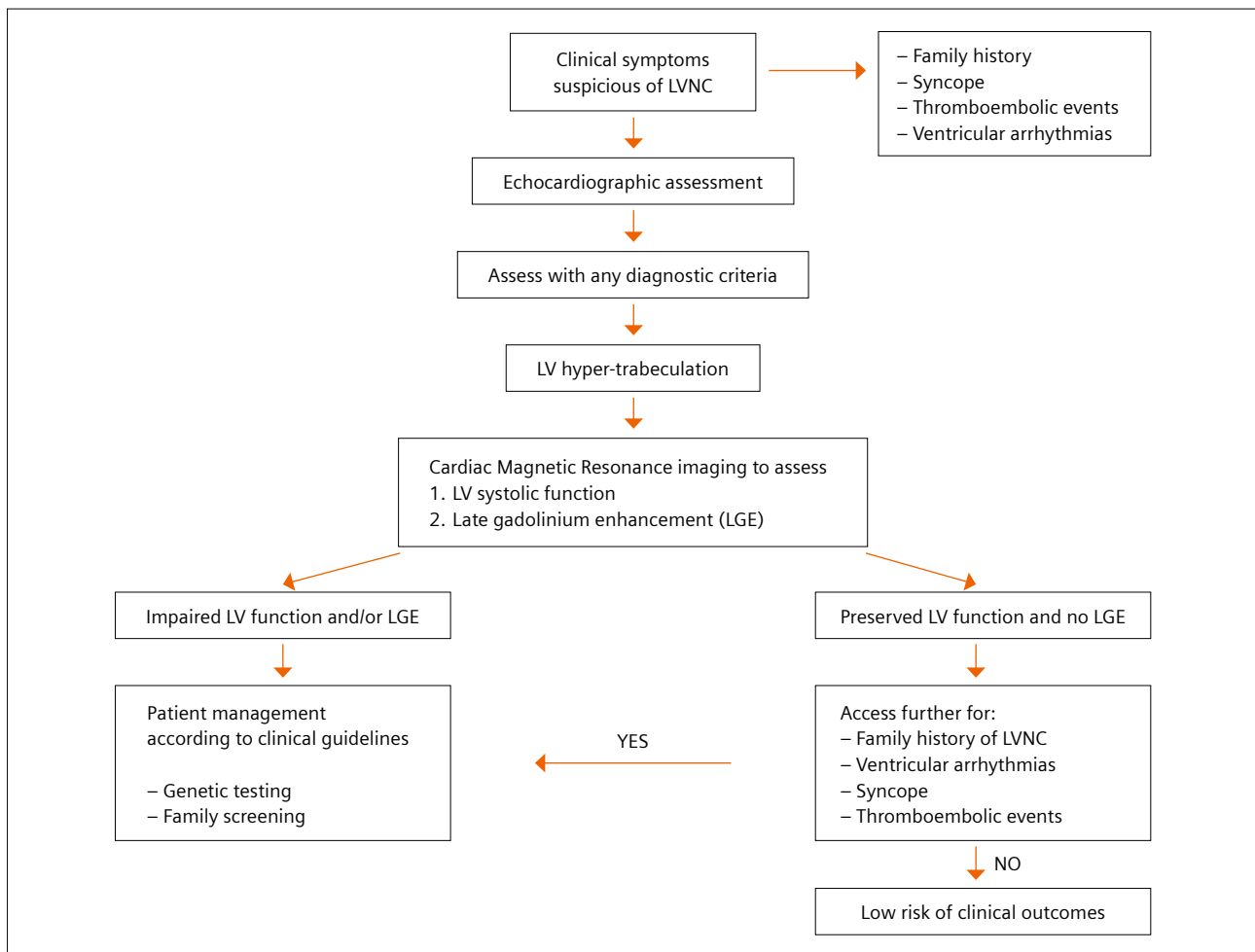
Hypertrabeculation and athletes

In the evaluation of athletes, echocardiographic studies have demonstrated a high prevalence of LV hypertrabeculation that fulfils at least one of the diagnostic criteria. The authors of the PESA study (Progression of Early Subclinical Atherosclerosis) assessed the relationship between LVNC phenotype on CMR imaging and accelerometer-measured physical activity. They found that the prevalence of LVNC phenotype according to several CMR criteria was significantly higher in those with the highest physical activity quintile [25]. The association between physical activity and LVNC phenotype was independent of LV volume. As a consequence, distinguishing pathological LVNC from

physiological remodelling remains a diagnostic challenge. In a cross-sectional echocardiographic study, a group of more than 1,100 athletes were found to have a higher prevalence of LV hypertrabeculation compared to controls (18.3% vs. 7.0%). However, during a long-term follow-up, all athletes were asymptomatic and free of adverse events [9]. In a subsequent study of more than 2,500 athletes, 36 were found to have prominent trabeculations that satisfied at least one echocardiographic criteria. Of these, only three patients were considered to be pathological with either LV dysfunction, a family history of LVNC, or a known pathogenic gene mutation [26]. Finally, in other studies there has been no reported cases of sudden cardiac death in athletes with hypertrabeculation [27, 28].

Management

Managing LVNC presents a significant clinical challenge given the variability in manifestations and the limited long-term efficacy of specific treatments. Although most



3 Diagnostic algorithm for left ventricular hyper-trabeculation

patients with LVNC remain asymptomatic, it is important to review patients regularly with cardiac imaging, as some may be at risk of heart failure, stroke, and/or sudden cardiac death. In particular, those with reduced LV function should be reviewed frequently and treated with evidence-based, guideline-directed pharmacologic therapy. For athletes, it has been suggested that only those who meet LVNC criteria with impaired LV function should be prohibited from participating in sport. Asymptomatic athletes with normal ventricular function should not have their activity restricted [29, 30].

In an effort to improve the overall diagnostic accuracy, a clinical algorithm has been developed to help guide clinicians in the assessment of patients with suspected LVNC [31]. Based on the most current evidence, we recommend all patients with hyper-trabeculation that fulfils any of the imaging-based criteria for either 2D echo or CMR should be assessed for impaired LV function and LGE. Those with normal LV function and no LGE should be screened for a family history of LVNC or sudden cardiac death (SCD), syncope, ventricular arrhythmias, and thromboembolic events to help predict the risk of adverse events and the need for further assessment. In the absence of these risk factors, patients can be reassured with less intensive long-term follow up (Fig. 3).

Conclusion

LVNC is a heterogenous condition with no universally accepted diagnostic criteria or gold standard. When evaluating patients and athletes with LVNC, it is important to take a comprehensive history, rely on more than one diagnostic method, and include LV parameters such as LV function and LGE. For those with impaired LV function and/or LGE, prohibiting vigorous sports activities should be considered and management goals should be based on clinical symptoms such as ventricular arrhythmias, syncope or thromboembolic events.

Acknowledgment

This article was adapted from the published original in *Medicina* [22].

References

- Maron BJ, Towbin JA, Thiene G, Antzelevitch C, Corrado D, Arnett D, et al. Contemporary definitions and classification of the cardiomyopathies: an American Heart Association Scientific Statement from the Council on Clinical Cardiology, Heart Failure and Transplantation Committee; Quality of Care and Outcomes Research and Functional Genomics and Translational Biology Interdisciplinary Working Groups; and Council on Epidemiology and Prevention. *Circulation* 2006;113(14):1807–16.
- Abustini E, Weidemann F, Hall JL. Left ventricular non-compaction: a distinct cardiomyopathy or a trait shared by different cardiac disease. *J Am Coll Cardiol*. 2014;64(17):1840–50.
- Risebro CA, Riley RP. Formation of the ventricles. *Scientific World Journal*. 2006;6: 1862–80.
- Sedmera D, Thompson RP. Myocyte proliferation in the developing heart. *Dev Dyn*. 2011;240(6):1322–34.
- Towbin J, Jefferies JL. Cardiomyopathies Due to Left Ventricular Noncompaction, Mitochondrial and Storage Diseases, and Inborn Errors of Metabolism. *Circ Res*. 2017;121 (7):838–854.
- Gati S, Rajani R, Carr-White GS, Chambers JB. Adult left ventricular noncompaction: reappraisal of current diagnostic imaging modalities. *JACC Cardiovasc Imaging*. 2014;7(12):1266–75.
- Gati S, Papadakis M, Papamichael ND, Zaidi A, Sheikh N, Reed M, et al. Reversible de novo left ventricular trabeculations in pregnant women: implications for the diagnosis of left ventricular noncompaction in low-risk populations. *Circulation*. 2014;130(6):475–83.
- Gati S, Papadakis M, Van Niekerk N, Reed M, Yeghen T, Sharma S. Increased left ventricular trabeculation in individuals with sickle cell anaemia: physiology or pathology? *Int J Cardiol*. 2013;168(2):1658–60.
- Gati S, Chandra N, Bennett RL, Reed M, Kervio G, Panoulas VF, et al. Increased left ventricular trabeculation in highly trained athletes: Do we need more stringent criteria for the diagnosis of left ventricular non-compaction in athletes? *Heart*. 2013;99(6):401–8.
- Andreini D, Pontone G, Bogaert J, Roghi A, Barison A, Schwitter J, et al. Long-Term Prognostic Value of Cardiac Magnetic Resonance in Left Ventricle Noncompaction: A Prospective Multicenter Study. *J Am Coll Cardiol*. 2016;68(20):2166–2181.
- Abela M, D'Silva A. Left Ventricular Trabeculations in Athletes: Epiphenomenon or Phenotype of Disease? *Curr Treat Options Cardiovasc Med*. 2018;20(12):100.
- Ross SB, Jones K, Blanch B, Puranik R, McGeechan K, Barratt A, et al. A systematic review and meta-analysis of the prevalence of left ventricular non-compaction in adults. *Eur Heart J*. 2020;41(14):1428–1436.
- Chin TK, Perloff JK, Williams RG, Jue K, Mohrmann R. Isolated noncompaction of left ventricular myocardium. A study of eight cases. *Circulation*. 1990;82(2):507–13.
- Jenni R, Oechslin E, Schneider J, Attenhofer Jost C, Kaufmann PA. Echocardiographic and pathoanatomical characteristics of isolated left ventricular non-compaction: a step towards classification as a distinct cardiomyopathy. *Heart* 2001;86(6):666–71.
- Stöllberger C, Finsterer J. Left ventricular hypertrabeculation/noncompaction. *J Am Soc Echocardiogr*. 2004;17(1):91–100.
- Gebhard C, Stähli BE, Greutmann M, Biaggi P, Jenni R, Tanner FC. Reduced left ventricular compacta thickness: a novel echocardiographic criterion for non-compaction cardiomyopathy. *J Am Soc Echocardiogr*. 2012;25(10):1050–7.
- Petersen SE, Selvanayagam JB, Wiesmann F, Robson MD, Francis JM, Anderson RH, et al. Left ventricular non-compaction. insights from cardiovascular magnetic resonance imaging. *J Am Coll Cardiol*. 2005;46(1):101–105.
- Jacquier A, Thuny F, Jop B, Giorgi R, Cohen F, Gaubert JY, et al. Measurement of trabeculated left ventricular mass using cardiac magnetic resonance imaging in the diagnosis of left ventricular non-compaction. *Eur Heart J*. 2010;31(9):1098–104.
- Grothoff M, Pachowsky M, Hoffmann J, Posch M, Klaassen S, Lehmkuhl L, et al. Value of cardiovascular MR in diagnosing left ventricular non-compaction cardiomyopathy and in discriminating between other cardiomyopathies. *Eur Radiol*. 2012;22(12):2699–709.
- Captur G, Muthurangu V, Cook C, Flett AS, Wilson R, Barison A, et al. Quantification of left ventricular trabeculae using fractal analysis. *J Cardiovasc Magn Reson*. 2013;15(1):36.
- Femia G, Zhu D, Choudhary P, Ross SB, Muthurangu V, Richmond D, et al. Long term clinical outcomes associated with CMR quantified isolated left ventricular non-compaction in adults. *Int J Cardiol*. 2021;328:235–240.
- Femia G, Semsarian C, Ross SB, Celermajer D, Puranik R. Left Ventricular Non-Compaction: Review of the Current

Diagnostic Challenges and Consequences in Athletes. *Medicina (Kaunas)*. 2020;56(12):697.

23 Stacey RB, Andersen MM, St Clair M, Hundley WG, Thohan V. Comparison of systolic and diastolic criteria for isolated LV noncompaction in CMR. *JACC Cardiovasc Imaging*. 2013;6(9):931–40.

24 Amzulescu MS, Rousseau MF, Ahn SA, Boileau L, de Meester de Ravenstein C, Vancaeraynest D, et al. Prognostic Impact of Hypertrabeculation and Noncompaction Phenotype in Dilated Cardiomyopathy: A CMR Study. *JACC Cardiovasc Imaging*. 2015;8(8):934–46.

25 de la Chica JA, Gómez-Talavera S, García-Ruiz JM, García-Lunar I, Oliva B, Fernández-Alvira JM, et al. Association Between Left Ventricular Noncompaction and Vigorous Physical Activity. *J Am Coll Cardiol*. 2020;76(15):1723–1733.

26 Caselli S, Ferreira D, Kanawati E, Di Paolo F, Picicchio C, Attenhofer Jost C, et al. Prominent left ventricular trabeculations in competitive athletes: a proposal for risk stratification and management. *Int J Cardiol*. 2016;223:590–595.

27 Harmon KG, Drezner JA, Wilson MG, Sharma S. Incidence of sudden cardiac death in athletes: a state-of-the-art review. *Br J Sports Med*. 2014;48:1185–1192.

28 Maron BJ, Doerer JJ, Haas TS, Tierney DM, Mueller FO. Sudden deaths in young competitive athletes: analysis of 1866 deaths in the United States, 1980–2006. *Circulation* 2009;119(8):1085–92.

29 Pelliccia A, Solberg EE, Papadakis M, Adami PE, Biffi A, Caselli S, et al. Recommendations for participation in competitive and leisure time sport in athletes with cardiomyopathies, myocarditis, and pericarditis: position statement of the Sport Cardiology Section

of the European Association of Preventive Cardiology (EAPC). *Eur Heart J* 2019;40(1):19–33.

30 Coris EE, Moran BK, De Cuba R, Farrar T, Curtis AB. Left Ventricular Non-Compaction in Athletes: To Play or Not to Play. *Sports Med*. 2016;46(9):1249–59.

31 Aung N, Zemrak F, Mohiddin S, Petersen S. LV Noncompaction Cardiomyopathy or Just a Lot of Trabeculations? *JACC Cardiovasc Imaging*. 2017;10(6):704–707.



Contact

Raj Puranik, MB BS, PhD, FRACP
 Clinical Associate Professor,
 The University of Sydney
 Consultant Cardiologist, Royal Prince
 Alfred Hospital and Alfred Cardiology
 100 Carillon Ave
 Camperdown NSW 2050
 Australia
 Phone: +61 2 9519 875
 raj.puranik@cmrs.org.au



Giuseppe Femia, BSc, MBBS, PhD,
 FRACP, FCSANZ
 The University of Sydney
 Australia
 giuseppe.femia@sydney.edu.au

Advertisement

Prepare your patients mentally for their MRI exam

Most patients who undergo an MRI exam, experience some level of anxiety. As a result, some move so much that they cause motion artifacts, cannot complete the scan, or do not even show up for the exam. Up to 75%¹ of all unsatisfactory scan outcomes can be eliminated by educating patients on the MRI exam.

Tap the full potential of your facility by preparing your patients for the scan with our patient education toolkit. A **video**, **poster**, **meditation**, and a **book for children** explain the process of an MRI exam in simple words and answer common questions:

- What does an MRI exam entail?
- What is important when having an MRI exam?
- What does an MRI exam feel like?




Download the patient education toolkit in your preferred language here:
siemens-healthineers.com/mri-patient-education

¹Törnqvist, E., Månsson, A., Larsson, E.-M., & Hallström, I. (2006). Impact of extended written information on patient anxiety and image motion artifacts during magnetic resonance imaging. *Acta Radiologica*, 47(5), 474–480. <https://doi.org/10.1080/02841850600690355>.

Cardiovascular Magnetic Resonance. Late Gadolinium Enhancement Imaging: A Technologist's Guide

Benny Lawton

Executive Cardiac MR radiographer, Advanced Diagnostics, St Joseph's Hospital, Malpas, Newport, Wales, UK

Introduction

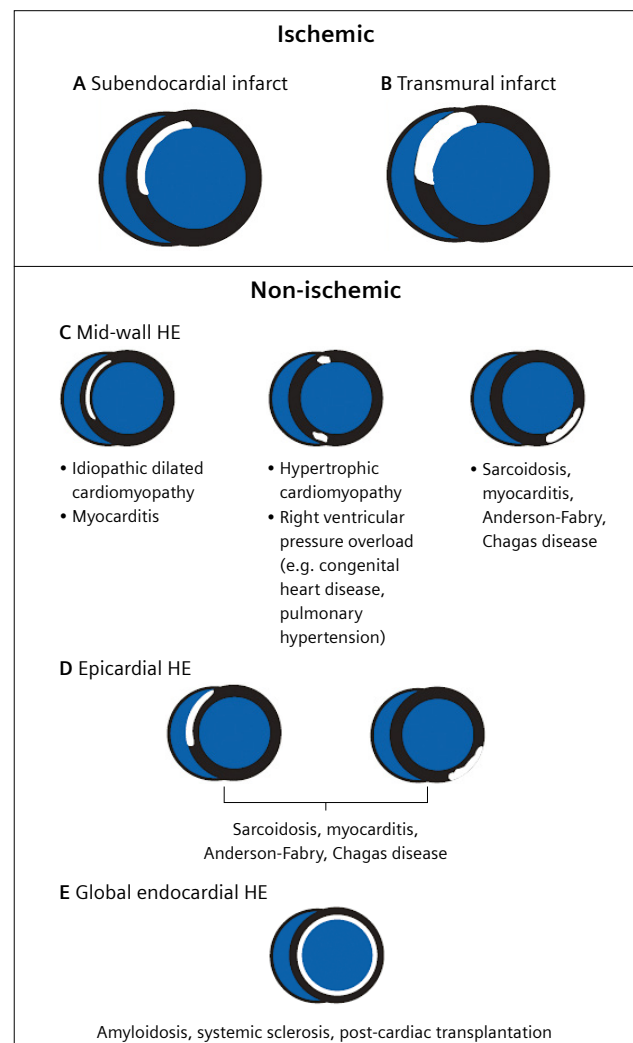
There is little doubt that one of the many great strengths of cardiac MRI (CMR) is its ability to assess tissue characterization within the myocardium. A key event in the evolution of CMR was first reported by M Saeed et al. in 1989. They described the technique of using T1-weighted MR images after the administration of an intravenous contrast injection to differentiate between healthy and infarcted myocardium [1]. Over 30 years later, this practice is now well established and provides vital prognostic and pathological information to guide patient management. The technique is now commonly referred to as late gadolinium enhancement (LGE) and is firmly established in nearly all CMR protocols.

Clinical application

The LGE technique is used to characterize various cardiac pathologies. By demonstrating the location of the scar/fibrosis, it is possible to distinguish ischemic from non-ischemic cardiac disease. In the early stages of ischemic infarction, scar will develop in the inner band of myocardium adjacent to the blood pool (subendocardial myocardium), and then over time spread to the outer wall of the myocardium (epicardium). Once this has occurred, the scar will now be present across the whole thickness of the myocardium (trans-mural). By visualizing the various patterns of fibrosis and scar in the myocardium, it is possible to classify many different non-ischemic cardiomyopathies. These different patterns of scar were very nicely illustrated by Mahrholdt et al. in 2005 [2] (Fig. 1).

Imaging technique

As users of technology from Siemens Healthineers, we have many options available to us when acquiring LGE images. In general practice, a 2D segmented inversion



1 Mahrholdt et al. [2] illustrate the different locations and patterns of myocardial scar, and the associated cardiac diseases. *Reproduced with permission from [2].*

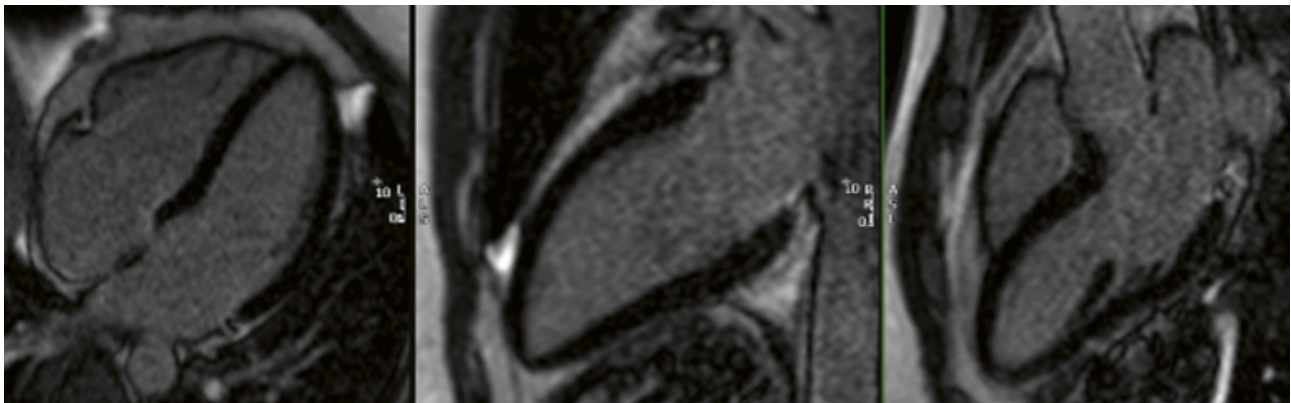
recovery (IR) gradient echo (GRE) or balanced steady state free precession (bSSFP) pulse sequence is used (Fig. 2). The LGE images should be acquired in all three long-axis positions, and a stack of short-axis images to include both ventricles. Two right ventricular long-axis imaging positions may also be required, depending on the imaging protocol. When positioning and acquiring your LGE images, it is of paramount importance that these images are prescribed in the same position as the cinematography and tissue characterization sequences. This will allow the reporting clinicians to effectively compare all the different sequences at the same position in the heart. A uniform slice thickness, slice gap, and field of view applied to all sequences will aid this process and provide consistent imaging throughout the CMR study.

Data acquisition for our LGE sequences should be set to late diastole to ensure that we are imaging when the myocardium is fully relaxed and motionless. Clicking on the Capture Cycle icon in the physio card will set our TR and acquisition window to the appropriate position in the heartbeat (Fig. 3). Always ensure that data collection does

not occur on top of the second R wave or within the next heartbeat, as this will cause a cardiac motion ghosting artifact on the images.

Inversion time

Setting the correct inversion time is a critical component of acquiring diagnostic and high-quality images. As already mentioned, the purpose of this technique is to identify areas of high signal (scar) within the myocardium. For this to be easily visualized, the healthy myocardium should be black, with a low signal. This technique is known as nulling the myocardium. After the administration of gadolinium, the magnetization of the healthy myocardium will fall below the level of 0. Over time, as the gadolinium washes out of the healthy myocardium, the magnetization will begin to increase. The perfect time to image the myocardium is when the magnetization is at 0 and therefore nulling the signal from healthy myocardium. Figure 4 [3] shows that when the healthy myocardium is nulled, the necrotic tissue will have a higher magnetization value, as the gadolinium present within it has shortened the T1 relaxation time.



2 LGE imaging using a 2D segmented PSIR sequence prescribed in 4C, 2C, and 3C long-axis orientations.



3 Screenshot of the physio signal window on a 1.5T MAGNETOM Sola. The green column in the heartbeat shows the optimal data acquisition time for an LGE sequence.

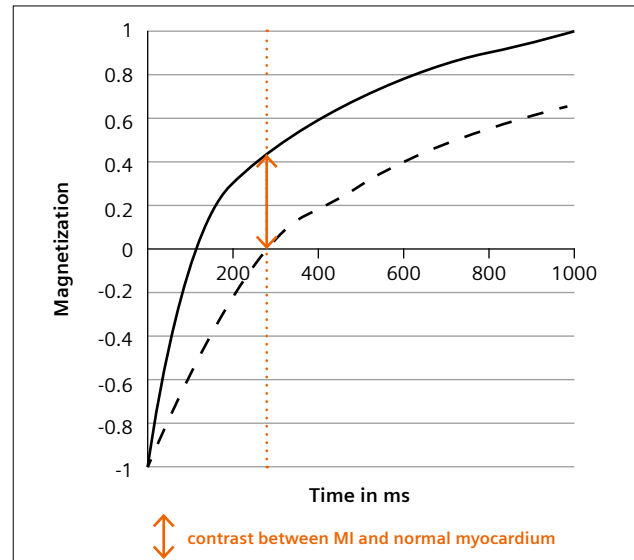
Necrotic tissue will therefore have a bright signal compared to the dark, healthy myocardium.

The TI scout sequence should be used approximately 7–10 minutes after administering the gadolinium. This valuable sequence will provide several images with different TI times, usually at intervals of between 20 and 80 milliseconds (Fig. 5). Scroll through the stack of images and simply choose the image in which the myocardium appears as black as the lung fields. Note the TI time displayed on this image and type it into the physio card for your LGE sequences.

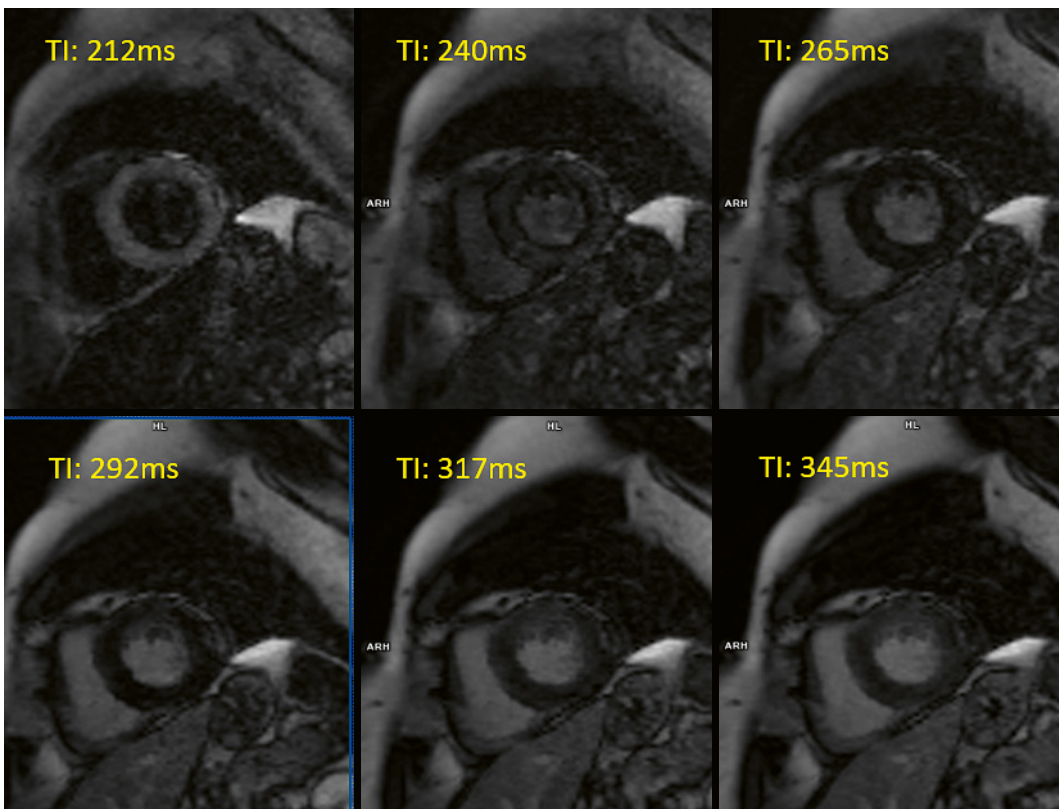
The TI scout is a valuable educational tool when learning how to null the myocardium and for differentiating between images that have an inversion time which is too low or too high. By studying the images, you will learn to understand the subtle differences of when an LGE image has an incorrect TI and how to correct it. An image which demonstrates a low TI will display a tramline nulling pattern. The myocardium will have a high signal, but at the endocardium and epicardium borders you will clearly see two dark lines circumferentially (Fig. 6). When a TI is set too high, the whole myocardium will have a homogenic high-signal appearance (Fig. 7).

It is essential that technologists understand several significant factors which influence the TI value of healthy myocardium. The contrast dose is the first consideration. In the 2020 update of its standardized cardiovascular magnetic resonance imaging (CMR) protocols [4], the Society

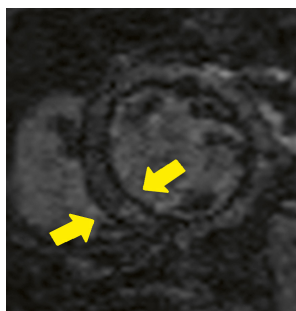
for Cardiovascular Magnetic Resonance (SCMR) recommends that a gadolinium contrast dose of between 0.1 and 0.2 mmol/kg (body weight) is given to the patient. In practice, a single dose of 0.1 mmol/kg is often used, but this remains at the discretion of the local clinicians and protocols. If a standard dose of 0.1 mmol/kg is admin-



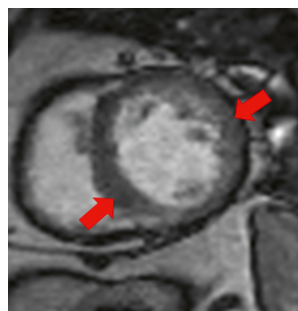
4 The dotted line represents the T1 relaxation time of healthy myocardium, whereas the solid line represents necrotic tissue.



5 TI scout images showing ascending TI measurements.



6 SA LGE image showing tramline nulling pattern (yellow arrows) as the TI is too low.



7 SA LGE image showing homogenic high signal in the myocardium as the TI is too high.

istered, LGE imaging will commence approximately 10 minutes after the injection. If imaging is started too early, the blood pool and healthy myocardium will both contain gadolinium, resulting in similarly high signal intensities. This will reduce the contrast between the subendocardial border of the myocardium and blood-pool interface, and therefore limit the ability to diagnose scar tissue in this region. Imaging too early will also make it impossible to appropriately null the healthy myocardium.

The age and physical nature of the patient can sometimes influence the wash-out time of the gadolinium contrast. In my experience, tall, thin, and younger adults will wash out contrast sooner than others. It is therefore prudent to perform a TI scout slightly earlier than you would normally, to avoid missing the optimal imaging window. I would also recommend starting LGE imaging slightly earlier in patients who have undergone a vasodilated stress perfusion examination, as this technique will also increase gadolinium wash-out.

Tips and tricks for successful LGE imaging

Cross-cut and phase-swap imaging

As described earlier in this article, scar/fibrosis can be described in a variety of sizes and locations within the myocardium. If a large amount of scar/fibrosis is present, it will be easy to detect and diagnose. However, in many cases there are subtle focal areas of scar/fibrosis which may be less identifiable. It is therefore important for technologists to be suspicious of all small areas of high signal within a properly nulled myocardium. It is our duty to help determine if this finding is a pathology or an artifact. There are two techniques which will assist us in verifying if an area of high signal is true scar/fibrosis or an imaging artifact.

The first technique is known as cross-cutting and should be used when detecting a small focal area of high

signal, even if you are confident that it is scar/fibrosis. Simply position your LGE sequence perpendicular to the area of high signal so that the new image is orthogonal to the original image. You can see from the example below (Fig. 8) that this technique will effectively demonstrate the area of high signal and provide detailed information on the total size and location of the scars/fibrosis. Figure 8 also shows that when a cross-cut slice is positioned from a short-axis image, it will provide additional information which is not necessarily identifiable on the original three long-axis images.

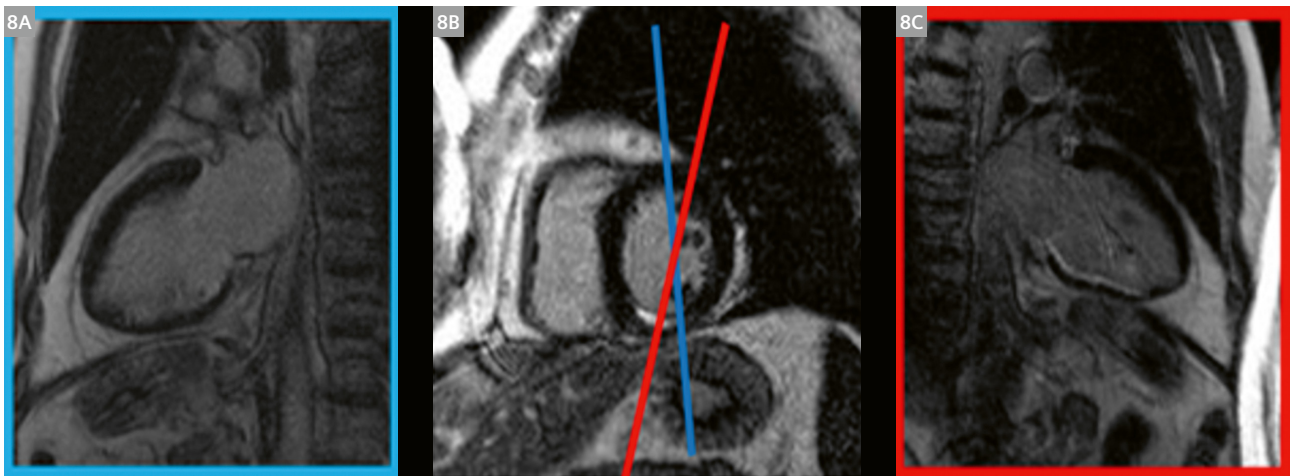
The phase-swap technique is required when there are areas of high signal across the heart which have the appearance of a ghosting artifact. By changing the phase-encoding direction when acquiring the image for a second time, any artifacts will move away from the area of interest. If an area of high signal does not change, you have proven that it is not an artifact and can be considered a true physiological finding. The example below (Fig. 9) shows how a ghosting artifact from a large pleural effusion has ghosted across the heart. By changing the phase-encoding direction, the artifact moved away from the heart. It is paramount that no artifacts are present on the images as they can result in a false-negative or false-positive diagnosis.

Fast imaging to reduce motion artifacts

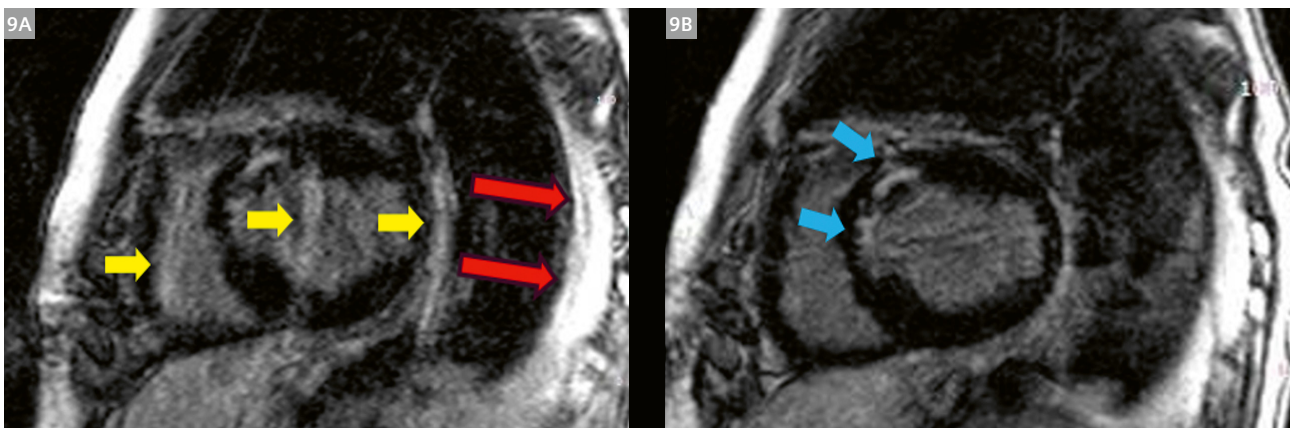
Like all CMR sequences, the 2D segmented LGE sequence will be negatively affected by motion artifacts. However, Siemens Healthineers provides us with imaging solutions which can deliver good-quality diagnostic images in the most challenging of patients.

The single-shot phase-sensitive inversion recovery (PSIR) sequences have been part of our protocols for many years. They provide a quick and easy solution for imaging patients who cannot hold their breath, are arrhythmogenic, or both. Clinically, I always run this sequence right after the TI scout as a free-breathing SA stack to provide immediate diagnostic LGE information of the whole myocardium in under 30 seconds. We then apply the 2D segmented LGE sequence in the three LA slice positions. Using the single-shot SA stack immediately gives you the safety net of having acquired the important LGE data just in case the patient aborts the scan prematurely. The single-shot images provide good temporal and spatial resolution, which means some clinicians are happy to report their findings on these images alone. However, in some patients where there may be subtle areas of scar/fibrosis, or the image quality is average, using a full SA stack of 2D segmented PSIR images will be required. Figure 10 shows an example of a single-shot SA stack image set.

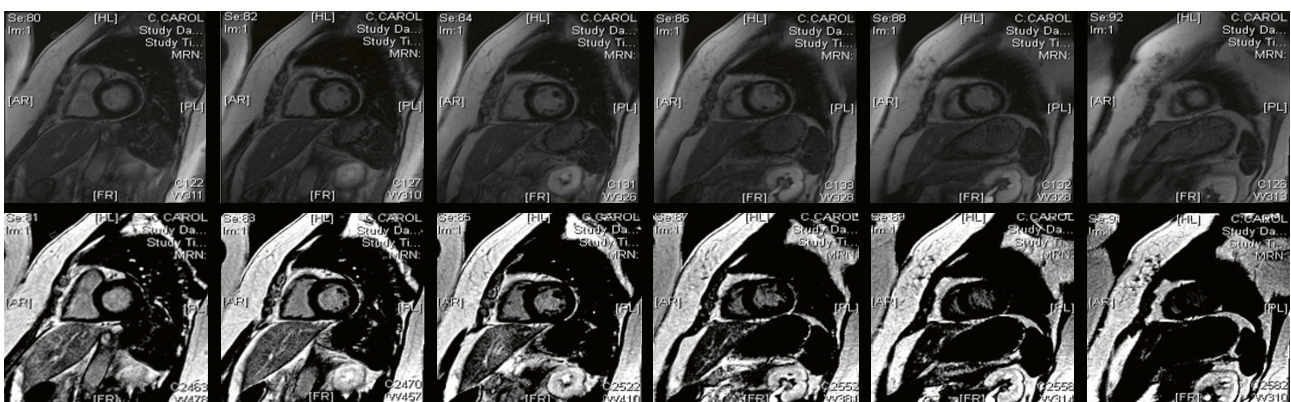
The latest, state-of-the-art LGE sequence to be released by Siemens Healthineers is called PSIR HeartFreeze.



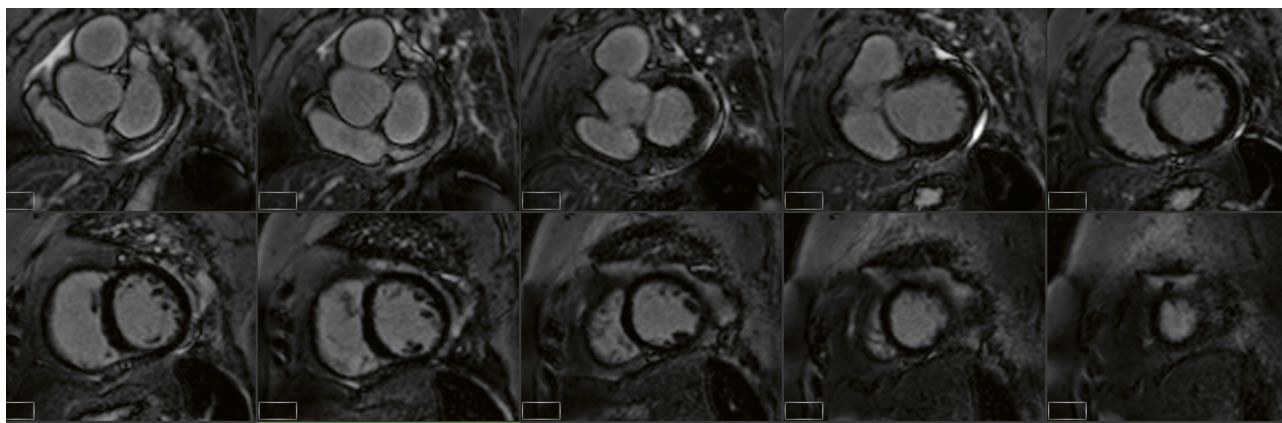
8 (8A) LGE short-axis image showing a small focal area of high signal in the inferior wall. The red line demonstrates a cross-cut slice position perpendicularly through the area of high signal. (8B) The resulting cross-cut image demonstrates a sub endocardial area of scar along the inferior wall. (8C) This image shows how the scar could have been missed by an ill-positioned 2C slice, which is demonstrated by the blue line on image (8A).



9 Image (9A) shows a large pleural effusion (red arrows) which is causing ghosting artifacts (yellow arrows) across an SA LGE image. Image (9B): After changing the phase-encoding direction and repeating the image, the ghosting artifact has been removed. Importantly, the two areas of focal scar in the septal myocardium have remained unchanged, therefore verifying that they are not artifact but rather a true pathology.



10 A selection of images taken for a short-axis stack using a single-shot PSIR LGE sequence. Top row: Phase images. Bottom row: Magnitude images.



11 A short-axis stack acquired using a single-shot PSIR HeartFreeze LGE sequence in a patient with atrial fibrillation. These images are the phase reconstruction using a motion-corrected algorithm.

It benefits from a newly developed motion compensation algorithm which provides high-resolution LGE imaging in a free-breathing acquisition. This sequence has proven to be a game changer for LGE imaging, with clinicians across the world now using it as part of their standard protocol. A study by Captur et al. [5] found greater reporting concordance and confidence when using the motion-correction free-breathing PSIR–SSFP sequence compared to a segmented PSIR–FLASH breath-hold sequence. The new sequence was also shown to reduce overall scanning time, which has paved the way for the development of a rapid CMR protocol. For those departments that still prefer to use a 2D segmented sequence for their patients, PSIR HeartFreeze offers a reliable alternative in acquiring good-quality images in patients who cannot hold their breath or are arrhythmogenic. Figure 11 displays LGE images that are good quality despite the data being acquired from a patient in atrial fibrillation.

Conclusion

In this article I have endeavored to describe the unique imaging method of LGE, which is an essential element in the CMR service. I have illustrated several imaging intricacies and offered advice to technologists on how to acquire good-quality images. As MRI technology evolves, so will our imaging practices. Siemens Healthineers continues to lead the way in developing and advancing its MRI hardware and software technologies. As well as benefiting our patients, this also provides robust, reproducible, and user-friendly imaging strategies and solutions for all CMR technologists and clinicians to employ and enjoy.

Acknowledgements

I would like to thank Dr Jonathan Rodrigues and Dr Amardeep Dastidar for their editorial contributions.

References

- 1 Saeed M, Wagner S, Wendland MF, et al. Occlusive and reperfused myocardial infarcts: differentiation with Mn-DPDP-enhanced MR imaging. *Radiology*. 1989;172(1):59-64.
- 2 Mahrholdt H, Wagner A. Delayed enhancement cardiovascular magnetic resonance assessment of non-ischaemic cardiomyopathies. 2005. *Eur Heart J*. 2005;26(15):1461-74.
- 3 Vogel-Claussen J, Rochitte KC, Wu IR, et al. Delayed Enhancement MR Imaging: Utility in Myocardial Assessment. *Radiographics*. 2006;26(3):795-810.
- 4 Kramer CM, Barkhausen J, Bucciarelli-Ducci C, et al. Standardized cardiovascular magnetic resonance imaging (CMR) protocols: 2020 update. *J Cardiovasc Magn Reson*. 2020;24;22(1):17.
- 5 Captur G, Lobascio I, Ye Y, et al. Motion-corrected free-breathing LGE delivers high quality imaging and reduces scan time by half: an independent validation study. *Int J Cardiovasc Imaging*. 2019;35(10):1893-1901.



Contact

Benny Lawton
Executive Cardiac MR radiographer
Advanced Diagnostics
St Joseph's Hospital
Harding Avenue, Malpas
Newport NP20 6ZE, Wales
United Kingdom
bennylawton@stjosephshospital.co.uk

High Spatial Resolution Coronary Magnetic Resonance Angiography: A Single Center Experience

Reza Hajhosseiny¹; Aurélien Bustin¹; Imran Rashid¹; Gastao Cruz¹; Karl P. Kunze^{1,2}; Radhouene Neji^{1,2}; Ronak Rajani³; Claudia Prieto¹; René M. Botnar¹

¹School of Biomedical Engineering and Imaging Sciences, King's College London, London, United Kingdom

²MR Research Collaborations, Siemens Healthcare Limited, Frimley, United Kingdom

³School of Cardiovascular Medicine and Sciences, King's College London, London, United Kingdom

Abstract

Coronary magnetic resonance angiography (CMRA) could potentially offer a safe, non-invasive alternative for the anatomical assessment of coronary artery disease (CAD), which is free of ionizing radiation and iodinated contrast agents. However, image acquisition with conventional free-breathing CMRA frameworks is limited by long and unpredictable scan times, whilst image degradation due to respiratory motion remains a challenge. Here we outline a CMRA framework, that aims to overcome some of these challenges by incorporating a highly undersampled Cartesian acquisition with a two-dimensional (2D) image navigator to enable 100% respiratory scan efficiency, 2D translational motion correction, and three-dimensional (3D) non-rigid motion estimation, which is then fully reconstructed using a 3D patch-based low-rank regularization framework (PROST)¹. We recently validated this framework against coronary computed tomography angiography (CCTA) in a single-center trial of 50 patients with suspected CAD. Diagnostic image quality was obtained in 95% of all coronary segments. The sensitivity, specificity, and negative predictive value were as follows: per-patient, 100%, 74%, and 100%; per-vessel, 81%, 88%, and 97%; and per-segment, 76%, 95%, and 99%, respectively. These findings emphasize the growing potential of this CMRA framework as a viable alternative to CCTA and invasive X-ray angiography for the anatomical assessment of CAD.

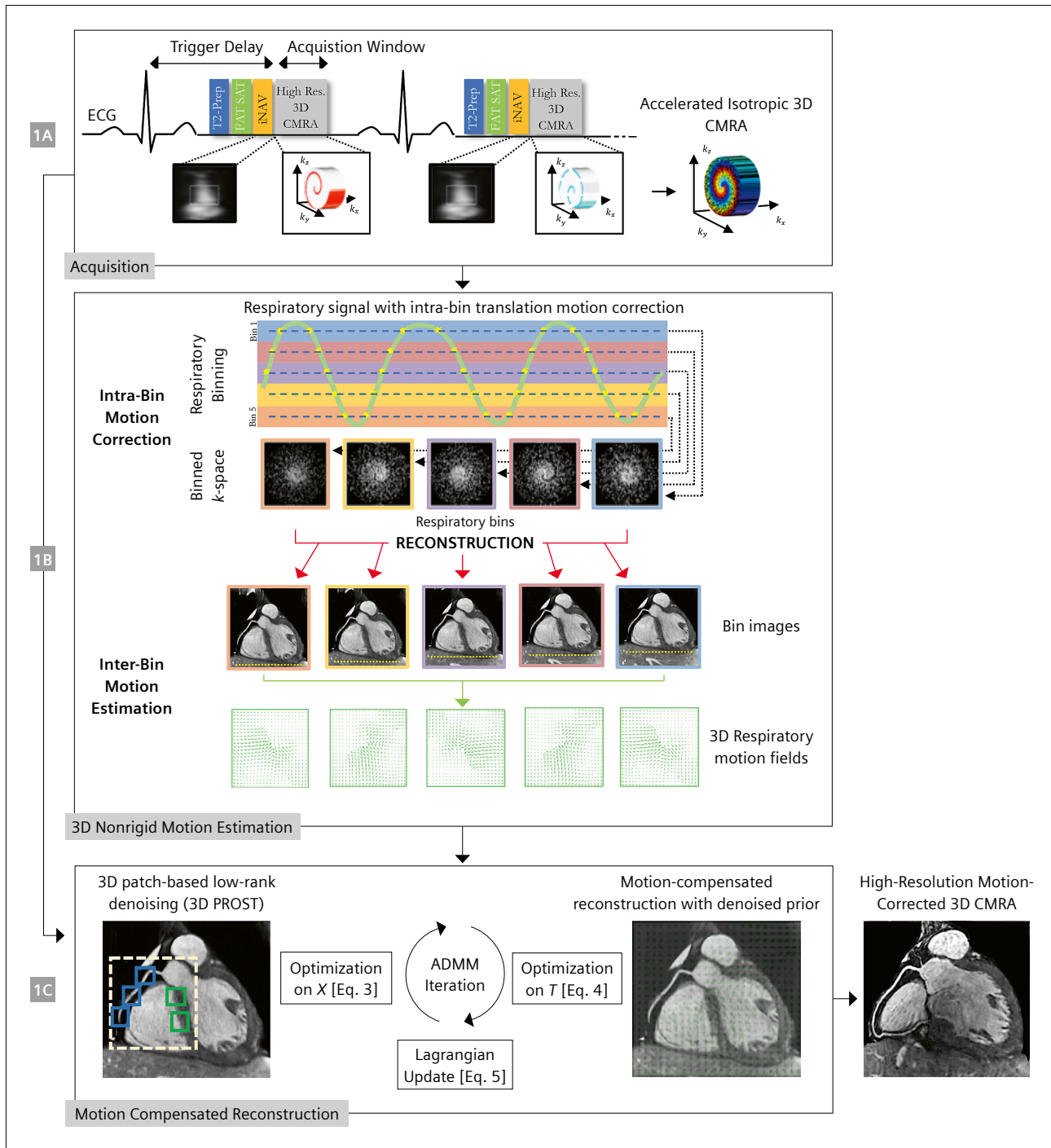
Introduction

Cardiovascular disease is the leading cause of mortality worldwide [1]. Among all causes of cardiovascular disease, atherosclerotic coronary artery disease (CAD) accounts for approximately half of all cases [1]. The early detection and long-term monitoring of CAD enable targeted risk stratification and prophylactic treatment of patients most at risk of progressing toward acute coronary syndromes. Invasive X-ray coronary angiography and non-invasive coronary computed tomography angiography (CCTA) are the gold standard imaging modalities for the assessment of CAD [2–7]. Despite being highly diagnostic, X-ray coronary angiography is limited by invasive complications (e.g., death, stroke, myocardial and vascular injury, pain, and bleeding), whilst both X-ray coronary angiography and CCTA are limited by the risks from ionizing radiation and contrast-mediated nephropathy. There is therefore a clear need for an alternative imaging modality for the early detection and long-term monitoring of CAD, which is free of the risks associated with X-ray coronary angiography and CCTA.

Coronary magnetic resonance angiography

Cardiovascular magnetic resonance (CMR) could be a safe, non-invasive alternative for the imaging of coronary artery stenosis without ionizing radiation or iodinated contrast

¹Work in progress. The application is currently under development and is not for sale in the U.S. and in other countries. Its future availability cannot be ensured.



1 Schematic overview of the proposed accelerated free-breathing 3D CMRA acquisition with sub-millimeter isotropic resolution, 100% scan efficiency, and non-rigid motion-compensated PROST reconstruction. **(1A)** CMRA acquisition is performed with an undersampled 3D variable density spiral-like Cartesian trajectory with golden angle between spiral-like interleaves (VD-CASPR), preceded by 2D image navigators (iNAV) to allow for 100% scan efficiency, and beat-to-beat translational respiratory-induced motion correction of the heart. **(1B)** Foot-head respiratory signal is estimated from the 2D iNAVs and used to assign the acquired data to 5 respiratory bins and translation-corrected respiratory bins. Subsequent reconstruction of each bin is performed using soft-gated SENSE, and 3D non-rigid motion fields are then estimated from the 5 reconstructed datasets. **(1C)** The final 3D whole-heart motion-corrected CMRA image is obtained using the proposed 3D patch-based (PROST) non-rigid motion-compensated reconstruction.

Abbreviations: CMRA = coronary magnetic resonance angiography; PROST = patch-based undersampled reconstruction;

ADMM = alternating direction method of multipliers.

Adapted and reproduced with permission from Bustin et al. [22].

agent. Large multi-center studies have demonstrated the clinical potential of coronary magnetic resonance angiography (CMRA) against X-ray coronary angiography for the anatomical assessment of CAD with per-patient sensitivity, specificity, and negative predictive value of up 94%, 82%, and 92% respectively [8–10]. However, widespread clinical implementation of CMRA is currently limited to suspected anomalous coronary arteries, suspected coronary artery aneurysms (e.g., Kawasaki's disease), coronary artery graft patency assessment, assessment of the proximal coronary arteries, and patients with renal impairment who are unable to receive iodinated contrast [11–13]. The very limited and specific clinical use of CMRA is due to long and unpredictable acquisition times, cumbersome scan planning, lower spatial resolution (usually 1–2 mm anisotropic), and motion-related (cardiac, respiratory, and patient) degradation of image quality.

In a similar fashion to CCTA, CMRA overcomes cardiac motion artifacts by using prospective electrocardiographic (ECG) gating to acquire data during the quiescent phase of the cardiac cycle when coronary artery motion is minimal [11], usually in mid-to-late diastole. In cases of cardiac arrhythmias and variable heart rates, which disproportionately impact the diastolic phase of the cardiac cycle, systolic imaging is the preferred option [11]. An alternative retrospective ECG gating approach is to continuously acquire data throughout the cardiac cycle and then reconstruct multiple cardiac phases and select the phase with the sharpest images or fewest motion artefacts [14, 15].

To compensate for the respiratory motion artifacts during free-breathing acquisitions, conventional CMRA estimates the respiratory displacement and deformation of the heart and surrounding tissues using the diaphragmatic 1D navigator approach [11, 16–18]. Here the liver-diaphragm interface lends itself for motion tracking, with the increased signal-to-noise ratio (SNR) of the right hemi diaphragm used as a surrogate to track the superior-inferior motion of the heart during the respiratory cycle, and with respiratory gating enabled to obtain image data at the quiescent phase of end of expiration [16, 19, 20, 17]. However, there is a non-linear relationship between the displacement of the diaphragm and the heart, requiring a patient-specific correction factor, which is usually set at 0.6 (population average) when gating is combined with respiratory motion correction [16]. Furthermore, only data within a small (end-expiration) respiratory gating window is accepted, significantly reducing scan efficiency and leading to prolonged and unpredictable acquisition times [21]. Moreover, prospective or retrospective translational motion compensation can only be applied in the superior-inferior direction [21]. Finally, this approach

adds complexity as detailed scan planning and defining separate imaging parameters for the navigator acquisition are required, further increasing scan time and costs [16]. In addition, a fully sampled 3D whole-heart CMRA acquisition at high spatial resolution is associated with long acquisition times (up to 30 minutes), regardless of cardiac and respiratory motion gating, which leads to patient discomfort and patient-related motion artifacts.

To overcome these limitations, we have leveraged recent advances in CMR technology including trajectory design, motion correction, and undersampled reconstruction techniques – to propose a novel, highly accelerated, high-spatial-resolution (sub-1 mm³), free-breathing, non-contrast, 3D whole-heart CMRA framework in a clinically feasible and 100% predictable acquisition time.

Proposed coronary magnetic resonance angiography framework

The proposed CMRA framework was developed on a 1.5T CMR scanner (MAGNETOM Aera, Siemens Healthcare, Erlangen, Germany) with a dedicated 32-channel spine coil and an 18-channel body coil. It combines a highly undersampled variable-density Cartesian acquisition with an image navigator (iNAV) to enable model-free 2D translational and 3D non-rigid motion estimation, and finally deploys a motion-corrected 3D patch-based low-rank image reconstruction (PROST) algorithm¹ to reconstruct the undersampled acquisition. These steps are outlined in more detail in the following sections and in the article by Bustin et al. [22].

Accelerated CMRA acquisition

An undersampled (3- to 4-fold) free-breathing 3D whole-heart, balanced steady-state free-precession (bSSFP) sequence with a 3D variable-density spiral-like Cartesian trajectory (VD-CASPR) with golden-angle step was employed as previously proposed [23] (Fig. 1). A low-resolution 2D iNAV preceded each spiral-like interleave to allow 100% scan efficiency, predictable scan time, and 2D translational motion estimation of the heart on a beat-to-beat basis. The 2D iNAVs were obtained by spatially encoding the startup profiles of the bSSFP sequence [24]. A spectrally selective SPIR (Spectral Presaturation with Inversion Recovery) fat saturation pulse with a constant flip angle (FA) of 130° was used to improve coronary depiction and minimize fat-related aliasing artifacts. An adiabatic T₂ preparation pulse [25, 26] was played at each heartbeat in order to enhance the contrast between blood and cardiac muscle and to avoid the use of extracellular contrast agents.

¹Work in progress. The application is currently under development and is not for sale in the U.S. and in other countries. Its future availability cannot be ensured.

Beat-to-beat 2D translational motion estimation

Beat-to-beat 2D translational motion correction was performed as previously proposed in [27, 28]. Briefly, foot-head (FH) and right-left (RL) translational respiratory motion of the heart was extracted from the iNAVs using a template-matching algorithm with normalized cross-correlation as similarity measure [24]. The reference template was manually selected during scan planning on a region encompassing the subject's heart. The FH respiratory signal was used to sort the acquired data into five respiratory states or bins. Intra-bin 2D translational motion estimation was performed by correcting the data for each bin to the same respiratory position (taken as the bin center) (Fig. 1). This correction was implemented by modulating the k -space data with a linear phase shift according to the previously estimated respiratory motion [27].

Bin-to-bin non-rigid motion estimation

In this framework, the acquired 3D CMRA data is under-sampled (3- to 4-fold), with the resulting binned k -spaces being highly accelerated (~15- to 20-fold). Soft-gating iterative sensitivity encoding reconstruction [27] was employed to reconstruct each respiratory bin. Bin-to-bin 3D non-rigid motion estimation was subsequently performed using spline-based free-form deformation [29], considering the end-expiration bin as reference image (Fig. 1).

3D patch-based non-rigid motion-compensated reconstruction (non-rigid PROST)

Following this step, the estimated 3D non-rigid motion fields are then directly incorporated into a general matrix description reconstruction framework [30, 31]. In contrast to previous CMRA studies where the data are acquired either fully sampled [27] or with modest undersampling factors [28], our proposed high-resolution (0.9 mm³) CMRA framework exploits higher undersampling factors (3- to 4-fold) to reach approximately 10-minute acquisition time. 3D patch-based low-rank undersampled reconstruction (3D PROST) has been proposed to highly accelerate sub-mm CMRA imaging with translational motion correction only [23]. 3D PROST reconstruction exploits the inherent redundancies of the complex 3D anatomy of the coronary arteries on a local (i.e., within a patch) and non-local (i.e., between similar patches within a neighborhood) basis, through an efficient iterative low-

rank decomposition and singular value thresholding. The proposed non-rigid PROST framework combines 3D PROST with the matrix formalism for non-rigid motion correction, and can be formulated as the unconstrained optimization (found at the bottom of the page), where X is the non-rigid motion-corrected 3D CMRA volume (or "motion-free" image), K is the 2D translational motion-corrected k -space data, E is the encoding operator composed of: A_b the sampling matrix for bin b , F the 3D Fourier transform, S_c the coil sensitivities for coil c , U_b the estimated 3D non-rigid motion fields for bin b and N_{bins} the number of respiratory bins. $\| \cdot \|_F$ and $\| \cdot \|_*$ denote the Frobenius and nuclear norms respectively, $P_p(\cdot)$ is the patch-selection operator at voxel p . Equation (1) can be efficiently solved by operator-splitting via alternating direction method of multipliers (ADMM).

Results from a single-center clinical study

The proposed CMRA framework was assessed in a cohort of patients with suspected CAD at Guy's and St Thomas' Hospitals, London, UK. The full results of this clinical study are described in the article by Hajhosseiny et al. [32]. In summary, 50 consecutive patients between 35 and 77 years of age who were referred for a clinically indicated CTCA were invited to undergo a CMRA within the proposed framework. In the absence of contraindications, each patient was treated with intravenous metoprolol in 5 mg increments with a maximum dose of 30 mg, aiming for a target heart rate (HR) < 65 bpm in order to maximize the diastolic acquisition window, reduce HR variability and cardiac motion artefacts. All patients were given 800 mg of sublingual glyceryl trinitrate to promote coronary vasodilation. To assess diagnostic performance, significant coronary stenosis was visually defined as luminal narrowing of $\geq 50\%$ in each of the coronary segments using an intention-to-read approach. The image quality of CMRA images (3D whole-heart dataset and individual vessels) was evaluated using the following scale: 0, non-diagnostic; 1, poor (limited coronary vessel visibility or noisy image); 2, average (coronary vessel visible but diagnostic confidence low); 3, good (coronary artery adequately visualized and diagnostic quality image); and 4, excellent (coronary artery clearly depicted).

All CMRA acquisitions were successfully completed in an imaging time of 10.7 ± 1.4 min (range 8.0–13.3 min), with 100% respiratory scan efficiency. All CMRA acquisi-

$$\textcircled{1} \quad L_{NR-PROST}(X, T, Y) := \underset{X, T_p, Y}{\operatorname{argmin}} \left\| EX - K \right\|_F^2 + \lambda \sum_p \left\| T_p \right\|_* + \frac{\mu}{2} \sum_p \left\| T_p - P_p(X) - \frac{Y_p}{\mu} \right\|_F^2$$

$$\textcircled{2} \quad E = \sum_b^{N_{bins}} A_b F S_c U_b$$

tions were performed in diastole with an average acquisition window of 88 ± 8 ms (range 81–111 ms). Mean age was 55 ± 9 years, 33/50 (66%) were male, and 12/50 (24%) had significant CAD on CTCA.

In total, 95% of CMRA segments were deemed diagnostic, while all left main stem segments were diagnostic on CMRA. Furthermore, 97%, 96%, and 87% of right coronary artery, left anterior descending artery, and left circumflex artery segments were diagnostic on CMRA. Finally, 97%, 97%, and 90% of proximal, middle, and distal CMRA segments were of diagnostic quality.

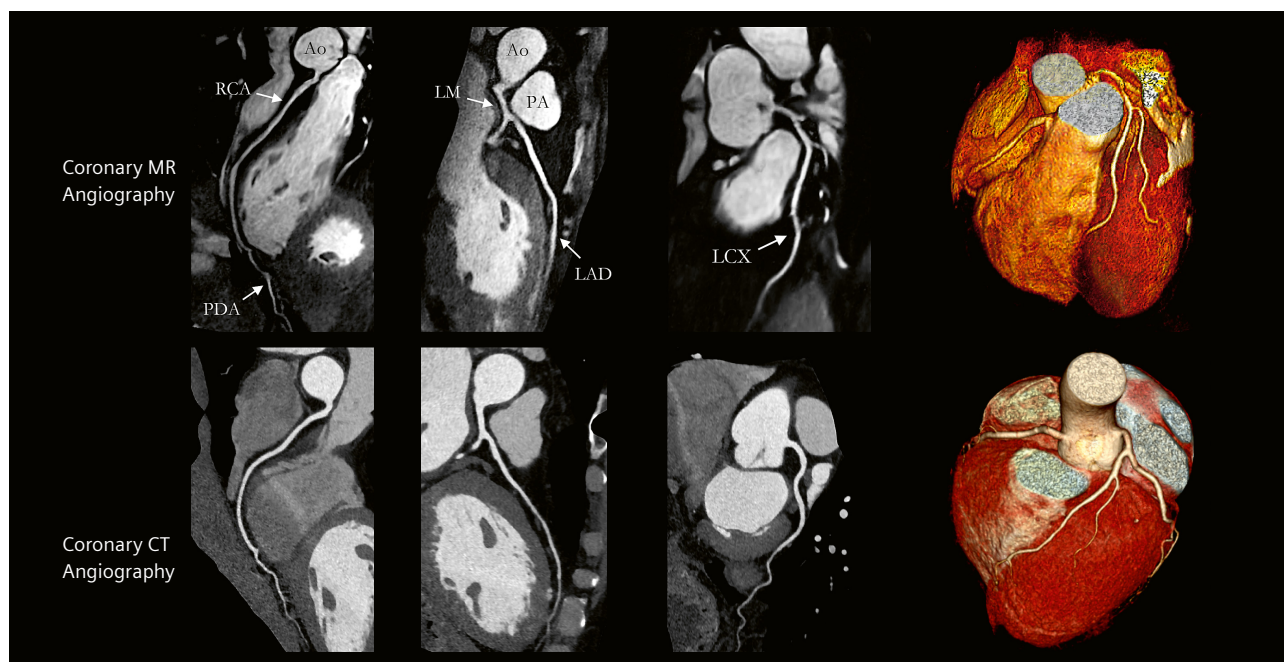
The sensitivity, specificity, positive predictive value, negative predictive value, and diagnostic accuracy of CMRA for detecting significant CAD were as follows:

- per-patient
100% (95% CI: 76–100%), 74% (95% CI: 58–85%), 55% (95% CI: 35–73%), 100% (95% CI: 88–100%), and 80% (95% CI: 67–89%) respectively;

- per-vessel
81% (95% CI: 57–93%), 88% (95% CI: 82–93%), 46% (95% CI: 30–64%), 97% (95% CI: 93–99%), and 88% (95% CI: 81–92%) respectively;
- per-segment
76% (95% CI: 55–89%), 95% (95% CI: 92–97%), 44% (95% CI: 30–60%), 99% (95% CI: 97–99%), and 94% (95% CI: 91–96%) respectively.

Example images from selected patients with suspected CAD are shown in Figures 2–8.

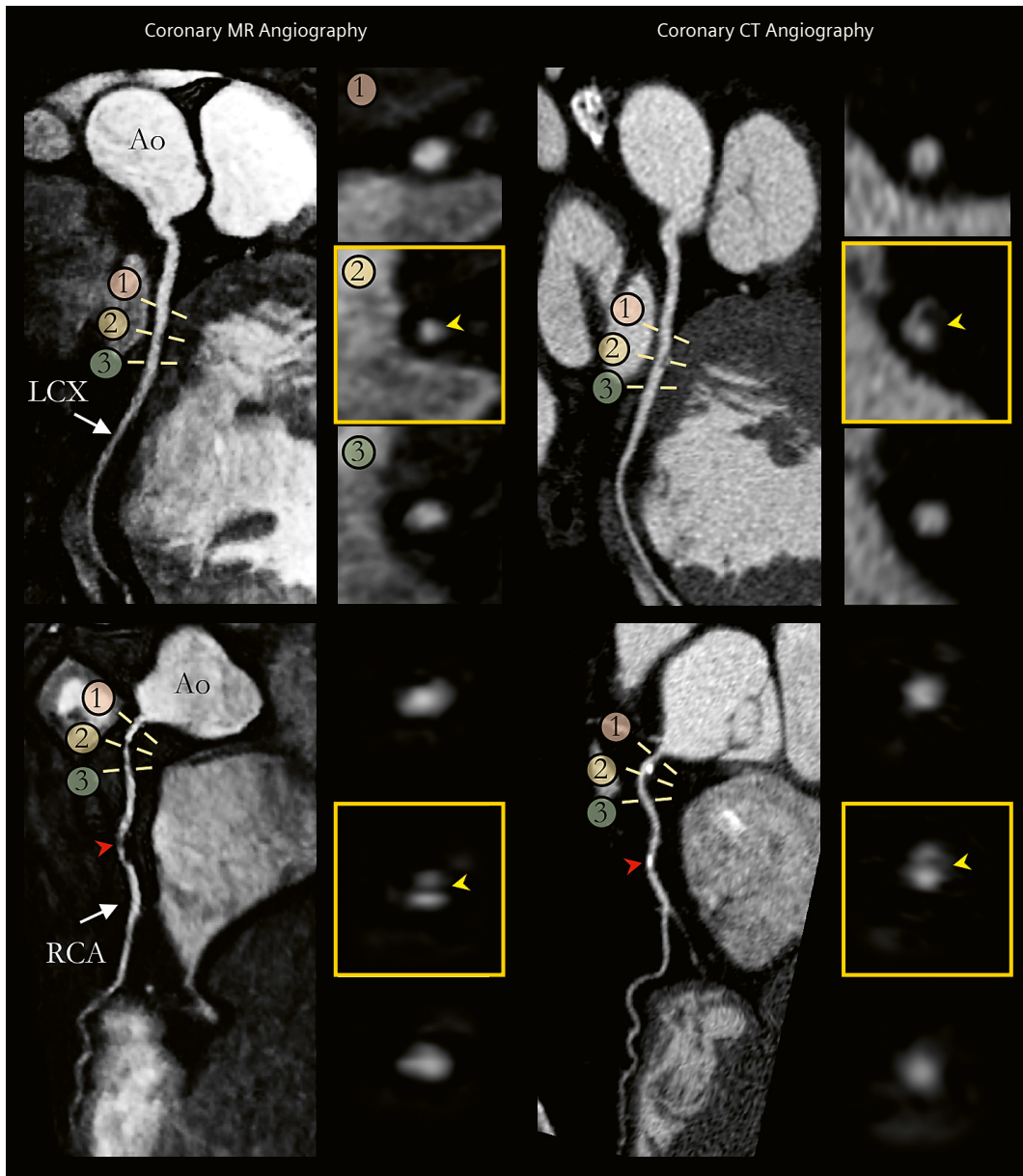
The proposed CMRA framework (without PROST regularization) has been implemented in-line in the scanner software, providing non-rigid motion corrected reconstructions in ~2–5 min (CPU).



- 2** Non-contrast whole-heart sub-millimeter isotropic CMRA images of a 53-year-old male patient with normal coronary arteries. Accelerated free-breathing CMRA images acquired and reconstructed with the proposed framework are shown in the top row, revealing the LAD, RCA, and LCX territories. The corresponding reformatted images obtained with contrast-enhanced CCTA are shown in the bottom row. 3D volume-rendered images for both modalities are shown in the right-hand column.

Abbreviations: CMRA = coronary magnetic resonance angiography; CCTA = coronary computed tomography angiography; LAD = left anterior descending artery; RCA = right coronary artery; LCX = left circumflex artery; PDA = posterior descending artery; PA = pulmonary artery; Ao = aorta.

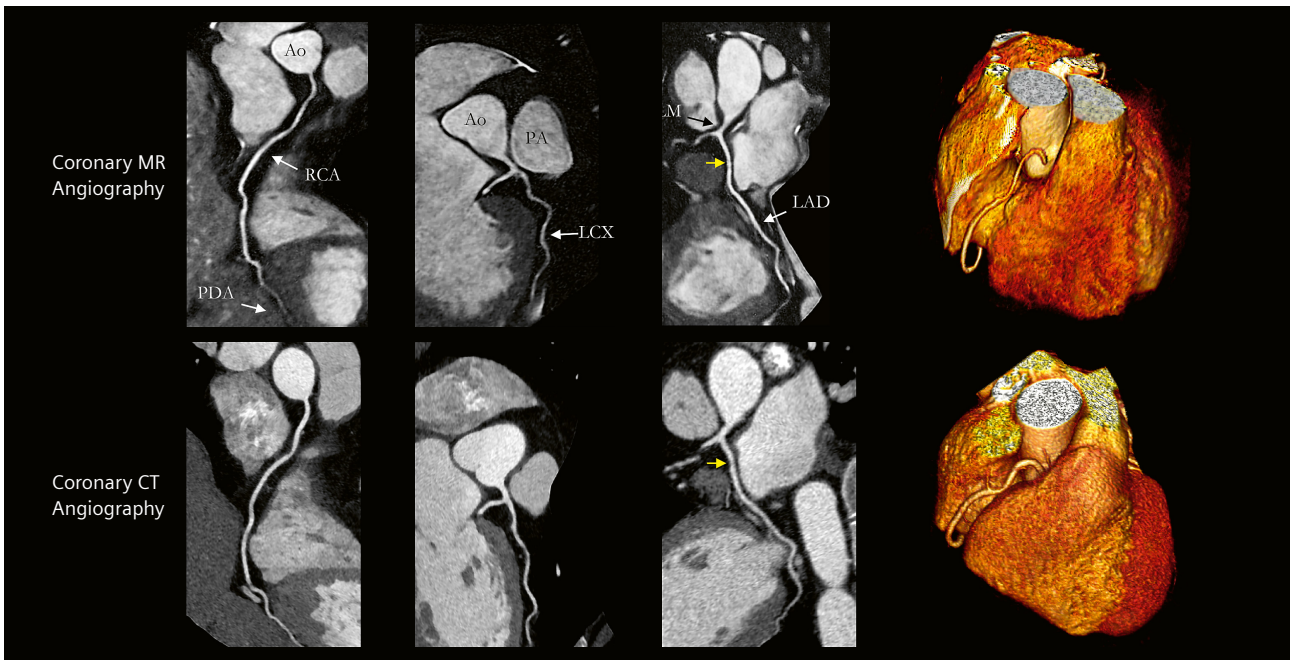
Adapted and reproduced with permission from Bustin et al. [22].



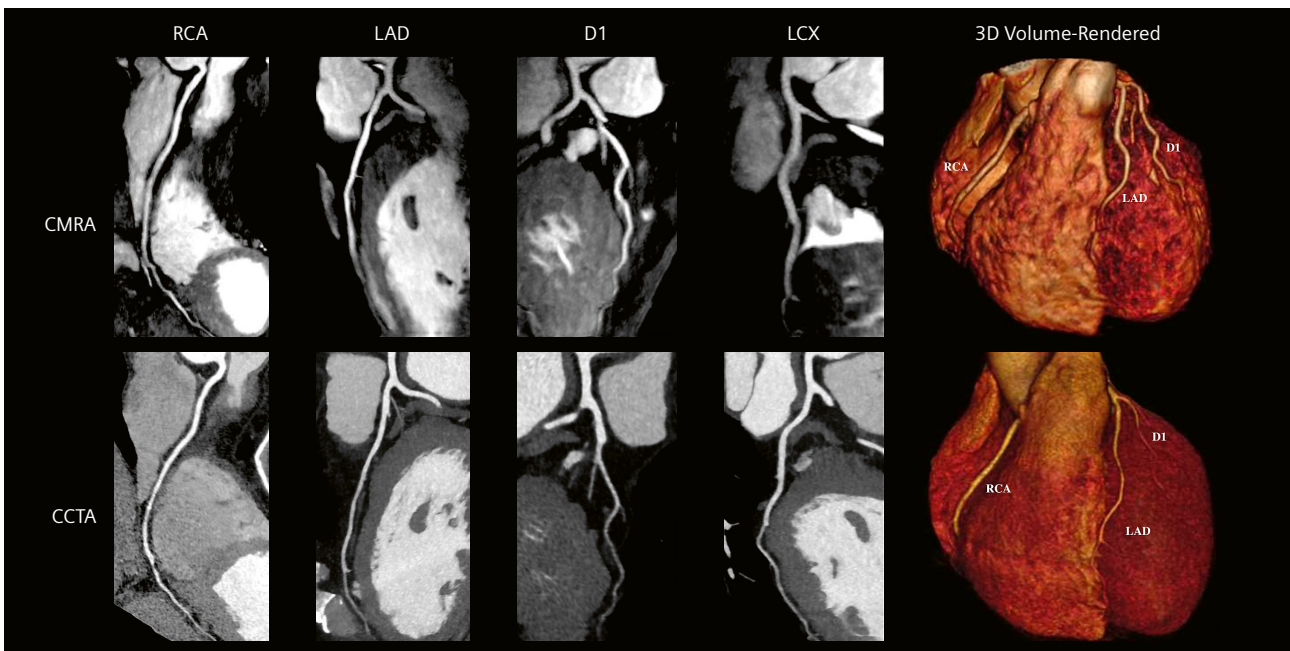
3 Reformatted non-contrast whole-heart sub-millimeter isotropic CMRA (left) and contrast-enhanced CCTA (right) images along the LCX (top) and RCA (bottom) are shown for a 54-year-old male patient. The CCTA images demonstrate mild (< 50%) disease with a calcified plaque within the proximal RCA, severe disease (> 50%) with a partially calcified plaque in the mid-segment of the RCA (red arrows), and mild (< 50%) disease with calcified plaque in the mid-segment of the LCX. Luminal narrowing is seen on the cross-sectional views at the sites of coronary plaque on the CMRA images (yellow arrows).

Abbreviations: CMRA = coronary magnetic resonance angiography; CCTA = coronary computed tomography angiography; LAD = left anterior descending artery; RCA = right coronary artery; LCX = left circumflex artery; Ao = aorta.

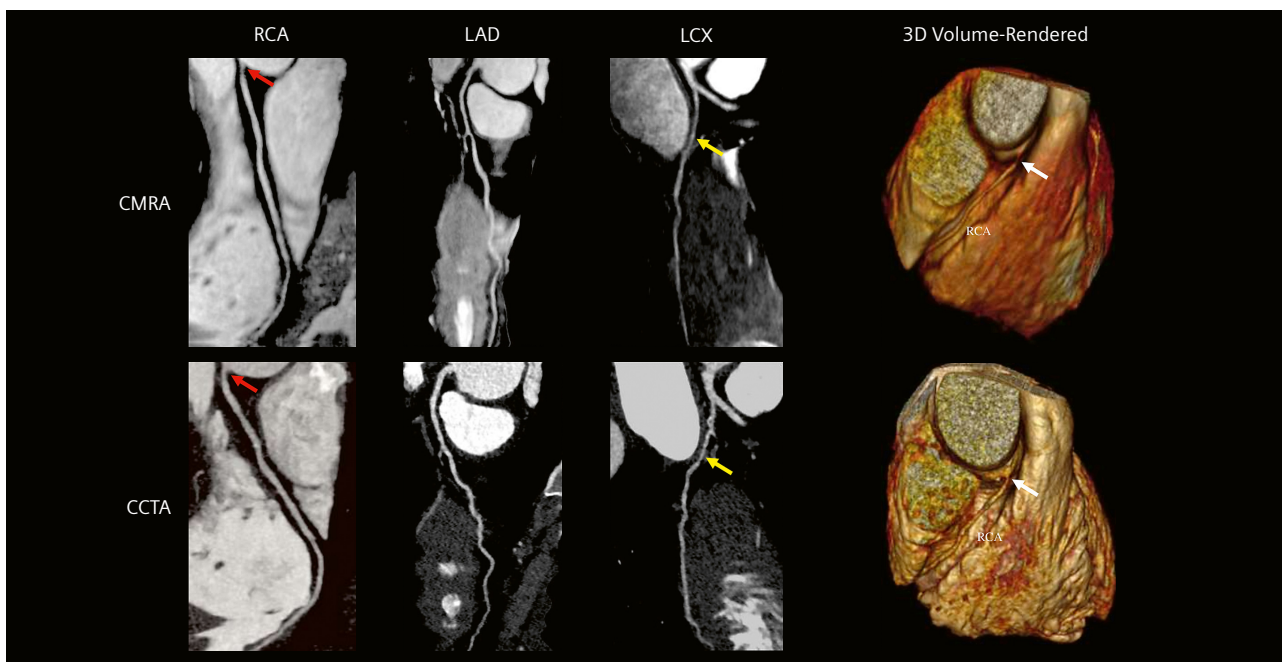
Adapted and reproduced with permission from Bustin et al. [22].



4 Non-contrast whole-heart sub-millimeter isotropic CMRA images of a 35-year-old male patient with normal coronary arteries. The CMRA images acquired and reconstructed with the proposed framework are shown in the top row, revealing the LAD and RCA. The corresponding reformatted images obtained with contrast-enhanced CCTA are shown in the bottom row. The 3D volume-rendered images are shown in the right-hand column, which were both correctly visualized on the CMRA images.
Abbreviations: CMRA = coronary magnetic resonance angiography; CCTA = coronary computed tomography angiography; LAD = left anterior descending artery; RCA = right coronary artery; LCX = left circumflex artery; LM = left main stem; PDA = posterior descending artery; PA = pulmonary artery; Ao = aorta.
 Adapted and reproduced with permission from Bustin et al. [22].



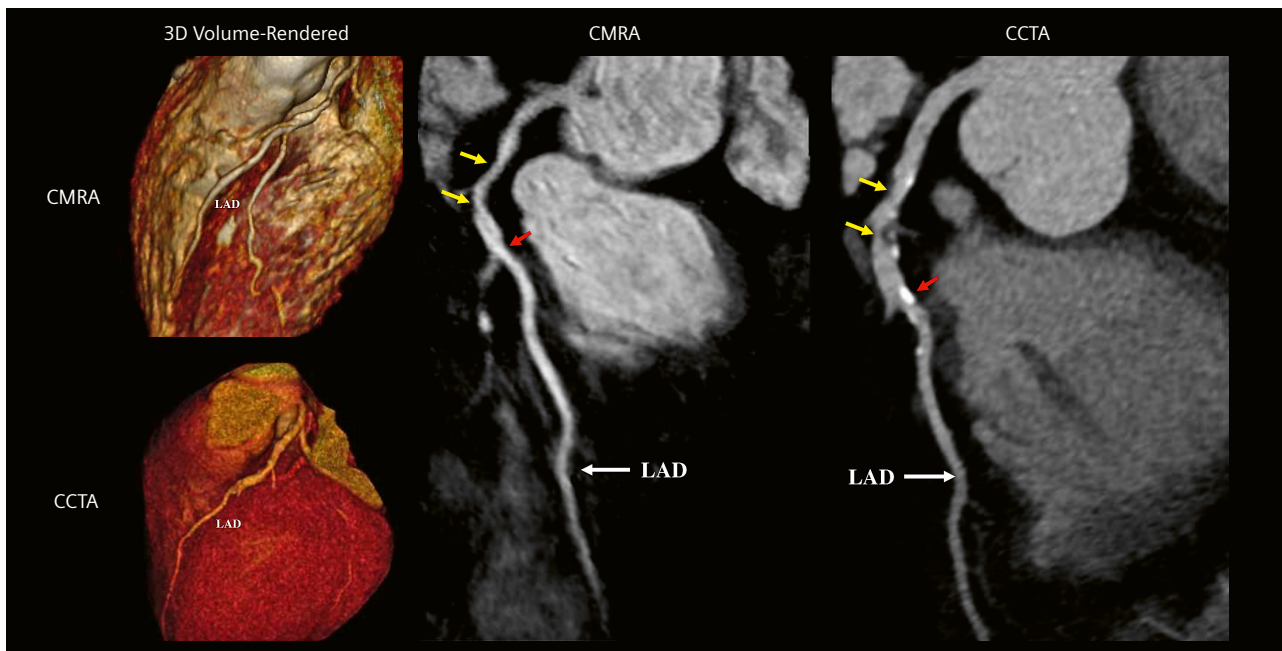
5 Curved multiplanar reformat and 3D volume-rendered non-contrast CMRA and contrast-enhanced CCTA in a 54-year-old male with no significant stenosis.
Abbreviations: CMRA = coronary magnetic resonance angiography; CCTA = coronary computed tomography angiography; RCA = right coronary artery; LAD = left anterior descending artery; D1 = first diagonal artery; LCX = left circumflex artery.
 Adapted and reproduced with permission from Hajhosseiny et al. [32].



6 Curved multiplanar reformat and 3D volume-rendered non-contrast CMRA and contrast-enhanced CCTA in a 44-year-old male with > 50% non-calcified stenosis in the ostial RCA (red arrows). This can also be seen in the 3D volume-rendered images (white arrows). The yellow arrows represent a > 50% stenosis in the proximal/mid LCX.

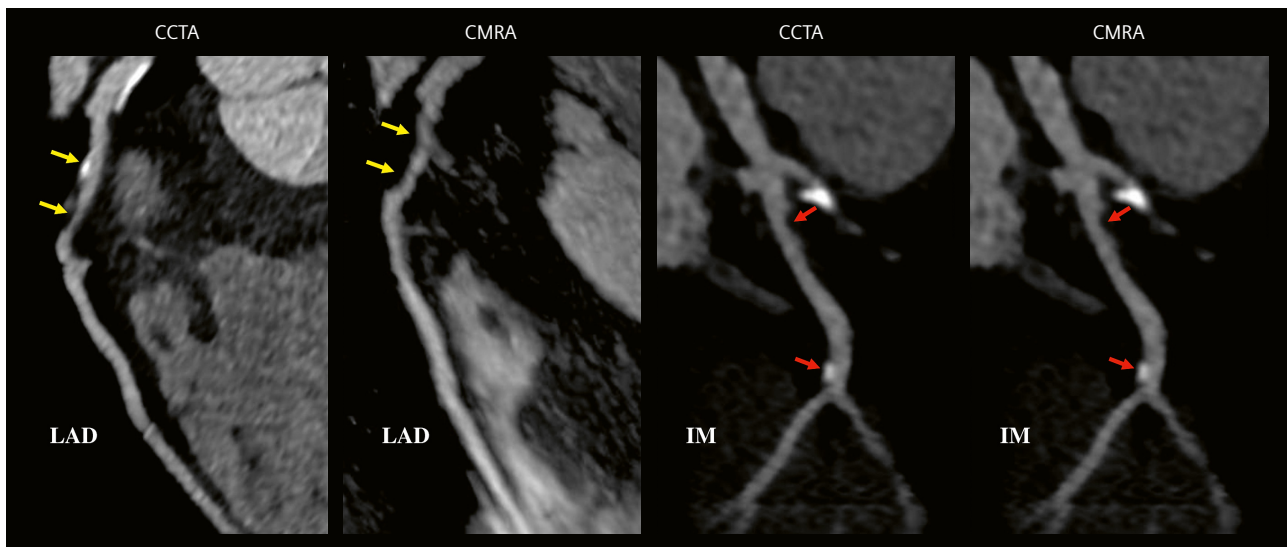
Abbreviations: CMRA = coronary magnetic resonance angiography; CCTA = coronary computed tomography angiography; RCA = right coronary artery; LAD = left anterior descending artery; LCX = left circumflex artery.

Adapted and reproduced with permission from Hajhosseiny et al. [32].



7 Curved multiplanar reformat and 3D volume-rendered non-contrast CMRA and contrast-enhanced CCTA in a 60-year-old male with > 50% partially calcified stenosis in the proximal-to-mid LAD on either side of the first diagonal artery (yellow arrows). The red arrows point to a focal calcified < 50% stenosis just distal to the second diagonal artery.

Abbreviations: CMRA = coronary magnetic resonance angiography; CCTA = coronary computed tomography angiography; LAD = left anterior descending artery. *Adapted and reproduced with permission from Hajhosseiny et al. [32].*



8 Curved multiplanar reformat non-contrast CMRA and contrast-enhanced CCTA in a 57-year-old male with > 50% partially calcified stenosis in the proximal LAD (yellow arrows). The red arrows point to focal < 50% stenosis in the proximal and distal ramus intermedius artery. **Abbreviations:** CMRA = coronary magnetic resonance angiography; CCTA = coronary computed tomography angiography; LAD = left anterior descending artery; IM = ramus intermedius artery. *Adapted and reproduced with permission from Hajhosseiny et al. [32].*

Conclusions

In this initial single-center clinical study, we have introduced a robust, contrast-free, sub-millimeter CMRA framework with predictable and clinically feasible scan times of approximately 10 minutes, achieving highly diagnostic image quality and diagnostic accuracy for excluding significant disease in patients with suspected CAD. This is the first clinical study to assess the diagnostic performance of a 3D contrast-free CMRA approach that enables a predictable scan time of approximately 10 minutes for 0.9 mm³ spatial-resolution. This was achieved by employing a robust motion corrected free-breathing acquisition with 100% respiratory scan efficiency, using image navigation for 2D translational motion estimation and respiratory data binning combined with 3D non-rigid motion compensated undersampled reconstruction employing a 3- to 4-fold undersampled Cartesian acquisition and a patched-based low-rank reconstruction. Future work will focus on multi-center clinical assessment of this novel framework to determine its clinical applicability in a larger cohort of patients with a wider spectrum of CAD.

References

- Benjamin EJ, Virani SS, Callaway CW, et al. Heart disease and stroke statistics-2018 update: A report from the American Heart Association. *Circulation* 2018;137(12):e67–e492. Available at: <http://www.ncbi.nlm.nih.gov/pubmed/29386200>.
- Kočka V. The coronary angiography – An old-timer in great shape. *Cor Vasa* 2015;57(6):e419–e424. Available at: <https://www.sciencedirect.com/science/article/pii/S0010865015001009>. Accessed August 14, 2018.
- Tavakol M, Ashraf S, Brenner SJ. Risks and complications of coronary angiography: a comprehensive review. *Glob J Health Sci*. 2012;4(1):65–93. Available at: <http://www.ncbi.nlm.nih.gov/pubmed/22980117>. Accessed August 14, 2018.
- Kolossváry M, Szilveszter B, Merkely B, Maurovich-Horvat P. Plaque imaging with CT-a comprehensive review on coronary CT angiography based risk assessment. *Cardiovasc Diagn Ther*. 2017;7(5):489–506. Available at: <http://www.ncbi.nlm.nih.gov/pubmed/29255692>. Accessed August 14, 2018.
- Hamilton M, Baumbach A. Non invasive coronary imaging with computed tomography. [journal on the Internet]. 2007; 5(20). Available at: <https://www.escardio.org/Journals/E-Journal-of-Cardiology-Practice/Volume-5/Non-Invasive-Coronary-Imaging-With-Computed-Tomography-Title-Non-Invasive-Cor>. Accessed August 14, 2018.
- Alfakih K, Byrne J, Monaghan M. CT coronary angiography: a paradigm shift for functional imaging tests. *Open Hear*. 2018;5(1):e000754. Available at: <http://www.ncbi.nlm.nih.gov/pubmed/29632679>. Accessed August 14, 2018.
- Doris MK, Newby DE. How should CT coronary angiography be integrated into the management of patients with chest pain and how does this affect outcomes? *Eur Heart J - Qual Care Clin. Outcomes* 2016;2(2):72–80. Available at: <https://academic.oup.com/ehjqcco/article-lookup/doi/10.1093/ehjqcco/qcv027>. Accessed August 14, 2018.
- Kim WY, Danias PG, Stuber M, et al. Coronary magnetic resonance angiography for the detection of coronary stenoses. *N Engl J Med*. 2001;345(26):1863–1869. Available at: <http://www.ncbi.nlm.nih.gov/pubmed/11756576>. Accessed July 26, 2019.
- Yang Q, Li K, Liu X, et al. Contrast-Enhanced Whole-Heart Coronary Magnetic Resonance Angiography at 3.0-T. A Comparative Study With X-ray Angiography in a Single Center. *J Am Coll Cardiol*. 2009;54(1):69-76.

- 10 Kato S, Kitagawa K, Ishida N, et al. Assessment of coronary artery disease using magnetic resonance coronary angiography: a national multicenter trial. *J Am Coll Cardiol*. 2010;56(12):983–91. Available at: <http://linkinghub.elsevier.com/retrieve/pii/S0735109710024691>. Accessed September 30, 2018.
- 11 Sriharan M, McParland P, Harden S, Nicol E. Non-Invasive Coronary Angiography. In: Branislav B. *Coronary Angiography - Advances in Noninvasive Imaging Approach for Evaluation of Coronary Artery Disease*. [book on the Internet]. London: InTech, 2011:99-122. DOI: 10.5772/22475. Available at: <http://www.intechopen.com/books/coronary-angiography-advances-in-noninvasive-imaging-approach-for-evaluation-of-coronary-artery-disease/non-invasive-coronary-angiography>. Accessed August 16, 2018.
- 12 Mangla A, Oliveros E, Williams KA, Kalra DK. Cardiac imaging in the diagnosis of coronary artery disease. *Curr Probl Cardiol*. 2017;42(10):316–366. Available at: <https://www.sciencedirect.com/science/article/pii/S0146280617300725?via%3DIihub#bib116>. Accessed August 16, 2018.
- 13 Hamdy A, Ishida M, Sakuma H. Cardiac MR assessment of coronary arteries. *CVIA 2017*;1(1):49–59. Available at: <https://doi.org/10.22468/cvia.2016.00066>. Accessed December 11, 2018.
- 14 Coppo S, Piccini D, Bonanno G, et al. Free-running 4D whole-heart self-navigated golden angle MRI: Initial results. *Magn Reson Med*. 2015;74(5):1306–1316. Available at: <http://www.ncbi.nlm.nih.gov/pubmed/25376772>. Accessed September 3, 2018.
- 15 Pang J, Bhat H, Sharif B, et al. Whole-heart coronary MRA with 100% respiratory gating efficiency: Self-navigated three-dimensional retrospective image-based motion correction (TRIM). *Magn Reson Med*. 2014;71(1):67–74. Available at: <http://doi.wiley.com/10.1002/mrm.24628>. Accessed August 18, 2018.
- 16 Henningsson M, Botnar RM. Advanced respiratory motion compensation for coronary MR angiography. *Sensors (Basel)*. 2013;13(6):6882–99. Available at: <http://www.ncbi.nlm.nih.gov/pubmed/23708271>. Accessed August 17, 2018.
- 17 Ehman RL, Felmlee JP. Adaptive technique for high-definition MR imaging of moving structures. *Radiology* 1989;173(1):255–263. Available at: <http://www.ncbi.nlm.nih.gov/pubmed/2781017>. Accessed August 17, 2018.
- 18 McConnell M V, Khasgiwala VC, Savord BJ, et al. Comparison of respiratory suppression methods and navigator locations for MR coronary angiography. *AJR Am J Roentgenol*. 1997;168(5):1369–1375. Available at: <http://www.ncbi.nlm.nih.gov/pubmed/9129447>. Accessed August 17, 2018.
- 19 Danias PG, McConnell M V, Khasgiwala VC, Chuang ML, Edelman RR, Manning WJ. Prospective navigator correction of image position for coronary MR angiography. *Radiology*. 1997;203(3):733–736. Available at: <http://www.ncbi.nlm.nih.gov/pubmed/9169696>. Accessed August 17, 2018.
- 20 Nehrke K, Börnert P, Groen J, Smink J, Böck JC. On the performance and accuracy of 2D navigator pulses. *Magn Reson Imaging* 1999;17(8):1173–81. Available at: <http://www.ncbi.nlm.nih.gov/pubmed/10499679>. Accessed August 17, 2018.
- 21 Correia T, Ginami G, Cruz G, et al. Optimized respiratory-resolved motion-compensated 3D Cartesian coronary MR angiography. *Magn Reson Med*. 2018;80(6):2618–2629. Available at: <http://www.ncbi.nlm.nih.gov/pubmed/29682783>. Accessed August 17, 2018.
- 22 Bustin A, Rashid I, Cruz G, et al. 3D whole-heart isotropic sub-millimeter resolution coronary magnetic resonance angiography with non-rigid motion-compensated PROST. *J Cardiovasc Magn Reson*. 2020;22(1):<https://doi.org/10.1186/s12968-020-00611-5>.
- 23 Bustin A, Ginami G, Cruz G, et al. Five-minute whole-heart coronary MRA with sub-millimeter isotropic resolution, 100% respiratory scan efficiency, and 3D-PROST reconstruction. *Magn Reson Med*. 2019;81(1):102–115.
- 24 Henningsson M, Koken P, Stehning C, Razavi R, Prieto C, Botnar RM. Whole-heart coronary MR angiography with 2D self-navigated image reconstruction. *Magn Reson Med*. 2012;67(2):437–445. Available at: <http://www.ncbi.nlm.nih.gov/pubmed/21656563>. Accessed August 17, 2018.
- 25 Nezafat R, Stuber M, Ouwerkerk R, Gharib AM, Desai MY, Pettigrew RI. B1-insensitive T2 preparation for improved coronary magnetic resonance angiography at 3T. *Magn Reson Med*. 2006;55(4):858–64.
- 26 Botnar RM, Stuber M, Danias G, Kissinger K V, Manning WJ. Improved coronary artery definition with T2-weighted, free-breathing, three-dimensional coronary MRA. *Circulation*. 1999;99(24):3139–3148.
- 27 Cruz G, Atkinson D, Henningsson M, Botnar RM, Prieto C. Highly efficient nonrigid motion-corrected 3D whole-heart coronary vessel wall imaging. *Magn Reson Med*. 2017;77(5):1894–1908. Available at: <http://doi.wiley.com/10.1002/mrm.26274>. Accessed August 20, 2018.
- 28 Correia T, Cruz G, Schneider T, Botnar RM, Prieto C. Technical note: Accelerated nonrigid motion-compensated isotropic 3D coronary MR angiography. *Med Phys*. 2018;45(1):214–222.
- 29 Rueckert D, Sonoda LI, Hayes C, Hill DL, Leach MO, Hawkes DJ. Nonrigid registration using free-form deformations: application to breast MR images. *IEEE Trans Med Imaging*. 1999;18(8):712–721.
- 30 Batchelor PG, Atkinson D, Irrazaval P, Hill DLG, Hajnal J, Larkman D. Matrix description of general motion correction applied to multishot images. *Magn Reson Med*. 2005;54(5):1273–1280.
- 31 Cruz G, Atkinson D, Buerger C, Schaeffter T, Prieto C. Accelerated motion corrected three-dimensional abdominal MRI using total variation regularized SENSE reconstruction. *Magn Reson Med*. 2016;75(4):1484–1498.
- 32 Hajhosseiny R, Rashid I, Bustin A, Munoz C, Cruz G, Nazir M.S, Grigoryan K, Ismail T.F, Preston R, Neji R, Kunze K, Razavi R, Chiribiri A, Masci P.G, Rajani R, Prieto C, Botnar R.M. Clinical comparison of sub-mm high-resolution non-contrast coronary MRA against coronary CTA in patients with low-intermediate risk of CAD: A single center trial. *J Cardiovasc Magn Reson*. 2021; IN PRESS.



Contact

Reza Hajhosseiny, M.D.
 School of Biomedical Engineering and Imaging Sciences
 King's College London
 3rd floor Lambeth Wing
 London, SE1 7EH
 United Kingdom
 Phone: +44 020 7188 7188
reza.hajhosseiny@kcl.ac.uk
 Twitter: @KCL_CardiacMR

Infrared Thermally Enhanced 3D TOF MOTSA MR Angiography for Visualizing the Arteries of the Face

Marc Mespreuve, M.D., Ph.D.¹; Karl Waked, M.D.²; Yannick De Brucker, M.D.³; Greta Vandemaele, Ph.D.⁴; Benoit Hendrickx, M.D., Ph.D.⁵

¹Department of Medical Imaging, University Hospital Ghent, Belgium

²Department of Plastic and Reconstructive Surgery, University Hospital Brussels, Belgium

³Department of Medical Imaging, University Hospital Brussels, Belgium

⁴Siemens Healthineers, MR Applications, Huizingen, Belgium

⁵University Hospital Brussels, and AZ Zeno, Knokke-Heist, Belgium

Three-dimensional time-of-flight magnetic resonance angiography and its limitations

Time-of-flight (TOF) magnetic resonance angiography (MRA) is one of the most important methods of non-contrast neurovascular MRA. TOF MRA is based on the principle of flow-related enhancement. Stationary tissues in an imaged volume become magnetically saturated by multiple repetitive radiofrequency (RF) pulses that reduce their steady-state magnetization levels. Fresh blood flowing into the imaged volume has not experienced these pulses and still has a high initial magnetization. The signal from the inflowing blood appears bright compared to the

background tissue. A maximum intensity projection (MIP) technique is then used to create an MR angiogram.

The 3D TOF angiography method is based on a 3D gradient echo (GRE) sequence. Often, a pre-saturation pulse is applied above or below the imaged volume to reduce the signals from venous inflow. Flip angles of 30°–60° are used to maximize the contrast between stationary tissues and blood. Short TE values (< 7 ms) are applied to minimize signal losses from phase dispersion. A maximal enhancement of the blood flow is observed when the vessel is perpendicular to the plane of imaging (in-plane flow is not visible) and has a larger diameter and a high flow. Various modifications of the TOF technique have been developed to reduce in-plane saturation effects and improve visualization of smaller vessels and slow flow. These modifications include the use of variable flip angles, fat suppression, magnetization transfer saturation pulses, and multiple overlapping thin slab acquisition (MOTSA).

The principle of combining infrared heat-induced enhancement with a 3D TOF MRA sequence, either with or without compressed sensing

The vascular anatomy of the face is extremely variable. Not only is the arterial course very tortuous, but the localization and depth of the facial arteries and their branches also varies significantly from person to person and even between each side of the face [1–3]. Hence, an ideal plane for the optimal inflow for the different facial arteries is always a compromise. Moreover, many of the vessels are small and have a slow flow.

Previous studies have described heating the face using an infrared (IR) lamp to enlarge the diameter of the vessels and accelerate the flow [4–6].

Recently, the use of compressed sensing (CS) has offered synergistic enhancement for parallel imaging with

3D TOF MOTSA sequence 1.5T	
TR (repetition time)	30 ms
TE (echo time)	6.8 ms
Number of slices per slab (% slice OS)	40 (20% OS)
FOV	180 × 180 mm ²
Flip angle	30 °
Matrix (% phase resolution)	241 × 256 (94%) pixels
Slice thickness (% slice resolution)	0.5 (50%) mm
Averages	2
Acceleration	GRAPPA2
Voxel size acquired	0.7 × 0.7 × 1.0 mm ³
Voxel size reconstructed	0.35 × 0.35 × 0.5 mm ³
Acquisition time	16:14 min

Table 1: MAGNETOM Aera XQ 3D TOF MOTSA sequence 1.5T
Gradient echo sequence with five overlapping slabs (-17.5%).

sparse sampling and iterative reconstruction. CS speeds up data acquisition with sparse data subsampling. Applying CS reconstruction to the raw data can achieve enhanced image quality. The acceleration makes it possible to significantly reduce the acquisition time, which is especially important for 1.5T MRA, as it involves quite long acquisition times. Compressed sensing applications have been demonstrated for the brain, where it has proven to be very useful in certain exams with lengthy scan times. TOF MRA is a lengthy scan technique, for which the application of compressed sensing has been demonstrated to almost halve scan time while still providing almost equivalent diagnostic information [7].

Technology

The patient is positioned with closed eyes in front of an infrared (IR) light source (300 W) with an InfraCare (Philips, Amsterdam, The Netherlands) screen (which filters out the UV light), at a distance of 30 cm and with their face parallel to the lamp for 15 minutes. The heat induces vasodilatation and enhances the vascular flow, both of which help to improve image acquisition [4–6]. At the same time, the patient is also asked to stimulate their facial muscles by slowly moving their lips and forehead and switching between several facial expressions during the exposure time. This is to further enhance the visualization of the facial arteries by vascular dilatation and increased flow

3D TOF MOTSA sequence 1.5T	
TR (repetition time)	26.3 ms
TE (echo time)	5.7 ms
Number of slices per slab (% slice OS)	44 (18% OS)
FOV	180 × 180 mm ²
Flip angle	20 °
Matrix (% phase resolution)	241 × 256 (94%) pixels
Slice thickness (% slice resolution)	0.5 (50%) mm
Averages	2
Acceleration	CS5
Voxel size acquired	0.75 × 0.7 × 0.94 mm ³
Voxel size reconstructed	0.47 × 0.47 × 0.47 mm ³
Interpolation	1.5
Acquisition time	11:35 min

Table 2: MAGNETOM Sola Fit XQ with Compressed Sensing 3D TOF MOTSA sequence 1.5T
Gradient echo sequence with seven overlapping slabs (-30%).

speed [8]. Immediately following IR exposure, the patient is transferred to the MRI unit.

After acquisition of the scout views, a 3D TOF MOTSA MRA sequence is acquired in an oblique coronal plane (tilting of 25° backwards in relation to the line between the glabella and the chin). The initial MRA protocol for a MAGNETOM Aera 1.5T scanner from Siemens Healthcare (with Numaris 4, software version *syngo* MR E11E) is summarized in Table 1 and was developed, based on a previously published study that discusses the MRA sequence in more detail [4]. Table 2 contains the data for a MAGNETOM Sola Fit 1.5T scanner from Siemens Healthcare (NumX *syngo* MR A20) with CS, and Table 3 contains the data for a MAGNETOM Vida 3T scanner from Siemens Healthcare (NumX *syngo* MR A20). During the examination, the patient is asked to remain completely still (this includes their eyes, lips, chin, and cheeks) with their eyes and mouth closed (without pressure on the lips), and their face parallel to the examination table. A multislab MOTSA technique is used to reduce the saturation effect of the signal from the inflowing blood.

Implementation and results

Various previous studies have proven the good results of this technique [4–6]. It is also currently in clinical use at several 3T MRI centers in Europe.

3D TOF MOTSA sequence 3T	
TR (repetition time)	30 ms
TE (echo time)	4.92 ms
Number of slices per slab (% slice OS)	40 (20% OS)
FOV	180 × 180 mm ²
Flip angle	30 °
Matrix (% phase resolution)	241 × 256 (94%) pixels
Slice thickness (% slice resolution)	0.5 (50%) mm
Averages	1
Acceleration	GRAPPA2
Voxel size acquired	0.8 × 0.8 × 1.0 mm ³
Voxel size reconstructed	0.4 × 0.4 × 0.5 mm ³
Interpolation	2
Acquisition time	9:21 min

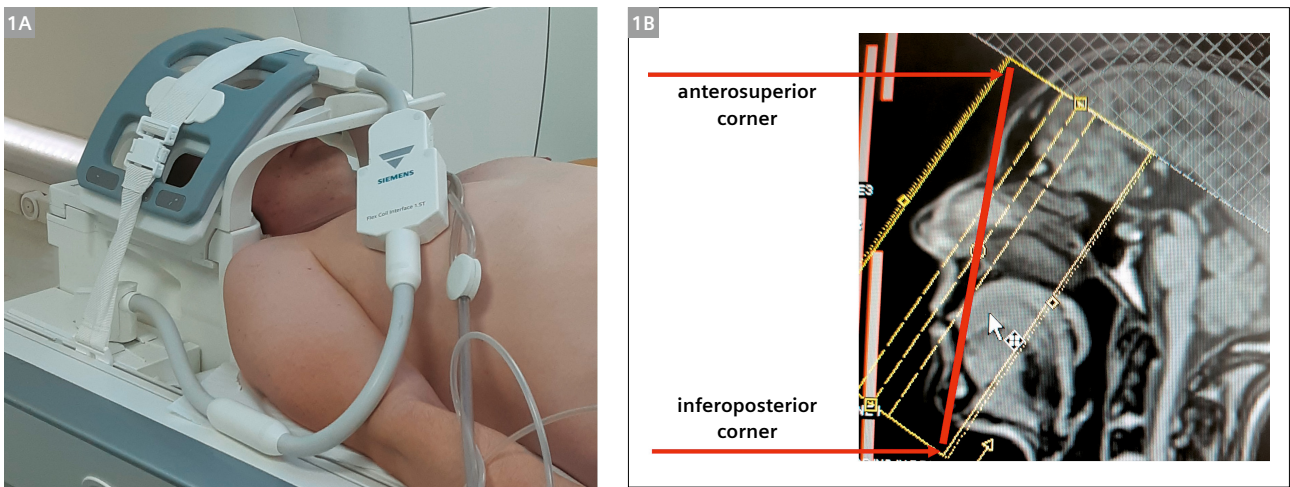
Table 3: MAGNETOM Vida 3D TOF MOTSA sequence 3T
Gradient echo sequence with seven overlapping slabs (-18%).

In the first series, all 3D TOF MOTSA MRA images were acquired on a 1.5T full-body MR system (MAGNETOM Aera, Siemens Healthcare, Erlangen, Germany), using a dedicated 20-channel head coil. Additionally, a flexible wrap-around 4-channel surface coil was mounted on top of the head coil (Fig. 1) [4]. Figure 2 shows a comparison of a 3D TOF MOTSA MRA without (A) and with (B) previous IR exposure.

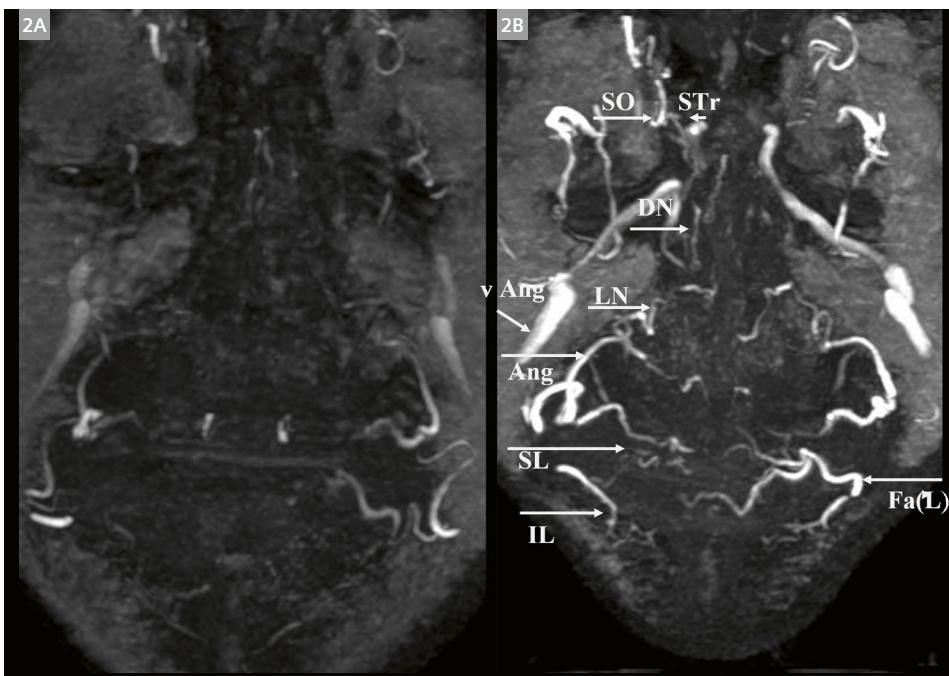
In order to reduce the examination time and obtain a stronger signal, further series with 3T MRI were added [6].

However, as more than 60% of all MR scanners globally are 1.5 Tesla machines, there is a need for an optimal 1.5T sequence and especially for a reduction in the examination time.

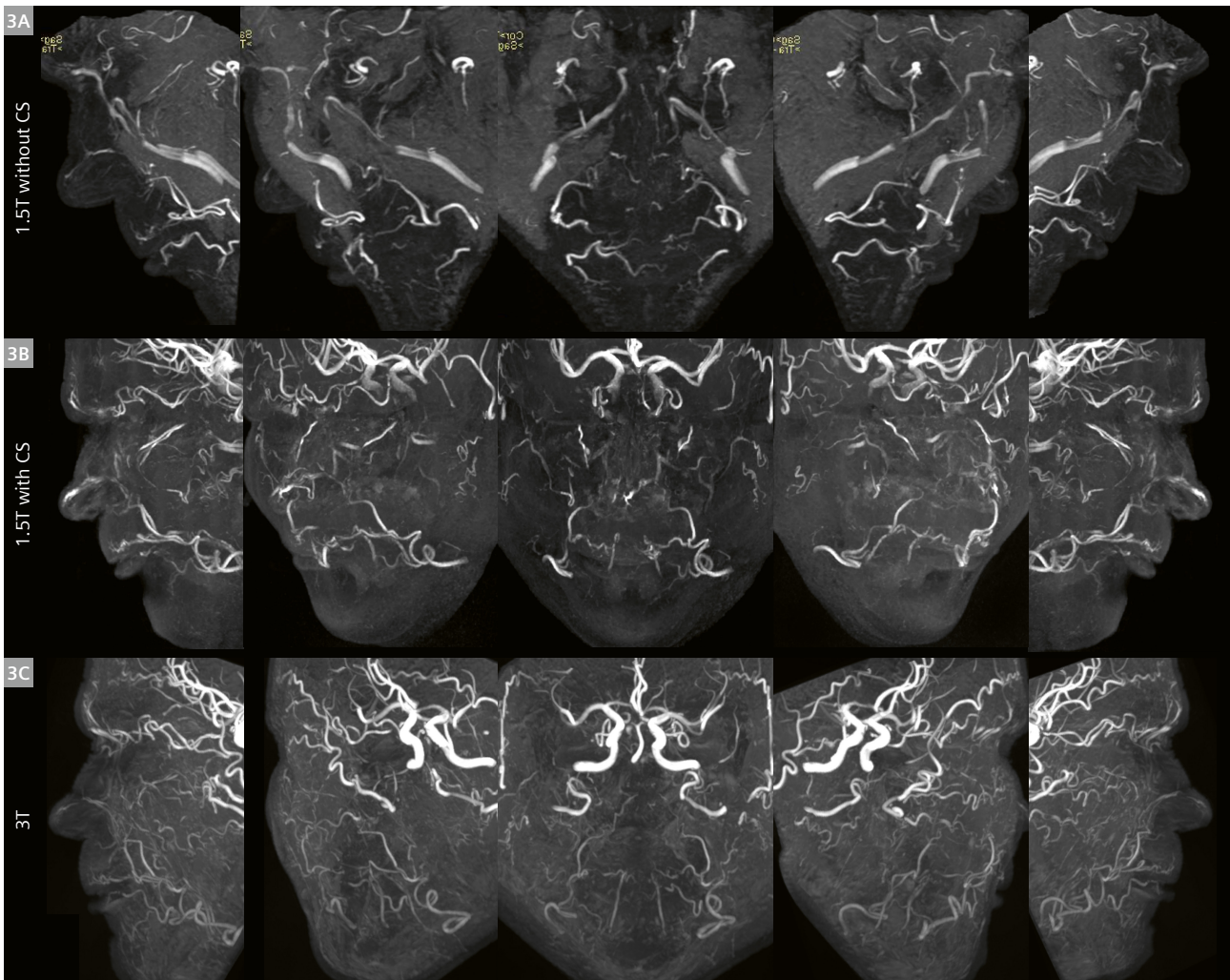
Figure 3 shows the same volunteer examined using a 1.5T MAGNETOM scanner with and without Compressed Sensing (MAGNETOM Aera and MAGNETOM Sola Fit, Siemens Healthcare, Erlangen, Germany), and using a 3T scanner (MAGNETOM Vida, Siemens Healthcare, Erlangen, Germany) in order to compare the individual results. The acquisition time was 9 minutes and 21 seconds for the 3T,



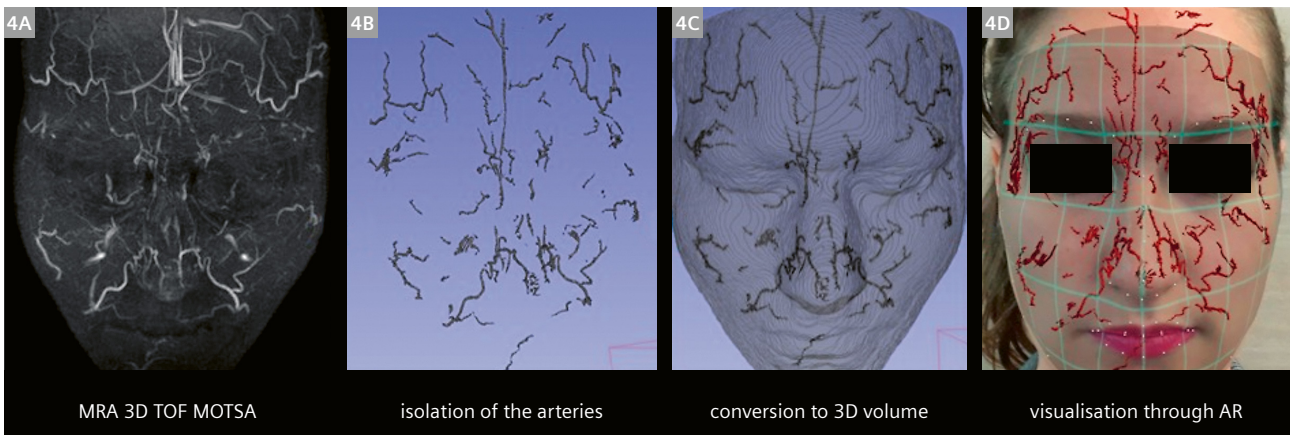
1 Position of the head coil and the flex coil for the MRA (1A), and position of the 3D TOF MOTSA slab block on the localizer (1B) (1A) Flexible wrap-around 4-channel surface coil can be mounted on top of the head coil to increase signal reception from the facial arteries. (1B) The line drawn from the glabella to the chin transects the slab position block from the anterosuperior corner to the inferoposterior corner. A magnetic saturation slab is positioned above the slab block.



2 MRA findings (MIP of 3D TOF MOTSA) without (2A) and with (2B) previous IR exposure The IR exposure results in a far better visualization of all facial vessels, with a larger caliber of the arteries and a higher visual signal. Superior (SL) and inferior labial artery (IL), angular artery (Ang), lateral nasal artery (LN), dorsal nasal artery (DN), supratrochlear artery (STr), supraorbital artery (SO), facial artery (Fa), and angular vein (vAng).



3 MRA findings (MIP of 3D TOF MOTSA)
 (3A) 1.5T without Compressed Sensing; (3B) 1.5T with Compressed Sensing; (3C) 3T.



4 MRA findings and data processing cycle in a 26-year-old female
 (4A) Frontal view of an MIP from the 3D TOF MOTSA.
 (4B) Image after isolation of the arteries.
 (4C) Conversion to a 3D volume using the MRI data (rotated MIP over 180° from right to left and native image DICOM data).
 (4D) Visualization using augmented reality (AR) and projection onto the patient's face with a smartphone camera.

16 minutes and 14 seconds for the 1.5T, and 11 minutes and 35 seconds for the 1.5T with CS (two averages). This illustrates the acceptability of 1.5T MRI examinations compared to 3T, and indicates that they are ready for general use.

Afterwards, the native DICOM images and the MIPs are processed by an experimental 3D software program which isolates the superficial subcutaneous arteries and creates a 3D volume. Using augmented reality, these patient-specific arterial 3D volumes are visualized and projected onto the patient's face (Fig. 4) with a smartphone.

Conclusion

Our experience shows that combining IR heat enhancement and a 3D TOF MRA sequence makes it feasible to visualize a large number of facial arteries in a radiation-free, contrast-free, and non-invasive way.

This thermally enhanced 3D TOF MRA imaging technique may provide a solution for acquiring much-needed information about the patient's individual anatomy in order to better plan and execute aesthetic and reconstructive procedures in the face, such as filler injections [6].

Using CS on a 1.5T MRI scanner significantly reduces the examination time to a more acceptable duration, meaning that the many 1.5T MRI systems in use worldwide could potentially be used for the purpose described above.

Contact

Prof. Dr. Marc Mespreuve
Department of Medical Imaging
University Hospital Ghent
Corneel Heymanslaan 10
9000 Ghent
Belgium
and
A.Z. St. Maarten
Liersesteenweg 435
2800 Mechelen
Belgium
marc.mespreuve@skynet.be



References

- 1 Loukas M, Hullett J, Louis RG Jr, Kapos T, Knight J, Nagy R, et al. A detailed observation of variations of the facial artery, with emphasis on the superior labial artery. *Surg Radiol Anat.* 2006;28(3):316–24.
- 2 Cotofana S, Lachman N. Arteries of the Face and Their Relevance for Minimally Invasive Facial Procedures: An Anatomical Review. *Plast Reconstr Surg.* 2019;143(2):416–426.
- 3 Tansatit T, Apinuntrum P, Phetudom T. Periorbital and Intraorbital Studies of the Terminal Branches of the Ophthalmic Artery for Periorbital and Glabellar Filler Placements. *Aesthetic Plast Surg.* 2017;41(3):678–688.
- 4 Hendrickx B, Waked K, Mespreuve M. Infrared Thermally Enhanced 3-Dimensional Time of Flight Magnetic Resonance Angiography Imaging for the Visualization of the Arteries of the Face. *Aesthet Surg J Open Forum.* 2020;2(2):ojaa020.
- 5 Mespreuve M, Waked K, Hendrickx B. Visualization techniques of the facial arteries, *J. Cosmet Dermatol.* 2021;20(2):386–390. Epub 2020 May 27.
- 6 Mespreuve M, Waked K, Collard B, De Ranter J, Vanneste F, Hendrickx B. The Usefulness of Magnetic Resonance Angiography to Analyze the Variable Arterial Facial Anatomy in an Effort to Reduce Filler-Associated Blindness: Anatomical Study and Visualization Through an Augmented Reality Application. *Aesthet Surg J Open Forum.* 2021;3(3):ojab018.
- 7 Runge V, Heverhagen J. Important Updates for Advanced Imaging Topics, with a Perspective on Improved Patient Throughput. *MAGNETOM Flash.* 2021;78:15–21.
- 8 Hotta K, Behnke BJ, Arjmandi B, Ghosh P, Chen B, Brooks R, et al. Daily muscle stretching enhances blood flow, endothelial function, capillarity, vascular volume and connectivity in aged skeletal muscle. *J Physiol.* 2018;596(10):1903–1917.

The DICOM files of the figures in this article are available for download at

<https://www.magnetomworld.siemens-healthineers.com/clinical-corner/protocols/dicom-images/3d-tof-motsa-mr>

- Phoenix is a unique *syngo* tool that allows you to click on an image, drag it into the measurement queue, and instantly duplicate the extracted protocol – TR, TE, bandwidth, number of slices, echo spacing, etc.
- Phoenix ensures reproducibility, e.g., for patient follow-up.
- Phoenix shares optimized protocols on the different MAGNETOM systems you work with.
- Phoenix supports multicenter protocol standardization.

You'll find DICOM images from various systems and all aspects of MRI at

<https://www.magnetomworld.siemens-healthineers.com/clinical-corner/protocols/dicom-images>

Meet Siemens Healthineers

Siemens Healthineers: Our brand name embodies the pioneering spirit and engineering expertise that is unique in the healthcare industry. The people working for Siemens Healthineers are totally committed to the company they work for, and are passionate about their technology. In this section we introduce you to colleagues from all over the world – people who put their hearts into what they do.

Solenn Toupin, Ph.D.

After earning a master's in engineering near my hometown in Brittany, western France, I had the invaluable opportunity to join Siemens Healthineers in 2014 while pursuing doctoral studies at the electrophysiology and heart modelling institute (LIRYC) in Bordeaux. In 2017, I completed my Ph.D. in interventional cardiovascular magnetic resonance imaging (CMR) and joined the French Scientific Partnership team as a clinical scientist. I bring my passion for cardiology and cardiovascular imaging to my main speciality of CMR. Within the team, my daily responsibilities focus on linking predevelopment researchers from Siemens Healthineers with local clinical partners through research projects that often involve prototypes and work-in-progress pulse sequences from Siemens Healthineers. I also enjoy teaching CMR to technicians, and I develop customer learning materials, which I teach both in person and online.



Bordeaux, France



How did you first come into contact with MRI?

I attended lectures on MRI physics while in engineering school, but my first real contact with MRI occurred when I was doing my master's thesis at LIRYC in Bordeaux. I think most CMR enthusiasts can relate to how fascinated I was the first time I saw a cine of a beating heart. My passion for CMR has continued to grow since then. CMR brings together two subjects that are close to my heart: education and technical innovation. Well-trained staff and robust pulse sequences are both necessary to deal with potential arrhythmia or breathing motion and to allow more patients to benefit from high-quality CMR exams.

What do you find motivating about your job?

My role as a clinical scientist provides me with the unique opportunity to bridge the gap between academy and industry. I also feel privileged to interact daily with experts on both sides: our academic partners and the research scientists at Siemens Healthineers. Successful collaborations rely on building long-term, trusting relationships with our partners, and I'd say that the most rewarding part of my job is being able to experience these bonds of trust. Being involved in each step of a collaborative research project, from the first experiments at the MR console to the final joint publication, makes me excited

about my job every day. I enjoy meeting well-known physicians and their teams throughout France, in cities such as Bordeaux, Paris, and Lille, and learning about their best practices. Ultimately, I'm driven by the way these MRI innovations – which started out as mere prototypes – benefit clinical routines and people's lives.

What are the biggest challenges in your job?

I'm responsible for supporting local academic partners with research on a wide range of collaborative topics that primarily focus on CMR. The biggest challenge is fulfilling the expectations of our partners while being experts ourselves. This allows us to create synergies between our partners' research projects and our own developments at Siemens Healthineers. It's all about asking questions, listening intently, and learning every day. Last year, I was proud to help facilitate a new collaboration with Professor Jérôme Garot and his team at the South Paris Cardiovascular Institute. The partnership was about validating artificial intelligence algorithms using the institute's unique database of stress CMR patients, which is the only one of its kind in the world. This project was challenging in many ways, but I'm excited about how the results of these algorithms may ultimately improve risk prediction for adverse cardiovascular events.

Another major challenge is having to switch from one research topic to another as we move from one partner's site to the next. In the same week, I can support research on arterial spin labelling perfusion in neonates, interventional CMR for ablation of arrhythmia, and high-resolution perfusion for stress CMR. The rapid pace of MRI innovations means that staying up to date is not an easy task. Hopefully, I can count on the support of other clinical scientists and application specialists from the whole MAGNETOM community.

What would you do if you could spend a month doing whatever you wanted?

I love to travel to dream destinations where I can discover new cultures and go scuba diving. If I couldn't travel to somewhere like that, I'd spend most of my vacation doing pottery. I still need to improve my skills on the potter's wheel before I can dare to offer my creations to my family and friends!

Visit MAGNETOM World

Find more portraits of our colleagues around the world!

www.magnetomworld.siemens-healthineers.com/meet-siemens-healthineers



The entire editorial staff at Toronto University / Toronto General Hospital, Toronto, ON, Canada and at Siemens Healthineers extends their appreciation to all the radiologists, technologists, physicists, experts, and scholars who donate their time and energy – without payment – in order to share their expertise with the readers of MAGNETOM Flash.

MAGNETOM Flash – Imprint

© 2022 by Siemens Healthcare GmbH,
All Rights Reserved

Publisher:

Siemens Healthcare GmbH
Magnetic Resonance,
Karl-Schall-Str. 6, D-91052 Erlangen, Germany

Editor-in-chief:

Antje Hellwich
(antje.hellwich@siemens-healthineers.com)

Guest Editor:

Bernd J. Wintersperger, MD EBCR FAHA
Associate Vice Chair Research (Heart-Lung-Vessel)
University of Toronto
Director Magnetic Resonance Imaging, Director Cardiac
Imaging, Toronto Joint Department of Medical Imaging
UHN|SHS|WCH
Toronto General Hospital, Toronto, Ontario, Canada

Editorial Board:

Christian Geppert, Ph.D.; Jane Kilkenny;
Nadine Leclair, M.D.; Rebecca Ramb, Ph.D.;
Wellesley Were

Review Board:

Gaia Banks, Ph.D.; Daniel Fischer; Daniel Giese, Ph.D.;
Carmel Hayes, Ph.D.; Michaela Schmidt

Copy Editing:

Sheila Regan, Jen Metcalf, UNIWORKS,
www.uni-works.org
(with special thanks to Kylie Martin)

Layout:

Agentur Baumgärtner,
Friedrichstr. 4, D-90762 Fürth, Germany

Production:

Norbert Moser,
Siemens Healthcare GmbH

Printer:

G. Peschke Druckerei GmbH,
Taxetstr. 4, D-85599 Parsdorf b. Munich, Germany

Note in accordance with § 33 Para.1 of the German Federal Data Protection Law: Despatch is made using an address file which is maintained with the aid of an automated data processing system.

MAGNETOM Flash is sent free of charge to Siemens Healthineers MR customers, qualified physicians, technologists, physicists and radiology departments throughout the world. It includes reports in the English language on magnetic resonance: diagnostic and therapeutic methods and their application as well as results and experience gained with corresponding systems and solutions. It introduces from case to case new principles and procedures and discusses their clinical potential. The statements and views of the authors in the individual contributions do not necessarily reflect the opinion of the publisher.

The information presented in these articles and case reports is for illustration only and is not intended to be relied upon by the reader for instruction as to the practice of medicine. Any health care practitioner reading this information is reminded that they must use their own learning, training and expertise in dealing with their individual patients. This material does not substitute for that duty and is not intended by Siemens Healthcare to be used for any purpose in that regard. The drugs and doses mentioned herein are consistent with the approval labeling for uses and/or indications of the drug. The treating physician bears the sole responsibility for the diagnosis and treatment of patients, including drugs and doses prescribed in connection with such use. The Operating Instructions must always be strictly followed when operating the MR system. The sources for the technical data are the corresponding data sheets. Results may vary.

Partial reproduction in printed form of individual contributions is permitted, provided the customary bibliographical data such as author's name and title of the contribution as well as year, issue number and pages of MAGNETOM Flash are named, but the editors request that two copies be sent to them. The written consent of the authors and publisher is required for the complete reprinting of an article.

We welcome your questions and comments about the editorial content of MAGNETOM Flash. Please contact us at
magnetomworld.team@siemens-healthineers.com

Manuscripts as well as suggestions, proposals and information are always welcome; they are carefully examined and submitted to the editorial board for attention. MAGNETOM Flash is not responsible for loss, damage, or any other injury to unsolicited manuscripts or other materials. We reserve the right to edit for clarity, accuracy, and space. Include your name, address, and phone number and send to the editors, address above.

MAGNETOM Flash is also available online:

www.siemens-healthineers.com/magnetom-world

Not for distribution in the US

On account of certain regional limitations of sales rights and service availability, we cannot guarantee that all products included in this brochure are available through the Siemens sales organization worldwide. Availability and packaging may vary by country and is subject to change without prior notice. Some/All of the features and products described herein may not be available in the United States.

The information in this document contains general technical descriptions of specifications and options as well as standard and optional features which do not always have to be present in individual cases, and which may not be commercially available in all countries.

Due to regulatory reasons their future availability cannot be guaranteed. Please contact your local Siemens organization for further details.

Siemens reserves the right to modify the design, packaging, specifications, and options described herein without prior notice. Please contact your local Siemens sales representative for the most current information.

Note: Any technical data contained in this document may vary within defined tolerances. Original images always lose a certain amount of detail when reproduced.

Siemens Healthineers Headquarters

Siemens Healthcare GmbH
Henkestr. 127
91052 Erlangen, Germany
Phone: +49 9131 84-0
siemens-healthineers.com